Compression Creep Rupture of an E-glass/Vinyl Ester Composite Subjected to Combined Mechanical and Fire Loading Conditions

Steven Earl Boyd

Dissertation submitted to the faculty of the Virginia Polytechnic Institute and State University in partial fulfillment of the requirements for the degree of

Doctor of Philosophy
in
Engineering Mechanics

John J. Lesko, chair
Scott W. Case
Judy S. Riffle
Demetri Telionis
Scott Hendricks

November 20, 2006
Blacksburg, Virginia

Keywords: Fire, Creep, Compression Creep Rupture, Viscoelastic Constitutive Modeling

Compression Creep Rupture of an E-glass/Vinyl Ester Composite Subjected to Combined Mechanical and Fire Loading Conditions

Steven Earl Boyd

(ABSTRACT)

Polymer matrix composites are seeing increasing use in structural systems (e.g. ships, bridges) and require a quantitative basis for describing their performance under combined mechanical load and fire. Although much work has been performed to characterize the flammability, fire resistance and toxicity of these composite systems, an understanding of the structural response of sandwich type structures and laminate panels under combined mechanical and thermal loads (simulating fire conditions) is still largely unavailable. Therefore a research effort to develop a model to describe the structural response of these glass/vinyl esters systems under fire loading conditions is relevant to the continuing and future application of polymer matrix composites aboard naval ships.

The main goal of the effort presented here is to develop analytical models and finite element analysis methods and tools to predict limit states such as local compression failures due to micro-buckling, residual strength and times to failure for composite laminates at temperatures in the vicinity of the glass transition where failure is controlled by viscoelastic effects. Given the importance of compression loading to a structure subject to fire exposure, the goals of this work are succinctly stated as the:

(a) Characterization of the non-linear viscoelastic and viscoplastic response of the E-glass/vinyl ester composite above T_g.

(b) Description of the laminate compression mechanics as a function of stress and temperature including viscoelasticity.

(c) Viscoelastic stress analysis of a laminated panel ($[0/+45/90/-45/0]_S$) using classical lamination theory (CLT).

Three manuscripts constitute this dissertation which is representative of the three steps listed above. First, a detailed characterization of the nonlinear thermoviscoelastic response of Vetrotex 324/Derakane 510A – 40 through T_g was conducted using the Time – Temperature – Stress – Superposition Principle (TTSSP) and Zapas – Crissman model. Second, the modeling approach and viscoelastic relaxation mechanism is validated by substituting the shear relaxation modulus into a compression strength model to predict lifetimes for isothermal and one sided heating of unidirectional laminates. Finally, viscoelastic stress analysis using CLT is performed for a general laminated panel to predict lifetimes under one sided heating. Results indicate that when temperatures remain in the vicinity of T_g, the laminate behavior is controlled by thermoviscoelasticity.

Acknowledgements

I would like to acknowledge and thank the following persons whose help made this work possible.

John J. “Jack” Lesko – Thank you for accepting me into the Materials Response Group and giving me a chance to work in an intellectually stimulating environment. I especially acknowledge your encouraging attitude and commending of my work even when I did not think I was going to be able to pull it together. You are a great mentor, colleague and friend.

Scott W. Case – Thank you for the many chats we had about how to proceed and model the experimental data.

Judy S. Riffle – I have enjoyed your instruction over the years.

Demetri Telionis and Scott Hendricks – Thank you for lending your academic experience to my committee. You are both excellent professors and researchers.

John V. Bausano – Thanks for performing the one sided heating experiments and being a sounding board for my confusion and budding ideas about how to approach and model the problem. I look forward to seeing your FE model.

Jason Cain and Nathan Post – Thanks for helping me make my composite panels over the years and for answering various questions I had about the post – cure study and the MTS 407 controller.

Theophanis Theophansis – Thank you for your invaluable lab expertise and for your work in developing the VARTM set-up.

Mac McCord – Thank you for helping me set-up my experiment and answering the many questions I had about proceeding to take the data.

Beverly Williams – Thank you for helping to keep our lives a little more organized.

Dave Dillard and Kurt Gramoll – Special thanks for providing your CLT codes and your wisdom concerning non-linear viscoelasticity.

Brian Clements and Dan Villareal – Thank you for taking data relevant to this work including compression strength tests and one sided heating tests.

Dave Simmons, and the machine shop – Thank you for making various parts which gave new life to old creep frames.

Table of Contents

Acknowledgements iv
Table of Contents v
List of Figures vii
List of Tables x
Chapter 1 : Introduction and Literature Review 1
1.1 Introduction 1
1.1.1 Polymer Matrix Composites in the Navy 1
1.1.2 PMC – Fire Risk Assessment 3
1.1.3 PMC – Fire Resistance, Flammability and Toxicity 4
1.1.4 PMC Structural Response in Fire – An Integrated Analysis 5
1.2 Literature Review 9
1.2.1 Fire and Polymers 9
1.2.2 Models of Polymer Viscoelasticity 13
1.2.3 Creep Rupture of Polymer Matrix Composites 17
1.2.4 Viscoelastic Stress Analysis of Polymer Matrix Composites 19
1.3 Research Objectives 21
Chapter 2 : The Thermo-Viscoelastic, Viscoplastic Characterization of Vetrotex 324/Derakane 510A – 40 through T_g 23
2.1 Abstract 23
2.2 Introduction 23
2.3 Analytical and Constitutive Modeling 28
2.3.1 Accelerated Characterization 28
2.3.2 The Data Reduction 30
2.3.3 The Constitutive Model 35
2.4 Experimental 36
2.4.1 VARTM, Post-Cure, and Coupon Preparation 36
2.4.2 Experimental Set-up 37
2.4.3 Material Properties 38
2.5 Results, Discussion, and Parameter Modeling 39
2.5.1 Viscoelastic and Viscoplastic Parameter Modeling 39
2.5.2 Stress and Temperature Master-Curve Modeling 42
2.5.3 Observations on the Nonlinearity with Stress and Temperature 43
2.6 Conclusions and Future Research 44
2.7 Acknowledgements 46
2.8 Figures 47
Chapter 3 : Compression Creep Rupture Behavior of a Glass/Vinyl Ester Composite Subject to Isothermal and One-sided Heat Flux Conditions 63
3.1 Abstract 63
3.2 Introduction 63
3.3 Experimental and Materials 68
3.3.1 Materials 68
3.3.2 Isothermal Experimental Set-Up 69
3.3.3 One-sided Heat Flux Experimental Set-up 70
3.4 Analytical Modeling 71

3.4.1 Ramberg – Osgood Plasticity Model 71
3.4.2 Time-Temperature and Time-Stress Superposition 72
3.4.3 Viscoelastic Shear Relaxation Modulus Representation 73
3.4.4 The Compression Strength Model with Viscoelasticity 76
3.4.5 Isothermal Compression Strength Estimation and Times to Failure 77
3.4.6 Time – Temperature Profile Determination in ANSYS 78
3.4.7 One-sided Compression Strength Estimation and Times to Failure 79
3.5 Results and Discussion 80
3.5.1 Isothermal Results 80
3.5.2 One-sided Heat Flux Results 81
3.6 Conclusions 82
3.7 Acknowledgments 84
3.8 Figures 85
Chapter 4 : Compression Creep Rupture Behavior of a Glass/Vinyl Ester Composite Laminate Subject to Fire Loading Conditions 97
4.1 Abstract 97
4.2 Introduction 97
4.3 Experimental and Materials 101
4.3.1 Materials 101
4.3.2 One-sided Heat Flux Experimental Set-up 103
4.4 Analytical Modeling 104
4.4.1 Laminate Constitutive Model 104
4.4.2 Time – Temperature Profile Determination 106
4.4.3 The Compression Strength Model with Viscoelasticity 107
4.4.4 Determination of the Viscoelastic, Viscoplastic Shear Modulus 108
4.4.5 The Viscoelastic and Viscoplastic Recursion Formulas 109
4.4.6 Comparison of the Viscoelastic Recursion Formulas 114
4.4.7 The Implicit CLT Algorithm 116
4.4.8 Prediction of Laminate Failure using Implicit CLT 118
4.5 Results and Discussion 122
4.6 Conclusions 124
4.7 Acknowledgements 125
4.8 Figures 126
4.9 Tables 134
Chapter 5 : Summary and Conclusions 137
5.1 Summary 137
5.2 Conclusions 141
References 147

List of Figures

Figure 1: A PMC radar/communications mast (the Advanced Enclosed Mast System) mounted on the destroyer U.S.S. Authur W. Radford together with a side view of the mast. 2

Figure 2: Design and subsequent fire testing for a composite helicopter hanger planned for placement topside on a large combatant (Naval Sea Systems Command). 2

Figure 3: General schematic of a composite laminate subject to compressive load and an incident heat flux detailing changes that take place in a composites exposed to fire (right) with the associated thermal conditions that must be tracked (left). 5

Figure 4: Flowchart identifying the approach to predicting structural integrity of polymer composite material systems and structures exposed to fire. 8

Figure 5: Cross-section of a decomposing glass/vinyl ester composite subject to one sided heating emphasizing residual resin content through thickness. (Photograph used by permission of A. Mouritz).................... 12

Figure 6: Typical temperature master-curves for V324/Derakane 510A – 40. 47

Figure 7: Stress master-curve at 90°C with fit model (dashed line). 48

Figure 8: Temperature shift factor a_T for the reference master-curve. 49

Figure 9: Low stress creep and creep recovery data at 110°C together with corresponding predictions from linear viscoelastic theory. 50

Figure 10: The viscoplastic permanent sets versus temperature and stress together with the power law predictions (Note the dramatic increase in the leathery and rubbery regions). 51

Figure 11: The viscoplastic permanent set versus varying creep times at 150°C and σ = 200 psi (1.38 MPa) (This fit is interdependent with the elevated stresses at t_1 = 120 min). 52

Figure 12: The shear modulus G_{12} versus temperature for V324/Derakane 510A – 40.. 53

Figure 13: Typical creep data for 110°C (fit model is represented by the dashed lines). 54

Figure 14: Typical recovery data at 110°C (fit model is represented by the dashed lines). 55

Figure 15: Schapery nonlinear parameter g_0 versus stress in the glassy region. 56

Figure 16: Schapery nonlinear parameter g_1 versus stress and temperature in the leathery to rubbery regions. 57

Figure 17: The stress shift factor a_σ versus stress and temperature. 58

Figure 18: The average value of Zapas - Crissman parameter n versus temperature. 59

Figure 19: The Zapas - Crissman coefficient C^n versus temperature. 60

Figure 20: The Zapas - Crissman exponent N versus temperature. 61

Figure 21: The temperature master-curve for σ = 200 psi (1.38 MPa) with fit model (dashed line). 62

Figure 22: Isothermal, compression creep rupture experimental set-up. 85

Figure 23: Combined centric compression loading and one sided heat flux exposure tests set-up and diagram. 86

Figure 24: Temperature master-curves for Vetrotex 324/Derakane 510A – 40 at various stress levels. 87

Figure 25: Tensile strength data for Vetrotex 324/Derakane 510A – 40 at temperature (T_g ≈105°C). 88

Figure 26: Results for Ramberg – Osgood fits to four tests at (a) 30°C, (b) 90°C, (c) 130°C, and (d) 160°C (the dashed line is the fit and the square indicates the yielding shearing strain and stress). 89

Figure 27: Summary of the Ramberg – Osgood fits to tensile strength data for (a) the shear modulus, (b) and (d) yielding shear stress and strain, and (c) the strain hardening with temperature (error bars indicate standard deviation at each temperature and dashed lines are stretched exponential fits) 90

Figure 28: Temperature shift factor from the tensile shear creep data reduction of shear coupons of Vetrotex 324/Derakane 510A – 40 91

Figure 29: Stress shift factor in stress and temperature from the tensile shear creep data reduction of shear coupons of Vetrotex 324/Derakane 510A – 40. 92

Figure 30: (*a*) The isothermal compression creep rupture data shifted using a (*b*) combined shift factor from the 1.38 MPa (200 psi) experimental master-curve. Note that the shifting is especially good above T_g (105ºC). 93

Figure 31: Polished cross-section of a shear coupon (8 layers) of Vetrotex 324/Derakane 510A – 40 used to determine the initial misalignment angle for the compression strength model 93

Figure 32: Shifted isothermal compression creep data of warp and weft coupons of Vetrotex 324/Derakane 510A – 40 with compression strength model prediction. 94

Figure 33: One-sided heat flux test for warp coupon #2a showing the time-temperature profile to failure. The front and back face temperatures are thermocouple readings and the interface temperatures were calculated by ANSYS. 95

Figure 34: Predicted times to failure versus rupture times for one-sided heat flux tests on warp coupons of Vetrotex 324/Derkane 510A – 40 using the compression strength model. 96

Figure 35: Compression creep failure of Vetrotex 324/Derakane 510A – 40 laminate ($[0/+45/90/-45/0]_S$) subject to a one sided constant heat flux.. 126

Figure 36: E_{11} and E_{22} as a function of temperature for Vetrotex 324/Derakane 510A – 40 (dashed lines are fits and error bars indicate the standard deviation). 127

Figure 37: Thermal strain versus temperature for thick block sample of Vetrotex 324/Derakane 510A – 40. 127

Figure 38: Strain hardening parameter and yield shearing strain versus temperature. Results from fits of the Ramberg – Osgood equation to stress – strain data for shear coupons of Vetrotex 324/Derakane 510A – 40.. 128

Figure 39: One sided heat flux experimental set-up. Image shows close-up view of a coupon seated in servo-hydraulic grips subject to heat flux from an IR lamp. 128

Figure 40: Time – temperature profile extension for constant heat flux test 5 kW/m^2 at a compressive load of 2800 lb. 129

Figure 41: Time – temperature extension for a constant heat flux 10 kW/m^2 test at a compressive load of 3000 lb. 129

Figure 42: Non-linear Kelvin – Voigt element mechanical analog. 130

Figure 43: A series of *l* non-linear Kelvin – Voigt elements. 130

Figure 44: Flowchart of the solution method used in predicting times to failure for laminates of Vetrotex 324/Derakane 510A – 40... 131

Figure 45: Compression creep rupture lifetimes of laminates ($[0/+45/90/-45/0]_S$) of Vetrotex 324/Derakane 510A – 40 subject to a one sided constant heat flux. 132

Figure 46: Compression creep rupture lifetimes of laminates ($[0/+45/90/-45/0]_S$) of Vetrotex 324/Derakane 510A – 40 subject to a one sided heat flux in which the front face temperature is held constant.. 133

List of Tables

Table 1: Comparison of glass transitions for various polymer composites. (Information provided by Dr. Judy Riffle, Dept. of Chemistry, Virginia Polytechnic Institute & State University.) 10

Table 2: Relevant material properties used in the analysis († values taken from Lattimer and Oullette [16]) 134

Table 3: Predictions for the constant heat flux tests. "N/A" refers to a test which was *not* used because of thermocouple failure. All calculations are performed using Matlab. .. 135

Table 4: Predictions for the constant front temperature tests. All calculations performed using Matlab.......... 136

Chapter 1: Introduction and Literature Review

1.1 Introduction

1.1.1 Polymer Matrix Composites in the Navy

Polymer matrix composites (PMC's) are an important class of engineering materials whose applications as a structural material are expanding for use in civil infrastructure, as topside structures on large naval vessels, and as shell materials in small vessels in the marine industry. In civil infrastructure PMC applications include the repair and retrofitting of decking and exposed structural members such as columns and beams in bridge structures. Many of the world's navies are currently investigating PMC's as replacements to conventional metals for use as topside structures such as helicopter hangers, radar/communications masts, and floors and bulkheads of deckhouse structures on larger combatants. PMC's are already used aboard some naval vessels as communications and radar installations. Figure 1 shows an example of the use PMC's on a naval vessel in the form of the Advanced Enclosed Mast System (AEM/S) [1] and Figure 2 shows a schematic for a helicopter hanger and its placement on a large combatant. Future uses of PMC's on naval vessels include propellers, propulsion shafts and rudders for frigates and aircraft carriers. Composites may even be used one day for smaller ship hulls.

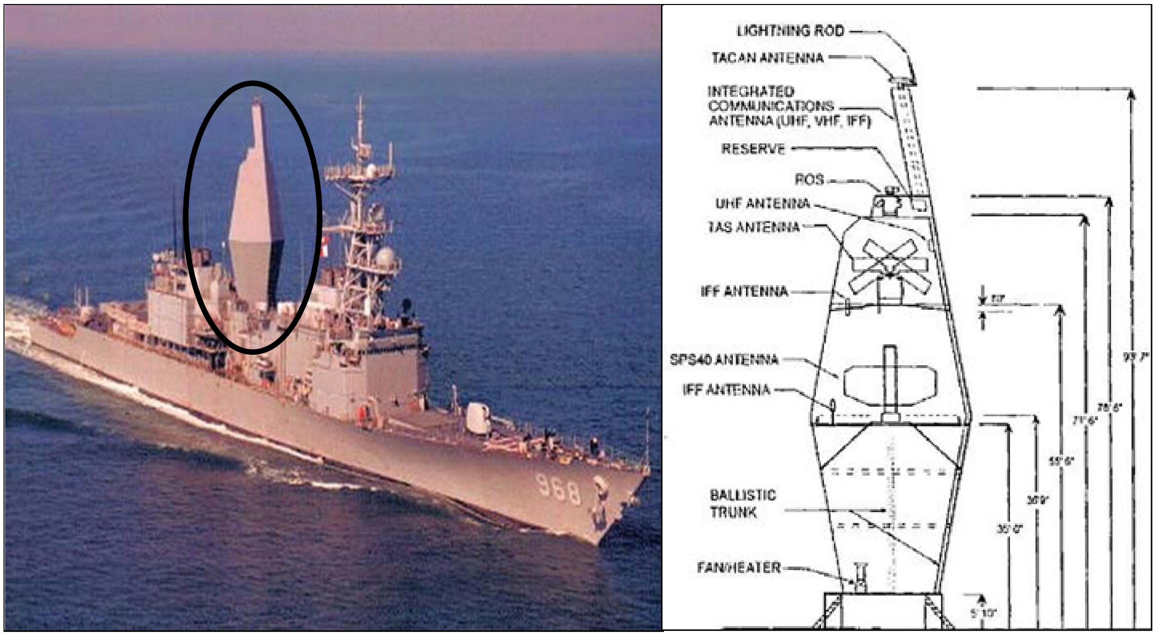

Figure 1: A PMC radar/communications mast (the Advanced Enclosed Mast System) mounted on the destroyer U.S.S. Authur W. Radford together with a side view of the mast.

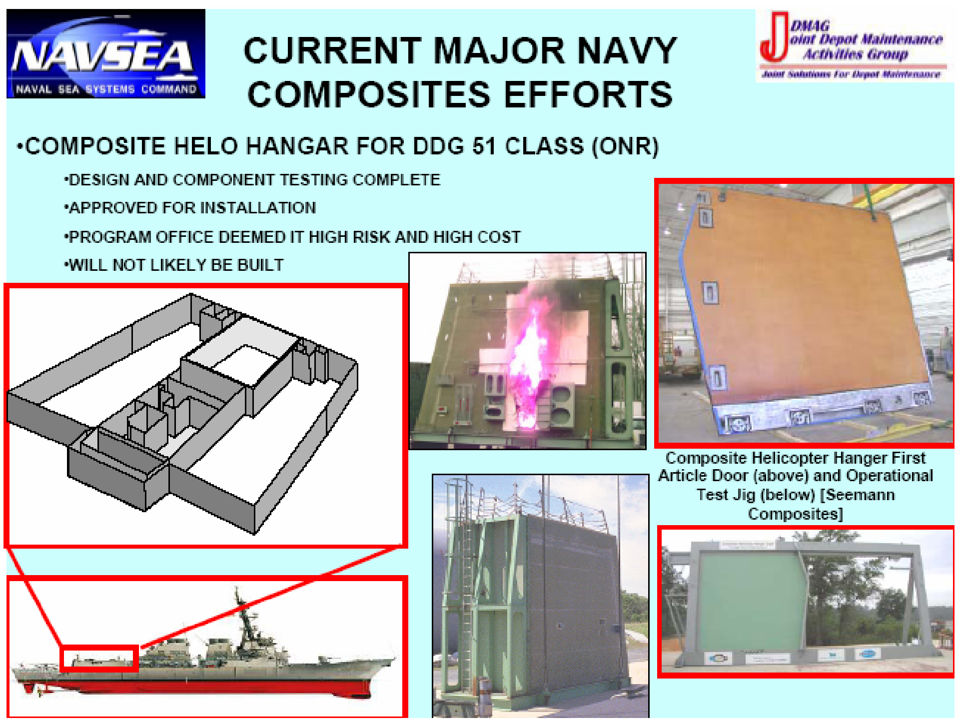

Figure 2: Design and subsequent fire testing for a composite helicopter hanger planned for placement topside on a large combatant (Naval Sea Systems Command).

Composites are beneficial in civil and naval applications due to their high specific strength, long fatigue life, excellent resistance to water corrosion, and overall good durability. The world's navies are interested in composites specifically to enhance the operational performance of naval vessels by extending their range and speed through weight savings, their stealth due to the low electromagnetic signature of composites, and their payload. Composites also lower operating cost for larger vessels by reducing fuel consumption due to weight savings and through reduced maintenance. However, their poor impact resistance, high cost, low rigidity, and various joining problems are impediments to their full application. One major impediment that must be removed if PMC's are to see a wider application to topside structures is their performance under fire exposure.

1.1.2 PMC – Fire Risk Assessment

Fires aboard naval vessels often start in the engine room or where aircraft are refueling. If a fire does break out, conventional metals which compose shipboard compartments quickly transfer heat from one to the other due to the high heat conductivity of metals and hasten flame spread and increase fire temperature. PMC's in contrast have a low heat conductivity which helps to stem the spread of fire out from its source. Although the rate of heat conduction for polymer matrix composites is low and may prevent fire from spreading quickly from one compartment to another, the overall performance of composites versus metals in fire is still worse due to the changes the organic matrix material undergoes in a fire exposure. Structurally, the organic matrix will soften with elevated temperatures, ablate and char, reducing strength and increasing buckling risk and eventually compartment collapse. Chemically, at very high temperatures the organic matrix will decompose releasing heat, dense smoke, soot, and toxic gases (especially in the case of brominated vinyl esters) which will obscure exit from the area of fire and pose significant health risk and survivability for any one remaining in the area. Before these composites can be fully implemented on board naval ships, questions regarding the fire resistance, flammability, toxicity, and structural integrity of the organic polymer matrix must be investigated.

1.1.3 PMC – Fire Resistance, Flammability and Toxicity

To date much work has been conducted to characterize the fire resistance, flammability and toxicity of PMC's [2-4]. At very high temperatures exceeding the matrix decomposition temperature the fire exposed surface will ignite releasing combustible gases and radiating heat energy. Ablation will occur and a pyrolysis front between a layer of char and the composite will begin to propagate through the composite as mass is lost (as shown in Figure 3). The interactions between solid and gaseous states are coupled and complicated but are well understood and quantified. The degree of smoke and soot generated as volatiles is characterized by ASTM E 662 and the quantities of particular gases produced such as carbon monoxide and carbon dioxide in addition to other composite specific gases (such as hydrogen bromide for a brominated vinyl ester) is estimated by ASTM E 1354. A significant contribution in this area has been accomplished by Sorathia et al. [5-7] and others [8-10] for the United States Navy. Fire resistance is defined by the time to ignition (ignitability) and heat release rate (HRR) and is determined by the standard test ASTM E 1354 (Oxygen Consumption Cone Calorimeter). Sorathia and Beck [11] and Hirschler [9] have made significant contributions to determining the fire resistance of a variety of polymers and composites. Flammability or fire growth and flame spread in which the HRR of the polymer is the most important catalyst is determined by a number of standardized tests including ASTM

E 84 (Tunnel Test), ASTM E 1354 (Cone Calorimeter), ASTM E 1321 (Lateral Ignition and Flamespread) and UL 94 (Oxygen Index). The tests range from small lab scale tests (ASTM E 1354) to full scale tests (ASTM E 1321). Ohlemiller [12, 13] and Sorathia [5] have conducted studies on a variety of composite materials including brominated vinyl-esters that characterize flamespread phenomena.

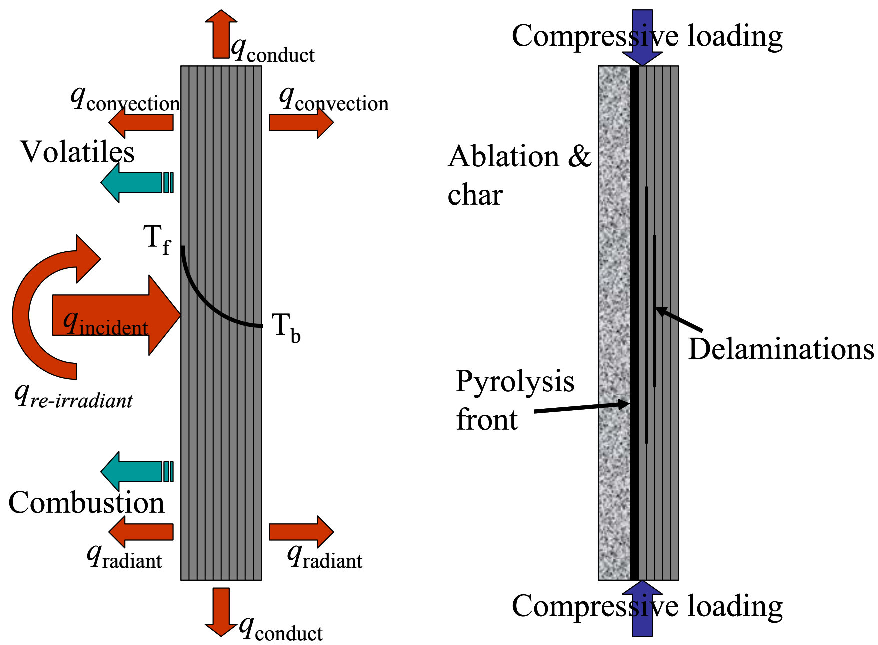

Figure 3: General schematic of a composite laminate subject to compressive load and an incident heat flux detailing changes that take place in a composites exposed to fire (right) with the associated thermal conditions that must be tracked (left).

1.1.4 PMC Structural Response in Fire – An Integrated Analysis

Although there are a number of standardized tests and numerous research efforts to characterize the flammability, fire resistance and toxicity of PMC's exposed to fire on naval ships, there are relatively few research efforts that have aimed to develop a mechanistic first principles based model to predict the structural response of PMC laminates or structures post – fire or under fire conditions. Aware of this shortfall in visualizing and understanding the entire problem, the main goal of this research effort is to develop tools that will model the response of PMC's to fire loading conditions and allow for the prediction of limit state variables in fire such as global and local buckling, deflection, thermo-mechanical property evolution as a function of fire (spatial assessment of heat fluxes and/or temperatures), and times to failure for PMC laminates and structures [14]. Though this research effort is focused on glass/vinyl ester systems currently being investigated by the United States Navy, the procedures described and modeling framework can be combined into an integrated tool applicable to other PMC's in other industries such as civil infrastructure, marine, and armor for civil and military applications given the availability of property evolution information as a function of temperature.

The broad focus of this research is to develop a framework for simulating fire exposure of Navy shipboard compartments (with a focus on PMC's) and the assessment of structural integrity during and subsequent to a particular fire scenario. The main feature of the analysis is *accurately* combining *all* aspects of the thermal and structural problem. To do so, a fire dynamics simulator (FDS from NIST [15]) will eventually be incorporated with a finite element (FE) structural analysis program (ANSYS or ABAQUS) for prediction. The FDS analysis will be used to determine the spatial and time dependent heat flux for a given compartment and fuel load. Component surface temperatures and the resulting material temperatures will be modeled as a function of time and position. These material temperatures will be used to assess the residual thermal-mechanical-damage response of the PMC, and therefore the structural capacity during and post - fire can be predicted using the FE analysis.

In order to accomplish these objectives, experiments and analysis are underway to determine the following:

- Characterization of the evolution of material properties as the PMC is exposed to a heat flux history, in particular including the:
    - Evolution of thermo-mechanical properties such as stiffnesses, coefficients of thermal expansion and thermal diffusivity as a function of temperature.
    - Change in the compression laminate strength as a function of time and temperature when subjected to a sustained compressive load and one sided heat flux.
    - Characterize the creep and creep rupture behavior and its effect on the evolution of strength and global stiffness.
    - Evolution of laminate properties and residual strength when irreversible damage and ablation occur.

- Combining the thermo-mechanical property evolution with a structural modeling package so as to assess structural integrity under non-uniform thermal and mechanical conditions.

- Integrating structural analysis and fire simulations in a manner that will allow for design and visualization of the problem.

A statement of the approach for predicting the structural performance of a PMC subject to fire exposure is summarized in Figure 4.

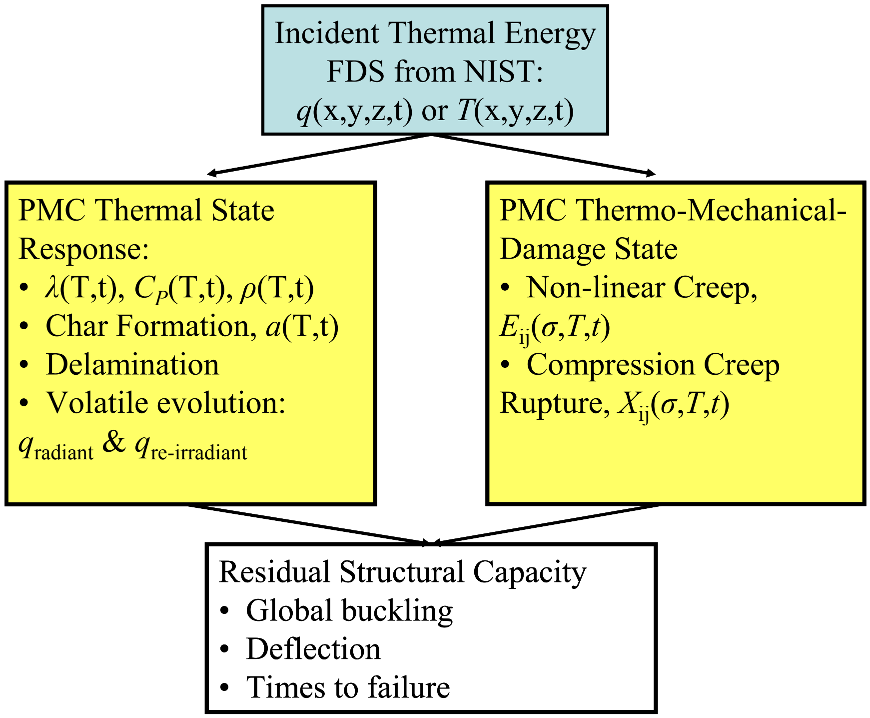

Figure 4: Flowchart identifying the approach to predicting structural integrity of polymer composite material systems and structures exposed to fire.

Of the areas listed in Figure 4, assessment of the PMC's thermal state response has already been undertaken by Lattimer and Oulette [16], Gibson et al. [17, 18], and Mouritz et al. [19-22] and others. These efforts focus on characterizing the thermo-mechanical material property evolution at temperatures where irreversible thermodynamic effects decompose the organic matrix and control the delayed failure of the structure; temperatures at and well above the thermal decomposition temperature. These high temperatures (heat fluxes greater than 50 – 75 kW/m^2) cause irreversible damage to the composite in the form of thermal decomposition of the matrix (ablation, char formation and pyrolysis) and typically a quick temperature controlled failure. As a continuation of the overall work to characterize the structural response under fire loading conditions, the current research effort seeks to study *reversible* phenomena that typically occur with lower heat fluxes (5 – 10 kW/m^2) and temperatures in the vicinity of the glass transition temperature T_g where viscoelastic effects (creep and creep rupture) control failure. Therefore, the contribution of this dissertation to the main research statement has been to determine the thermo-mechanical damage state of the composite due to non-linear creep and resulting creep rupture at elevated temperatures and incorporate this characterization into the structural model for the assessment of residual structural integrity and failure prediction.

1.2 Literature Review

1.2.1 Fire and Polymers

Chemical composition and the glass transition temperature are very important indicators of how well a polymer matrix will perform chemically and structural when exposed to fire. There are two general classifications of polymer matrices which define how PMC's perform during fire exposure. Polymers with a high aromatic content (e.g. phenolic, epoxies) tend to form char insulating the exposed surface and impeding further fire damage (diminishing the convection of gases). Halogenated polymers evolve gases upon ignition which displaces oxygen and slows or eliminates the burning; however, smoke and toxicity generation is a concern. Phenolic polymers exhibit lower peak heat release rates (PHRR) and higher char yields. However, their mechanical properties are not considered adequate, without modification, for structural applications. Styrenated resins (polyesters and vinyl esters) and the halogenated epoxies possess higher PHRR and lower char yields. Upon exposure to flame or heat, the matrix material of the polymer composite first undergoes *reversible* changes in physical properties (non-linear viscoelasticity and progressive thermal softening of the material properties), see Figure 3. These *reversible* changes will act in the early stages of fire exposure at temperatures in the vicinity of the glass transition T_g and may cause the structure to exceed buckling or deflection limit criteria. The glass transition temperature T_g as a result is a very important property of polymer matrices because it is the temperature at which the polymer's properties will change most significantly and whose value will best determine to which application a polymer composite is best suited. Table 1 illustrates various polymer matrix glass transitions and some of their applications. Styrenated resins and phenolics have the lower T_g with epoxies performing better with elevated temperatures. Styrenated vinyl ester systems such as Ashland Composite Polymers Derakane 510A – 40 are presently used by the United States Navy in experimental applications for top-side structures.

Table 1: Comparison of glass transitions for various polymer composites. (Information provided by Dr. Judy Riffle, Dept. of Chemistry, Virginia Polytechnic Institute & State University.)

Polymer System	Glass Transition Temperature, T_g	Current Applications
Vinyl Esters - Styrene Unsaturated Polyesters - Styrene Phenolics	Moderate (≈120 - 160°C)	Civil Engineering, Infrastructure, Automotive, ships
Cyanates	High (260°C)	Electronic Materials, Adhesives and Matrices, Civilian Aircraft
Epoxies	High (≈240°C)	Military
Functional Arylene Ethers	High (200 - 280°C)	Tougheners
Functional Imides Phthalonitrile	Very High (200 - 400°C)	Aerospace/Electronic

As the temperature increases the polymer matrix ignites and begins to burn starting coupled and complex multi-stage decomposition reactions such as pyrolysis, the formation and evolution of gases, and the forming of a layer of carbonaceous char which can propagate through the composite on continued heating (see both Figure 3 and Figure 5). There are a number of important works that have investigated the thermal degradation and transport of volatiles in polymer composites subject to fire exposure and their effect on the composite's residual thermal properties and strength. Pering et al. [23]

was among the first to attempt to correlate mass loss with residual strength for polymer composites subject to intense heating. Griffis et al. [24] actually presented a 1D finite difference model (modified Crank – Nicolson scheme) for the time – temperature profile which they used to predict front and rear temperatures of a AS/3501-6 graphite/epoxy composite. Other researchers Chen et al. [25] and Griffis et al. [26] improved the time – temperature profile predictions and added a mechanical component to the analysis to predict times to failure, although unsuccessfully.

Other researchers such as Hendersen and Wiecek [27], Milke and Vizzini [28] and McManus and Springer I and II [29, 30] developed and continued to improve the thermal evolution model for polymers subject to very high temperatures. Hendersen and Wiecek developed a 1D transient heat transfer model which accounted for the endothermic decomposition of the matrix by modeling the storage and mass transfer associated with the evolution of gases on the exposed surface. Milke and Vizzini developed a 3D transient heat transfer model with non-uniform boundary conditions; however, they did not account for the evolution of pyrolysis gases in their analysis. McManus and Springer developed one of the most sophisticated and complete treatments of the physics of a combusting polymer composite including formation of a char layer, mass loss, vapor (water) and volatile formation along with diffusion of the gases and combined it with a 3D elasticity model to predict delaminations through thickness. Though these models accurately predicted temperatures in the polymer matrix under intense heating, experimental validation was sometimes lacking and a mechanical model to predict residual strength and material properties as a function of heat exposure (temperature) was not attempted.

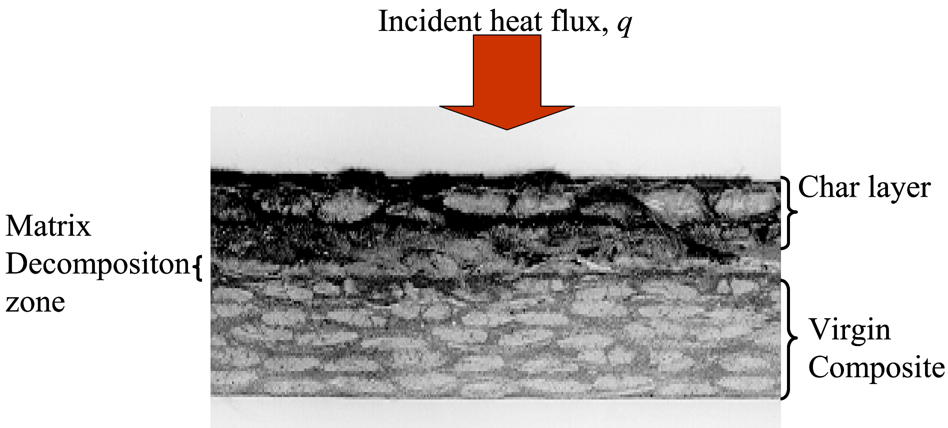

Figure 5: Cross-section of a decomposing glass/vinyl ester composite subject to one sided heating emphasizing residual resin content through thickness. (Photograph used by permission of A. Mouritz).

More recently, other research efforts have sought to combine an accurate treatment of the high temperature thermal response/physical properties of combusting polymer composites with mechanistic based models of residual tensile and compression strength and structural stability. Among them are investigations by Gibson et al. [17, 31], Seggewiß [32, 33] and Mouritz and Mathys [19-22]. Mouritz and Mathys [20] investigated changes in tensile and flexural properties of three composite systems most frequently used on board naval ships (polyesters, vinyl esters, and phenolics) exposed to constant heat fluxes of 25 – 100 kW/m^2 for 325 s to 1800 s (30 min). They noted significant decrease in stiffness and failure load with increasing heat flux and attributed it to matrix degradation due to the formation of char. They developed a rule of mixtures model based on the ratio of char depth to remaining composite to estimate residual tensile and flexural failure load. Gibson et al. continued with the work of Mouritz and Mathys and developed a thermal response model to predict a time – temperature profile for a decomposing polymer composite which included effects due to endothermic matrix decomposition and volatile gas convection. This thermal model is used as input into a later research effort to predict residual laminate properties (cross-ply [0/90] glass/vinyl ester laminates) and strength at constant heat fluxes from 10 to 75 kW/m^2. Gibson et al. [18, 34] proposed a two – layer model using a simple rule of mixtures model to estimate the remaining tensile strength of a polymer composite containing char and composite layers. Utilizing the idea of progressive thermal softening of stiffnesses and changes in coefficients of thermal expansion, they also estimated the critical buckling load under uniform compression and used the value to estimate times to failure for laminates subject to a compressive load and constant heat flux. In addition they calculated the elements of the A-B-D matrix versus time for a polymer composite exposed to a constant heat flux. For the most part the modeling approach was validated by existing experimental data; however, the lifetime predictions for compression were much better than those for tension especially at the higher heat fluxes. Seggewiß has shown a comparison of the tensile and compressive lifetimes for carbon/polyester systems in their principle orientations with heat fluxes up to 280 kW/m^2.

1.2.2 Models of Polymer Viscoelasticity

The preceding work has been concerned with the very high temperature thermal response/physics of PMC's where endothermic matrix decomposition controls failure. However, at lower temperatures in the vicinity of the glass transition temperature T_g (well below the thermal decomposition temperature) delayed failure of laminates subject to load and lower heat fluxes is controlled by viscoelastic and viscoplastic effects. As mentioned previously the most significant changes to polymer matrix properties and thus polymer composite properties such as a precipitous drop in the elastic modulus occur in the area of the glass transition. For polymers these changes in properties are not only temperature dependent but time and stress dependent as well.

The time dependence of the properties of polymer matrix composites is well documented in the literature. Certain environmental variables such as elevated temperature, stress, moisture, and, more recently, the phenomena of physical aging can alter the properties of polymers over time. Leaderman [35] was the first to suggest that temperature was an "accelerating factor" in the time dependence of polymer properties. He realized that short creep tests conducted under controlled conditions at different temperatures appeared to give a representation of the polymer properties over different time scales. The effects of elevated temperature appeared to accelerate or shift the long – term viscoelastic behavior to shorter times. Schapery [36] developed a non-linear modification to the Boltzmann hereditary integral based on irreversible thermodynamics to account for the effects of elevated stress. Lou and Schapery [37] were among the first to apply Schapery's nonlinear hereditary integral (the time-stress superposition principle) to the analysis of unidirectional glass fiber-epoxy composites. At this time the physical meaning of the vertical shifts g_0, g_1 and g_2 and the stress shift factor a_σ of the Schapery model were being questioned. The stress shift factor was suggested to obey Eyring's [38] rate process at high stress by Lou and Schapery. Daugste [39] was among the first to suggest that it may also have a temperature dependence (he also suggested that the temperature shift factor may have a stress dependence).

Griffith [40] explored the nature of the shift factor when multiple accelerating mechanisms were acting to influence the viscoelastic behavior and used this analysis to create combined temperature and stress master-curves. Griffith also gave a detailed account of the possible presence of a vertical shift, a_G, as a function of temperature; these are the vertical shifts that are encountered when forming smooth temperature master-curves and are not related to the vertical shifts, g_0, g_1 and g_2 of the Schapery model. Hiel [41] and Tuttle and Brinson [42] performed a nonlinear viscoelastic (Schapery) analysis on unidirectional graphite fiber-epoxy composites and were among the first to note that their composites were exhibiting a noticeable viscoplastic strain or permanent set in the recovery data. Their approach was simply to subtract the permanent set from the recovery data and then conduct the data reduction on corrected data (it should be noted that their creep and recovery tests were conducted below T_g of the epoxy where plastic strains are often negligible and as a result this method had reasonable success for them). Tuttle and Brinson also developed a numerical iteration scheme to predict creep strains using classical lamination theory (CLT) which was later adopted by Tuttle et al. [43].

Until then a power law was used to model the transient compliance in Schapery's model as suggested by Findley, Onaran, and Lai [44-46] and experimentally observed in creep data. However, Gramoll et al. [47, 48] and Cysz and Szyszkowski [49] demonstrated that the power law kernel required laborious calculations of the hereditary integral (at each time step the previous stress history had to be stored and used in the subsequent calculation). The power law kernel for the transient compliance also became unstable at large times diverging instead of modeling the rubbery region plateau behavior illustrated by most polymers. As a result Xiao [50] and Brouwer [51] used a modified power law in their analysis. The modified power law although it picked up the rubbery region behavior of a polymer matrix composite, was difficult to include within the Schapery model and again required laborious calculations of the hereditary integral. Ha and Springer [52, 53], Tuttle et al. [54, 55], and Guedes et al. [56, 57] adopted a Prony series kernel (a generalized Kelvin – Voigt series first proposed by Zeinkeiwicz et al. [58]) which is used today by most researchers.

The first data reduction to combine time-temperature with time-stress superposition principles (TTSP with TSSP) successfully was performed by Peretz and Weitsman [59, 60] on FM-73 adhesive. Ha and Springer [53] and Tuttle et al. [43] also utilized the TTSSP on unidirectional graphite fiber-epoxy composites. In addition Ha and Springer incorporated a viscoplastic component based on the viscoplastic strain rate after Naghdi [61, 62]. Tuttle et al. also incorporated a viscoplastic component after Zapas and Crissman [63, 64] and used the model to predict cyclic, thermo-mechanical loading. Both of these studies were limited in scope because the analysis and resulting success of the approach to TTSSP was limited to the glassy region of the polymer matrix. Also, to our knowledge the only other study to examine the nonlinear viscoelastic behavior of composites in the vicinity of and above T_g was performed by Xiao [65]; however, severe nonlinearity in the composite kept him from employing a full Schapery-type analysis. However, Xiao was able to conclude that his stress shift factor, a_σ, had a clear temperature dependence which he modeled using temperature dependent coefficient parameters (his approach to modeling the stress and temperature dependence of a given nonlinear parameter was used in the chapter 1 manuscript).

In the current study a combined time-temperature and time-stress superposition (TTSSP) within an accelerated characterization scheme is employed to describe nonlinear viscoelastic behavior of an E-glass/vinyl ester composite with elevated temperature and stress. A viscoplastic strain component is included using the Zapas - Crissman model to account for the observed permanent sets in the recovery data. Since the polymer matrix is understood to be the main source of the viscoelastic, viscoplastic response of the composite especially in a non-fiber reinforced direction, the characterization focuses on the shear response through T_g as a main source of the viscoelastic behavior. Chapter 1 will present a manuscript which will give a detailed presentation of the viscoelastic and viscoplastic data reduction of Vetrotex 324/Derakane 510A - 40.

1.2.3 Creep Rupture of Polymer Matrix Composites

There is a wealth of information in the literature on the creep rupture of metals and metal matrix composites but comparatively few studies on the creep rupture of PMC's. Many of these studies report numerous methods for the modeling of creep deformation and rupture behavior including damage models using a continuum mechanics approach or energy criterion (Kawai et al. [66] and Guedes [67], respectively), a general life prediction approach using time-temperature equivalence (Miyano et al. [68-70]), mechanistic models like Sherby – Dorn [71], parameter models like Larson – Miller [72], and a detailed characterization of creep deformation behavior applied to a suitable failure criterion modified for the inclusion of creep (Dillard et al. [73]). These different models have been successfully applied to PMC's to predict tensile creep rupture in the vicinity of T_g.

Kawai, Masuko, and Sagawa [66] utilized a continuum mechanics model to describe the creep deformation and rupture behavior as an evolution of damage in carbon fiber reinforced epoxy laminates (T800H/epoxy). They compared their results with Dillard's [73] approach of modifying the Tsai – Hill failure criterion to include time dependent strengths and found good agreement. Mechanistic and parameter model approaches were also investigated. Lyons [74] investigated both Sherby – Dorn and Larson – Miller models and settled on the Sherby – Dorn model which assumes that the steady state creep rate is proportional to the stress and the temperature through an activation energy process of the Zhurkov type [75, 76]. Lyons performed the Sherby – Dorn analysis on glass filled thermoplastic resin systems (polyamides and polyphthalimides) constructing reasonable master-curves for the prediction of delayed failures. Dillard [73] also chose to represent his creep rupture strength condition in a form of the Larson – Miller, Sherby – Dorn, and Zhurkov types.

Miyano et al. [68-70] have forwarded models predicting creep rupture behavior based purely on time-temperature equivalence. Miyano et al. collected rupture times at different temperatures and stresses and shifted the data to form temperature master-curves. The resulting shift factors were modeled using an Arrhenius relationship and the corresponding activation energies were calculated. Miyano et al. then used the master-curves to successfully predict rupture strengths. Guedes [67], working with creep and creep rupture data taken by Dillard et al. [73], represented the creep compliance functions as a Prony series and calculated the change in free energy that accumulated during creep loading. The energy criterion model that Guedes derived successfully predicted Dillard's creep rupture data and compared well with the modified Tsai – Hill failure criteria utilized by Dillard.

Of all the approaches reviewed the one of Dillard et al. [73] is closest to the one selected for the current study. An approach which accounts for rupture data over a wide temperature range and number of stress levels and which utilizes an existing creep deformation analysis is desired. Also, given that the dominant loading mode for a bulkhead structure composed of a glass/vinyl ester system subject to fire exposure is compressive, a model which accounts for a state of compression loading through a compression mechanics analysis such as the Budiansky and Fleck model [77] is needed. The Budiansky and Fleck model also estimates the effect of initial fiber misalignments on the residual strength, a detail which is very important to this research considering that the compressive loading combined with the significant initial misalignment angle of the fiber tows of Vetrotex 324 (a woven roving) profoundly effect the residual strength and stiffness. Using the Budiansky and Fleck model as a starting point, a compression strength failure criterion is developed that includes nonlinear viscoelastic effects (in the form of the shear modulus G_{12} and is used to predict both isothermal and one-sided heat flux compression creep rupture data.

1.2.4 Viscoelastic Stress Analysis of Polymer Matrix Composites

The main goal of current work is to develop a mechanistically based model based on first principles to characterize the non-linear viscoelastic behavior and predict delayed failure of a glass/vinyl ester composite subject to fire loading conditions. For an orthotropic laminate subject to a constant compressive load and a temperature profile, knowledge of both the time – temperature profile, an estimation of the state of stress in each ply, and application of these two inputs to the compression strength failure criterion are required to solve the problem. A FE implementation will eventually be developed to solve the structural problem; however, CLT gives a simple, straight forward method for calculating the state of stress for now and validating the modeling approach.

A CLT based approach for calculating the long term viscoelastic response and delayed failure of polymer matrix composites was developed here at Virginia Tech by

Dillard and Brinson [78]. A detailed description of this forward explicit CLT algorithm may be found in Dillard [78-80] and Tuttle and Brinson [42]. Dillard et al. used the non-linear Findley model with a viscoelastic recursion based on a power law kernel within CLT to predict long term viscoelastic response and delayed failure of a graphite/epoxy composite. Tuttle and Brinson performed a similar analysis except used the Schapery model to describe the non-linear viscoelastic behavior. Ha and Springer [53] used the Schapery model with a Prony series kernel and a viscoplastic strain within CLT to predict the response of a graphite epoxy composite under conditions of changing stress and temperature. Tuttle et al. [54], Pasricha [43] and Guedes et al. [56, 57] continued with this approach except used the Zapas – Crissman model for the viscoplastic strain component.

Dillard [79] was the only author to mention stability problems with the forward explicit CLT algorithm. Dillard reported that the convergence characteristics of the algorithm depended on the time-step size, the type of laminate considered (worse for two angle laminates), convergence to the correct state of stress was required if stresses changed significantly through the laminate (such as loading or discounting a ply), and on modifying the stress inputs to the non-linear viscoelastic functions using a pseudo-central difference technique. Gramoll et al. [47] continued the work of using CLT to calculate the long term viscoelastic response of polymer matrix composites, but had similar problems with the forward explicit CLT algorithm and eventually developed an implicit method (the non-linear differential equation method – NDEM) which is unconditionally stable and allows modeling of laminate strain and stress out to very long times regardless of time step size. The implicit CLT algorithm is simple and can easily be adapted to orthotropic laminates. The stress – strain equations of CLT and the equilibrium equations are not solved using the A-B-D matrix, but are solved with the Newton – Raphson method which has better convergence properties. The method of Gramoll et al. [47] was successfully adopted as the solution method for the current work. For additional information on stability issues and a verification of the implicit method see Gramoll et al. [47].

1.3 Research Objectives

The main goal of this research effort is to develop analytical models and methods to predict laminate level (a laminate panel as opposed to a structural component containing the laminate) limit state variables such as local compression failure due to micro-buckling, residual strength and stiffness, and estimated times to failure. Given the importance of compressive loading at elevated temperatures in the response of composite structures exposed to fire, the areas of focus for this work are succinctly stated as the:

- Characterization of the non-linear viscoelastic and viscoplastic response of the E-glass/vinyl ester composite at and above the glass transition temperature T_g (see Boyd et al. [81]).
- Description of the compression mechanics as a function of stress and temperature using a developed compression strength failure criterion (based on Budiansky and Fleck [77]) which includes viscoelasticity (see Boyd et al. [82]).
- Incorporation of the material characterization and failure criterion into a viscoelastic stress analysis using classical lamination theory (CLT).

The next three chapters in this dissertation include manuscripts (both published and submitted) that address each of the three points listed. Though there are co-authors listed, every manuscript was written and the modeling and analysis performed by the author of this dissertation, Steven Earl Boyd. Chapter 2 addresses the first point characterizing the non-linear viscoelasticity of a glass/vinyl ester composite; the manuscript was published in the Journal of Engineering Materials and Technology in October 2006 [81]. Chapter 3 addresses the second point and focuses on creep rupture of warp (unidirectional 0°) laminates of a glass/vinyl ester composite subject to both isothermal and one-sided heating; this manuscript has been submitted to Composites, Part A: Applied Science and Manufacturing. The final point is addressed in chapter 4 where a viscoelastic stress analysis using implicit CLT is used to predict times to failure for pseudo-quasi-isotropic laminate ($[0/+45/90/-45/0]_S$) of a glass/vinyl ester composite subject to one sided heating; this manuscript has yet to be submitted to a journal.

Chapter 2: The Thermo-Viscoelastic, Viscoplastic Characterization of Vetrotex 324/Derakane 510A – 40 through T_g[1]

2.1 Abstract

The increased use of fiber reinforced plastics (FRP) in ship topside structures necessitates the need to understand how such structures respond to fire exposure. For this reason we have characterized the nonlinear, thermo-viscoelastic behavior of Vetrotex 324/Derakane 510A – 40 using tensile loading of $[\pm 45]_{2S}$ laminates. Nonlinearity is observed at elevated stress and temperatures above T_g. The data reduction sufficiently modeled the experimental master-curves over the whole temperature range, but suffered from inconsistencies in the creep data and recovery data, perhaps due to accumulated damage during the creep cycle. Our results indicate that the nonlinear viscoelastic behavior significantly contributes to structural behavior under fire loading conditions.

Keywords: Fire, Viscoelasticity, Viscoplasticity, Schapery, TTSSP, Zapas – Crissman

2.2 Introduction

Currently, the Navy is investigating Vetrotex 324/Derakane 510A – 40, a glass woven roving reinforced, vinyl ester composite, for use in topside structures on naval vessels. Due to the stringent codes for both structural integrity and fire resistance in effect on naval vessels, a research effort has been undertaken to model the fire loading behavior of this composite. Numerous tests have been conducted subjecting samples to a

[1] Boyd SE, Lesko JJ, Case SW. The Thermo-Viscoelastic, Viscoplastic Characterization of Vetrotex 324/Derakane 510A – 40 through Tg. Journal of Engineering Materials and Technology 2006;128(4):586-94.

one-sided heat flux and compression loading [22, 33, 83]. Data reduction and analysis of the tests revealed a gap in our modeling efforts suggesting that the nonlinear, viscoelastic behavior of the composite required inclusion in the structural modeling. Obviously, high temperatures and non-uniform temperature profiles through the thickness are the controlling factors under fire loading conditions. Our previous modeling efforts have included these effects [83, 84]. Therefore, the purpose of this effort is to quantify the nonlinear, viscoelastic behavior of V324/ Derakane 510A – 40 at high temperatures (in the vicinity of and exceeding T_g) and stresses to complete the treatment of temperature effects in the main structural model.

The time dependence of the properties of polymer matrix composites is well documented in the literature. Certain environmental variables such as elevated temperature, stress, moisture, and, more recently, the phenomena of physical aging can alter the properties of polymers over time. Leaderman [35] was the first to suggest that temperature was an "accelerating factor" in the time dependence of polymer properties. He realized that short creep tests conducted under controlled conditions at different temperatures appeared to give a representation of the polymer properties over different time scales. The effects of elevated temperature appeared to shorten or shift the viscoelastic behavior to shorter times. Schapery [36] developed a nonlinear modification to the Boltzmann hereditary integral based on irreversible thermodynamics to account for the effects of elevated stress. Lou and Schapery [37] were among the first to apply Schapery's nonlinear viscoelastic integral (the time-stress superposition principle) to the analysis of unidirectional glass fiber-epoxy composites. At this time the physical meaning of the vertical shifts g_0, g_1 and g_2 and the stress shift factor a_σ of the Schapery model were being questioned. The stress shift factor was suggested to obey Eyring's [38] rate process at high stress by Lou and Schapery. Daugste [39] was among the first to suggest that it may also have a temperature dependence (he also suggested that the temperature shift factor may have a stress dependence).

Griffith [40] explored the nature of the shift factor when multiple accelerating mechanisms were acting to influence the viscoelastic behavior and used this analysis to create combined temperature and stress master-curves. Griffith also gave a detailed accounting of the possible presence of a vertical shift, a_G, as a function of temperature; these are the vertical shifts that are encountered when forming smooth temperature master-curves and are not related to the vertical shifts, g_0, g_1 and g_2 of the Schapery model. Hiel [41] and Tuttle and Brinson [42] performed a nonlinear viscoelastic (Schapery) analysis on unidirectional graphite fiber-epoxy composites and were among the first to note that their composites were exhibiting a noticeable viscoplastic strain or permanent set in the recovery data. Their approach was simply to subtract the permanent set from the recovery data and then conduct the data reduction on corrected data (it should be noted that their creep and recovery tests were conducted below T_g of the epoxy where plastic strains are often negligible and as a result this method had reasonable success for them). Tuttle and Brinson also developed a numerical iteration scheme to predict creep strains using classical lamination theory (CLT) which was later adopted by Tuttle, Pasricha, and Emery [54].

Until then a power law was used to model the transient compliance in Schapery's model as suggested by Findley, Onaran, and Lai [44-46] and experimentally observed in creep data. However, Gramoll, Dillard, and Brinson [47, 48] and Cysz and Szyszkowski

[49] demonstrated that the power law kernel required laborious calculations of the hereditary integral and suffered from stability issues. As a result Xiao [50] used a modified power law in his analysis and Tuttle, Pasricha, and Emery [54, 55] adopted a Prony series kernel (a generalized Kelvin – Voigt series for a viscoelastic solid) which is used today by most researchers.

To our knowledge the first data reduction to combine time-temperature with time-stress superposition principles (TTSP with TSSP) successfully was performed by Peretz and Weitsman [59, 60] on FM-73 adhesive. Tuttle, Pasricha, and Emery also utilized the TTSSP on unidirectional graphite fiber-epoxy composites and incorporated a viscoplastic component after Zapas and Crissman [63, 64] and used the model to predict cyclic, thermo-mechanical loading. Both of these studies were limited in scope because the analysis and resulting success of the approach to TTSSP was limited to the glassy region of the polymer matrix. Also, to our knowledge the only other study to examine the nonlinear viscoelastic behavior of composites in the vicinity of and above T_g was performed by Xiao [65]; however, severe nonlinearity in his composite kept him from employing a full Schapery-type analysis. Xiao was able to conclude that his stress shift factor, a_σ, had a clear temperature dependence (His approach to modeling the stress and temperature dependence of a given nonlinear parameter was used in the present data reduction). More recently Guedes, Morais, Marques, and Cardon [57] have incorporated the Zapas – Crissman viscoplastic component into an iterative scheme to predict creep strains for the estimation of residual life under multiple types of viscoelastic loading.

In the current study a combined time-temperature and time-stress superposition (TTSSP) within an accelerated characterization scheme is employed to describe nonlinear viscoelastic behavior with elevated temperature and stress. The TTSSP provides a solid framework in which to describe a wide range of nonlinear viscoelastic responses. However, while performing creep testing a sizable viscoplastic deformation or permanent set was consistently observed in the recovery data becoming large in the leathery region (in the vicinity of T_g of the polymer matrix). A viscoplastic strain component was included and a variation of the Zapas - Crissman model was adopted into the modeling effort. The polymer matrix is understood to be the main source of the viscoelastic, viscoplastic response of a polymer matrix composite especially in a non-fiber reinforced direction. Since Vetrotex 324 is woven roving with two directions of fiber reinforcement, the characterization focused on the shear response through T_g as a main source of the viscoelastic behavior. A decision was made to characterize the shear creep response and assume the warp and weft direction properties were time, temperature, and stress independent.

A full thermo-viscoelastic, viscoplastic characterization of Vetrotex 324/Derakane 510A – 40 was conducted over a broad temperature range meant to exceed T_g of the polymer matrix by 50°C. Short term creep/creep recovery tests were performed at elevated stress levels at each temperature up to 50% of the ultimate strength at that particular temperature so as to avoid rupture of the coupon or gage/adhesive failure. A detailed data reduction was carried out focusing on identifying the nature of the nonlinear response with increasing temperature and stress. Particular attention was paid to the glassy, leathery, and rubbery regions in the temperature response. Difficulties and inconsistencies in the data are identified along with their effect on the versatility and viability of the data reduction. At the very least the data reduction must accurately model both stress and temperature master-curve responses in shear. A more detailed discussion of the analytical modeling expressions utilized in the data reduction, the results, and a detailed discussion of the modeling performance follow in this manuscript.

2.3 Analytical and Constitutive Modeling

2.3.1 Accelerated Characterization

The idea of accelerated characterization is the use of short term test data in the modeling of long term properties. It has been observed that certain factors such as elevating the temperature or stress level have the effect of accelerating the viscoelastic process and contracting the time scale over which the viscoelastic phenomenon takes place. The time-temperature superposition principle (TTSP) postulates that for short term, linear creep data, successive horizontal shifts in the time scale are enough to form a smooth master-curve. These master-curves give satisfactory representations of the material properties over long times and are useful for analytical and constitutive modeling. Figure 6 illustrates some of our temperature master-curves that were formed by this process. It is important to note here that, even for linear creep data, some vertical shifting (that is a_G) may be required. For our work vertical shifting was required for the rubbery region temperatures (140°C to 170°C) but was not found to have any particular temperature dependence; vertical shifting was used only because it was necessary to form a smooth master-curve.

An accelerated characterization technique which addresses the effects of elevating the stress levels was developed by Schapery [36, 85] and has been successfully used by numerous authors [37, 41, 42, 50, 59]. Schapery's isothermal, nonlinear, viscoelastic hereditary integral is derived from concepts of irreversible thermodynamics and has been successfully combined with the TTSP by Xiao [65], Tuttle, Pasricha, and Emery [54], and Peretz and Weitzman [60]. Unlike TTSP (which is a linear theory), Schapery's theory requires the use of vertical shifting in the characterization of the viscoelastic nonlinearity; nonlinearity that may also utilize both creep and creep recovery data in determination of the parameters. As in the TTSP the Schapery theory allows for the construction of stress master-curves giving a long term representation of the behavior of the material subject to isothermal conditions at constant stress. Figure 7 illustrates the stress master-curve at 90°C. These two theories combined provide a good framework for characterizing the thermo-viscoelastic behavior of many polymer matrix composites.

A crucial part of the accelerated characterization framework is the accurate determination of the temperature and stress shift factors. Typically, linear creep data is assembled from short term creep tests and shifted horizontally (in the time scale) to form a master-curve. If the linear data is strongly consistent and proportional without a lot a variation or scatter, a master-curve of the linear data will yield the temperature shift factor, a_T. The stress shift factor is defined as one for linear creep data and determined later on from nonlinear creep data. The "linear" data in this study showed a fair amount of variation and there was no linear data found above 110°C ($T_g \approx 105$°C); therefore, a low stress, reference master-curve was constructed using linear data up to 110°C, and the lowest stress level tested in the leathery and rubbery regions. The stress shift factor was defined to be one for the tests composing the master-curve and the temperature shift factor found from the horizontal shifts. The temperature dependence of the temperature shift factor is well documented in the literature [86]. The temperature shift factor followed an Arrhenius type dependence up to T_g and a Williams – Landell – Ferry dependence above T_g as illustrated in Figure 8.

2.3.2 The Data Reduction

As a result of the lack of strongly consistent linear creep data, the linear creep analysis was replaced by an analysis at a reference stress level. A reference stress of 50 psi (345 kPa) was selected because it was the lowest stress level tested at temperatures greater than 110°C. A reference stress master-curve was constructed by combining these tests with linear stress tests below 110°C (as a result 110°C was chosen as the reference temperature). For this master-curve all the nonlinear parameters of the Schapery model were defined to be one. The creep compliance was modeled from this master-curve data using a one term per decade generalized Kelvin - Voigt series,

$$
\begin{aligned}
S(\psi(t,T),\sigma_{\mathrm{Ref}}) &= S_0(\sigma_{\mathrm{Ref}}) + \sum_{k=1}^{m} S_k(\sigma_{\mathrm{Ref}})\left(1 - e^{-\psi(t,T)/\tau_k}\right) \\
\psi(t,T) &= \int_{0^-}^{t} \frac{d\xi}{a_T(T)}
\end{aligned}
\tag{1}
$$

Note that required temperature shift, a_T, and some vertical shifts, a_G, have already been accounted for in the formation of the reference master-curve; therefore, S_0 and S_k represent the reference stress compliance coefficients over the entire temperature range.

As mentioned previously, while conducting the short term creep tests a significant permanent set or viscoplastic strain was observed in the recovery data especially in the leathery temperature region. Also, application of the linear viscoelastic expressions for creep and creep recovery,

$$
\begin{aligned}
S_{\text{creep}}(t,T,\sigma_{\text{Ref}}) &= S_0(\sigma_{\text{Ref}}) + \frac{1}{a_G(T)}\sum_{k=1}^{m} S_k(\sigma_{\text{Ref}})\left(1-e^{-t/a_T(T)\tau_k}\right) \\
S_{\text{recovery}}(t,T,\sigma_{\text{Ref}}) &= \frac{1}{a_G(T)}\sum_{k=1}^{m} S_k(\sigma_{\text{Ref}})\left(1-e^{-t_1/a_T(T)\tau_k}\right)e^{-(t-t_1)/a_T(T)\tau_k}
\end{aligned} \tag{2}
$$

did not adequately describe the linear data well. Figure 9 demonstrates that an excellent fit to the creep data yielded an over prediction for the corresponding recovery data and an excellent fit to recovery data would under predict the corresponding creep data. It was surmised that some kind of damage was occurring during the creep cycle that was resulting in a “flatter” than expected recovery and a permanent set. Equation (2) required the addition of a viscoplastic term to account for the observed permanent sets.

Tuttle, Pasricha, and Emery [54] and Guedes, Morais, Marques, and Cardon [57], have all successfully included a viscoplastic functional model known as the Zapas – Crissman model. A derivation of this model is given in [63] and its application to a viscoelastic, viscoplastic analysis in [54]. The model adds a viscoplastic strain to the elastic and viscoelastic strains in the form of a power law in stress and time,

$$
\varepsilon_{\text{VP}}(t,T,\sigma) = \left\{C(T)\sigma^{N(T)}t\right\}^{n(\sigma,T)} \tag{3}
$$

The viscoplastic parameters, C, N, and n, are found from fits to viscoplastic strain versus stress and creep data. According to their definitions, the parameters C and N should be stress independent but temperature dependent (refer to [54] for a detailed derivation of Eq. (3)); however, depending on how the time dependence of the viscoplastic strain is determined, n could be stress and temperature dependent. Figure 10 illustrates the stress dependence of the viscoplastic strain over all temperatures tested and demonstrates that a power law dependence on the creep stress is a good assumption.

The time dependence in the Zapas – Crissman model was a source of difficulties during the data reduction. The previous recommendation for its estimation from Tuttle, Pasricha, and Emery was that *n* was a "linear" parameter, only a function of temperature, and determined from fits to linear creep data and then fixed for subsequent fits to nonlinear data. This interpretation was not viable for this data reduction considering the way in which we determined the compliance coefficients. Determining *n* according to Tuttle, Pasricha, and Emery essentially reduces *n* to a parameter that allows for a better fit to experimental creep data than a Prony series kernel alone. Although this method gives better fits, it strips *n* of any possible physical significance it may have as a key parameter in a rate process for the viscoplastic permanent set versus time (see Fig. 6). Also, we regard the parameters of the Zapas – Crissman model to be decidedly nonlinear and believe that all the data should be involved in their estimation, not just the linear data.

Ideally, the viscoelastic and viscoplastic parameters should be determined from separate fit analyses so as to reduce a negative interdependence of the parameters when the data is fit. For example, for a given fit to creep data, parameter *n* changes the shape of the fit model to better fit the data and thus the corresponding value of a_σ. As a verification step, creep tests were performed at constant temperature and stress for different durations (short to long creep cycles) and the viscoplastic strain plotted versus time. Figure 11 shows the results of this for 150°C and 200 psi (1.38 MPa) in which we find that the power law assumption is reasonably good but that the value of *n* obtained is half the value of the average obtained for *n* when it is fit to all the 150°C elevated stress creep tests. Due to time and material limitations and a necessity to improve our data fits, we decided to determine n by fitting to all creep tests in the leathery and rubbery region and to accept any possible influences of the value of n on the value of a_σ.

The elevated stress analysis was performed at each temperature through the use of the Schapery nonlinear, viscoelastic hereditary integral [85] for a uniaxial loading,

$$\varepsilon(t,\sigma) = g_0(\sigma)S_0 + g_1(\sigma)\int_{0^-}^{t} \Delta S(\psi - \psi') \frac{d(g_2(\sigma)\sigma)}{d\tau} d\tau \tag{4}$$

The viscoelastic strain depends on both the stress history $\sigma(\tau)$ and the accelerating factors of elevated temperature and stress through the shift factors in the reduced time expressions.

$$\psi = \psi(t,T,\sigma) = \int_{0^-}^{t} \frac{d\xi}{a_T(T)a_\sigma(\sigma)} \qquad \psi' = \psi'(\tau,T,\sigma) = \int_{0^-}^{\tau} \frac{d\xi'}{a_T(T)a_\sigma(\sigma)} \tag{5}$$

Together the nonlinear parameters of the Schapery model a_σ, g_0, g_1 and g_2 represent horizontal and vertical shifts of the reference creep data which are often both required for an accurate fit to nonlinear creep data. It is important to note here that ***not all*** of the vertical shifting parameters may be required to describe the nonlinearity in stress.

For an applied creep loading, a Prony series kernel representing the transient compliance, and the addition of a viscoplastic component, Eq. (4) yields expressions for the nonlinear creep and creep recovery compliances,

$$
\begin{aligned}
S_{\text{creep}}(t,T,\sigma) &= g_0(T,\sigma)S_0(\sigma_{\text{Ref}})\ldots \\
&\quad + \frac{g_1(T,\sigma)g_2(T,\sigma)}{a_G(T)}\sum_{k=1}^{m} S_k(\sigma_{\text{Ref}})(1-e^{-t/a_\sigma(T,\sigma)a_T(T)\tau_k})\ldots \\
&\quad + C^n(T)\sigma^{N(T)\cdot\bar{n}(T)-1}t^{\bar{n}(T)} \\
S_{\text{recovery}}(t,T,\sigma) &= \frac{g_2(T,\sigma)}{a_G(T)}\sum_{k=1}^{m} S_k(\sigma_{\text{Ref}})(1-e^{-t_1/a_\sigma(T,\sigma)a_T(T)\tau_k})e^{-(t-t_1)/a_\sigma(T,\sigma)a_T(T)\tau_k} \\
&\quad + C^n(T)\sigma^{N(T)\cdot\bar{n}(T)-1}t_1^{\bar{n}(T)}
\end{aligned}
\tag{6}
$$

Note that the Schapery model parameters, g_0, g_1, g_2 and a_σ, are not only functions of stress but also, intuitively, functions of temperature and all of the Zapas – Crissman parameters are only functions of temperature with $\bar{n}$ as the average value of n at a particular temperature. Also, the data and resulting fits indicate that the viscoplastic component is only appreciable in the leathery to rubbery region (temperatures above 90°C). As a result the viscoplastic part of Eq. (6) is only used for temperatures of 110°C and greater.

Ultimately, we desire to include the effects of creep into the structural model for V324/ Derakane 510A – 40 subject to fire loading conditions. Since the composite laminate will be in a state of compressive creep rupture, our modeling approach emphasizes the accurate representation of the creep behavior, while ignoring the recovery behavior. This was both convenient and necessary considering the inconsistencies observed in the recovery data at all temperatures and stresses and in both creep and recovery data at temperatures above T_g (problems with the recovery data will be discussed in more detail below). Therefore, except for the viscoplastic analysis, we ignored our recovery data and set g_2 equal to unity across all temperatures and stresses. The expression for the creep compliance from Eq. (6) was then fit to each creep stress level over all the temperatures tested to determine the non-liner parameters.

2.3.3 The Constitutive Model

The constitutive model for the inclusion of creep into the structural response of Vetrotex 324/Derakane 510A – 40 subject to fire loading conditions is presented in this manuscript with the goal of predicting creep strains under conditions of changing temperature and stress. The framework of the time-temperature and time-stress (Schapery) superposition principles together with an estimation of the viscoplastic strain was sufficient to model these strains.

This methodology is identical to that presented in other papers such as Guedes, Morais, Marques, and Cardon [57], Tuttle, Pasricha, and Emery [54] and Tuttle, Mescher, and Potocki [87] will be briefly presented here. Vetrotex 324 is a woven roving and our macro-mechanical approach considers each weave to be a layer subject to the following total strain given a stress history *σ(t)*,

$$\begin{Bmatrix} \varepsilon_{11}(t) \\ \varepsilon_{22}(t) \\ \gamma_{12}(t) \end{Bmatrix} = \begin{bmatrix} S_{11} & S_{12} & 0 \\ S_{12} & S_{22} & 0 \\ 0 & 0 & S_{66}(t) \end{bmatrix} \begin{Bmatrix} \sigma_{11}(t) \\ \sigma_{22}(t) \\ \tau_{12}(t) \end{Bmatrix}_{\mathrm{EL+VE}} + \begin{Bmatrix} 0 \\ 0 \\ \gamma_{12}(t) \end{Bmatrix}_{\mathrm{VP}} \tag{7}$$

Here we have assumed that the only time dependent compliance term is the matrix dominated shear compliance S_{66}; the fiber dominated terms S_{11}, S_{12}, and S_{22} are assumed to be time independent. The strains induced by the arbitrary stress history can be further reduced to elastic, viscoelastic, and viscoplastic strains,

$$
\begin{Bmatrix} \varepsilon_{11}(t) \\ \varepsilon_{22}(t) \\ \gamma_{12}(t,T,\sigma) \end{Bmatrix}_{\text{Creep}} = \begin{bmatrix} S_{11} & S_{12} & 0 \\ S_{12} & S_{22} & 0 \\ 0 & 0 & g_0^{66}(T,\sigma)S_0^{66}(\sigma_{\text{Ref}}) \end{bmatrix} \begin{Bmatrix} \sigma_{11}(t) \\ \sigma_{22}(t) \\ \tau_{12}(t) \end{Bmatrix}_{\text{EL}}
$$

$$
+ \begin{Bmatrix} 0 \\ 0 \\ g_1^{66}(T,\sigma)\int_{0^-}^{t} \Delta S_{66}(\psi-\psi')\frac{d}{d\tau}\left\{g_2^{66}(T,\sigma)\tau_{12}(\tau)\right\}d\tau \end{Bmatrix}_{\text{VE}} \tag{8}
$$

$$
+ \begin{Bmatrix} 0 \\ 0 \\ \left(C^{66}(T)\int_{0^-}^{t} \tau_{12}^{N^{66}(T)}(\tau)d\tau\right)^{n^{66}(T)} \end{Bmatrix}_{\text{VP}}
$$

In this equation the elastic, viscoelastic and viscoplastic components of the strain are represented by *EL*, *VE* and *VP*, respectively. This formulation, once all the viscoelastic, viscoplastic parameters are found, gives a sufficient constitutive model for estimating the creep strain for a given loading, temperature, and time.

2.4 Experimental

2.4.1 VARTM, Post-Cure, and Coupon Preparation

Vetrotrex 324 24 oz/yd E-glass woven roving was purchased in 200 lb rolls from St. Gobain and 5 gallon drums of Derakane 510A – 40 (38% styrene) were donated by the Dow Chemical Company. The composites were manufactured at Virginia Tech using a simple vacuum assisted resin transfer method (VARTM) set-up. A chemical cure package of 1% (per total resin volume) organic peroxide (Crompton's HI-Point 90) and 0.108% Cobalt Naphthenate catalyst was used (it should be noted that this cure package was eventually changed because of a preponderance of dry fibers in the panels, but that change did not affect this study).

The post-cure procedure for this room-temperature cured system was divided into three stages. The first post-cure was a 2°C/min ramp to 130°C followed by a 2 hour hold and then gradual cool-down. This first post-cure removed much of the remaining styrene gas from the composite panels. After this, the $[\pm 45°]_{2S}$ panels were cut up in to 9 in by 1 in (22.9 cm by 2.5 cm) coupons and prepared for gaging. Measurements Group CEA-06-500UW-350 gages were used for their durability over a wide temperature range and a grid size of 500 mil (12.7 mm) allowed for global strain measurement across the 0.25" (6.35 mm) tows of the Vetrotex 324 woven roving. These gages were mounted longitudinally and transversely back-to-back on each coupon to correct for both bending and temperature using M-Bond 610 adhesive. The 610 is an elevated cure adhesive so the coupons were clamped up and post-cured a second time with a 10°C/min ramp to 130°C followed by a 2 hour hold and gradual cool down. A final post-cure was performed to remove any remaining stress history and straighten the coupons after clamping by placing the coupons between weighted glass and heating with a 10°C/min ramp to 200°C followed by a 2 hour hold and gradual cool down. For some tests, the expected strain exceeded the abilities of the CEA gage/610 adhesive system and EP-06-500AE-350 gages with AE-15 adhesive were used instead.

2.4.2 Experimental Set-up

All creep tests were performed on three separate tension lever arm creep frames each equipped with an oven. The lever arm frames were usually tested simultaneously from a central data acquisition system using Measurements Group 2310 strain amps together with National Instrument's 2080 BNC board, a DAQ card and acquisition software. Creep loading was applied through single acting Bimba pneumatic cylinders controlled by solenoid valves so that loading was accomplished within 2 to 7 seconds. The K-type thermocouples that controlled the heating of all three of the ovens were calibrated to within 1-2°C of each other and temperature control was maintained to within ±1°C of the set temperature by Omega CN76000 series temperature controllers. The coupon set temperatures were acquired by taping the thermocouples to the coupons with Measurements Group MJG-2 Mylar tape; the temperatures were independently monitored with Omega HH-21 series digital thermometers.

2.4.3 Material Properties

The material properties and modeling parameters were found from an extensive test matrix of the shear coupons extending over nine temperatures (30, 60, and 90°C – Glassy; 110, 120, and 130°C – Leathery; 140, 150, and 170°C - Rubbery) and low to high stress levels. Tests were conducted to the highest possible stress while avoiding rupture during the creep cycle for the temperature and collection of reliable data given the limitations of the gage/gage adhesive. In the glassy region our test stress went to 5000 psi (34.47 MPa), in the leathery region to 1500 psi (10.34 MPa), and in the rubbery region only to 400 psi (2.76 MPa). The instantaneous response of the compliance given by the creep data was checked against quasi-static tensile tests which were performed at each of the creep testing temperatures. At least two to three tensile tests were done and the shear modulus was measured as function of temperature as presented in Fig. 7.

Because the testing matrix was so aggressive in terms of the number of stress and temperature combinations tested, it was not possible to repeat every test. Only 10% of the approximately 100 creep/creep recovery tests were repeated, mostly in the rubbery region. Of those repeated a ±10% variation was observed between replicate tests in the rubbery region and a ±5% variation in the glassy region (no attempt was made to combine replicate tests; each test was analyzed and fit to separately). A method of accelerated characterization involving short term creep/creep recovery tests balanced with the desire to have 2 – 3 decades worth of reliable creep data without risking rupture was implemented with a creep cycle of 120 minutes followed by 20 to 48 hours of recovery data. Figures 8 and 9 show typical creep and creep recovery data at 110°C.

2.5 Results, Discussion, and Parameter Modeling

2.5.1 Viscoelastic and Viscoplastic Parameter Modeling

As previously discussed, the parameters of Schapery's nonlinear viscoelastic hereditary integral and the viscoplastic Zapas – Crissman model were found through fits to creep data only (with g_2 set to unity). Again, our approach was to use only the number of nonlinear parameters which were needed to adequately describe the nonlinearity at each temperature. Determination of the parameters was more successful in the glassy region than in the leathery and rubbery region; in fact, the data reduction was very difficult to do in the rubbery region. In the glassy region (30 - 90°C), the nonlinearity in stress was best described through one vertical shift, g_0, and a horizontal shift, a_σ. At 110°C fits using g_0 and/or g_1 together with a_σ were not satisfactory until all vertical shifting was discarded and the Zapas – Crissman model applied. At temperatures of 110°C and greater, a vertical shift of g_1 (with g_0 set to one), a_σ and the Zapas – Crissman model adequately represented the creep data. Our approach to fitting the creep data was to balance the degree of the creep fit with how consistent in stress the nonlinear parameters were. We also made no assumptions about either the stress or temperature dependencies before fitting Eq. (6) to the creep data as other investigators have (Tuttle, Pasricha, and Emery [54] and Peretz and Weitsman [60])—we simply fit all data with respect to stress and then looked for trends in stress then in temperature.

The Schapery nonlinear parameters used were g_0, g_1, and a_σ. The parameters were found to obey the following expressions in stress,

$$
\begin{aligned}
g_0(T,\sigma) &= \begin{cases} 1 + a(T)e^{b(T)\left(\frac{\sigma}{\sigma_{\text{Ref}}}\right)} & 30^\circ\text{C} \le T \le 90^\circ\text{C} \\ 1 & T > 90^\circ\text{C} \end{cases} \\
g_1(T,\sigma) &= \begin{cases} 1 & T < 120^\circ\text{C} \\ 1 + a(T)e^{b(T)\left(\frac{\sigma}{\sigma_{\text{Ref}}}\right)} & T \ge 120^\circ\text{C} \end{cases} \\
a_\sigma(T,\sigma) &= a(T)e^{b(T)\left(\frac{\sigma}{\sigma_{\text{Ref}}}\right)} \qquad 30^\circ\text{C} \le T \le 170^\circ\text{C}
\end{aligned}
\tag{9}
$$

Here the generic temperature coefficients *a(T)* and *b(T)* were compared across the temperatures over which the stress expression was valid and were mostly found to be some type of exponential or piecewise linear in temperature.

The data fit points (results of the fits to individual creep data at each stress and temperature) and fits for the Schapery parameters are presented in Figs. 10 – 12. These figures demonstrate that there was not a distinct linear region versus a nonlinear region as demonstrated for other composites in the literature [37, 41, 42, 50, 59]. These expressions are valid for all the stresses fit at a particular temperature and are only one for the reference stress. This distinction in our analysis is probably due to two causes; our linear data was not strongly consistent (we observed only mild proportionality at lower temperatures and stresses) and there was a consistency problem with the recovery data at all temperatures and stresses. The recovery data were found to be nonlinear in stress regardless the temperature and stress level and were inconsistent (as discussed above and in Fig. 4) with corresponding creep data. Although selection of the expressions in Eq. (9) is arbitrary, they are comparable to what other investigators have reported [42, 43, 50, 60].

The Zapas – Crissman model proved useful in the leathery to rubbery region and showed a strong temperature and stress dependence. As mentioned in a previous section, the power law assumptions on the viscoplastic strain versus temperature and stress proved to be good. First, a power law was fit to viscoplastic strain versus stress dependence of the form,

$$\varepsilon_{\mathrm{VP}}(\sigma) = \left(Ct_1\right)^n \sigma^{N \cdot n} \tag{10}$$

Second, parameter n was fit as a nonlinear parameter to each creep tests and showed no strong stress dependence but did show temperature dependence as illustrated in Fig. 13. At this point the parameters C^n and N could be found from the coefficient and exponent of the power law fits at each temperature (Eq. (10) with t_1 equal to the length of each creep cycle) and Figs. 14 and 15 illustrate this temperature dependence. Note here the spike at 120°C in the leathery region. The viscoelastic data showed the greatest permanent sets in the leathery region (temperatures of 110°C - 130°C). Also, the viscoplastic strain was relatively small in the glassy region and was neglected and moderately large in the rubbery region where its inclusion was the only way to achieve a good fit to the creep data. Expressions used to model the temperature dependence of the Zapas – Crissman parameters were also arbitrary and mostly either logarithmic or piecewise linear.

2.5.2 Stress and Temperature Master-Curve Modeling

The stress and temperature master-curve modeling were reasonable. Figures 2 and 16 show typical stress and temperature master-curves, respectively. The stress master-curve of Fig. 2 was created by shifting the fit model horizontally and taking out the vertical shifting to form a smooth curve; this was done automatically after fitting the elevated stress data at each temperature. The temperature master-curve of Fig. 16 was generated using Eq. (11) after the nonlinear parameters were accurately modeled as functions of temperature and stress.

$$
\begin{aligned}
S(t,T,\sigma) = {} & g_0(T,\sigma)S_0(\sigma_{\text{Ref}}) + g_1(T,\sigma)\sum_{k=1}^{m} S_k(\sigma_{\text{Ref}})\left(1 - e^{-t/a_T(T)a_\sigma(T,\sigma)\tau_k}\right) \\
& + C^n(T)\sigma^{N(T)\cdot\bar{n}(T)-1}t^{\bar{n}(T)}
\end{aligned}
\tag{11}
$$

There were four key points to consider when using the model Eq. (11) to generate master-curves. First, whatever code or software is chosen to do nonlinear least squares fitting will find g_0, g_1 and a_σ based on the nonlinear fit model; that is, the fitting algorithm is going to shift the fit model and *not* the data. This will result in a difference between the model and the data which should be small but will deviate from the experimental data. Second, the Zapas – Crissman model does not lend itself to master-curve modeling because the viscoplastic component is not a function of reduced time but of time. The Zapas – Crissman model simply does not shift as the viscoelastic model does and becomes unstable at longer times. As a result, the temperature and stress master-curve displayed in Figs. 2 and 16 were generated from Eq. (11) by ignoring the viscoplastic component. Third, another source of discontinuities was the intermittent temperature dependence of the some of the nonlinear and Zapas – Crissman parameters. At the temperatures of 90°C to 120°C g_0 gradually decreased to one, Zapas – Crissman went into effect at 110°C, and g_1 gradually increased from one. The discontinuous nature of these functions could not be avoided, but creating gently transitions from the value over the active region back to one did smooth out the kinks and discontinuities in the predicted temperature master-curves. Another issue with the temperature master-curves is the necessity of vertical shifting (that is a_G not g_1) in the rubbery region for the lower stress master-curves. As a result, we expect some differences between the modeling and our temperature master-curves and find this appropriate considering that the underlying data had a variation of ±10%. Figure 21 illustrates the model versus a temperature master-curve at 200 psi (1.38 MPa).

2.5.3 Observations on the Nonlinearity with Stress and Temperature

Several key observations were made regarding the nonlinearity of Vetrotrex 324/Derakane 510A – 40 during this study. The response of the composite was found to be very nonlinear with temperature. Above T_g, there were no linear stress levels and the statistical variation between replicate tests was approximately ±10%. Also, all the data obtained at 170°C was noticeably inconsistent with the other rubbery region temperatures. This is apparent when looking at the temperature and stress shift factor figures (Figs. 3 and 12) and the Zapas – Crissman model parameter figures (Figs. 13 - 15). As a result, a decision was made to exclude the 170°C data from the analysis. Given that our T_g was 105°C, our results suggest that it may be difficult to obtain reliable creep data at more than T_g + 50°C. High temperatures also affected the reliability of our strain gage readings. The CEA gage/610 system is rated to be reliable to ±5.5% shearing strain through temperatures of 175°C; however, the gages (especially the transverse gage) failed at approximately 3-4% shearing strain at temperatures greater than 130°C. This disappointing consequence kept us from reaching some of the stress levels in the leathery to rubbery regions that we desired.

The nonlinearity with stress was characterized as expected through the use of the Schapery nonlinear parameters. Most notable was the problem with the recovery data. All recovery data was nonlinear and "flatter" than expected. As mentioned previously, a good fit to creep data would always over-predict the corresponding recovery data. Even in the glassy region where lower stress creep data exhibited reasonable proportionality, the recovery data was noticeably stress dependent. The data reduction attempted to account for nonlinear viscoelastic and viscoplastic effects, but made no attempt to account for any damage that may have occurred during the creep cycle that would have altered the recovery behavior. Another limitation noticed in the glassy to leathery region was the stress limit imposed by the ductility of the composite. Tests conducted at stresses in the vicinity of yield for a given temperature gave unreliable data due to the high strains encountered and a risk of sudden rupture.

2.6 Conclusions and Future Research

An accelerated characterization method has been successfully applied to Vetrotex 324/Derakane 510A – 40. Creep tests were conducted at nine different temperatures up to and exceeding T_g and stress and temperature master-curves formed from the data. The time-temperature and time-stress (Schapery) superposition principles (TTSSP) have provided a flexible framework in which to characterize nonlinear viscoelastic behavior above T_g even when there is no distinct linear data. A viscoplastic functional model developed by Zapas and Crissman has been added to account for the profound viscoplastic behavior observed in the leathery to rubbery regions. The Zapas – Crissman model provides good modeling of the stress and time dependence of the viscoplastic strain.

Nonlinear behavior was observed in the viscoelastic response of V324/Derakane 510A – 40. The composite was noticeably nonlinear in the vicinity of and above T_g at all stress levels. Although there was some proportionality observed in the glassy to leathery region at low stress levels, there was no distinct “linear” region for the Schapery nonlinear parameters and the recovery data was nonlinear at all temperatures and stresses. The viscoplastic response was negligible in the glassy region but peaked in the leathery region (about T_g + 15°C - 25°C) and remained significant into the rubbery region. The nonlinearity was more pronounced at creep stress levels in the vicinity of yield for a given temperature. These stress levels produced a profound viscoelastic response and posed a risk of sudden rupture regardless of the temperature.

Modeling of the stress and temperature master-curves was reasonable. A main problem in the modeling was the power law form of the Zapas – Crissman model and how best to include its effect in the temperature and stress master-curve modeling. Although Zapas – Crissman is good for modeling individual tests, its power law form causes it to monotonically increase becoming unstable. Other functional forms are currently being investigated for the viscoplastic component that will not be so sensitive to variations in model parameters and be well behaved for short to long time periods.

Our continuing research objective is to incorporate creep phenomena into a structural model for the failure time prediction of a V324/Derakane 510A – 40 composite panels subject to fire loading conditions. We will accomplish this by coding into a finite element program the nonlinear viscoelastic and viscoplastic behavior as incremental functions of time, temperature, and stress.

2.7 Acknowledgements

The authors acknowledge the support of the Office of Naval Research Code 334, Award # N00014-04-1-0195. Additionally, the many helpful discussions with Dr. Soojae Park of IBM are gratefully acknowledged.

2.8 Figures

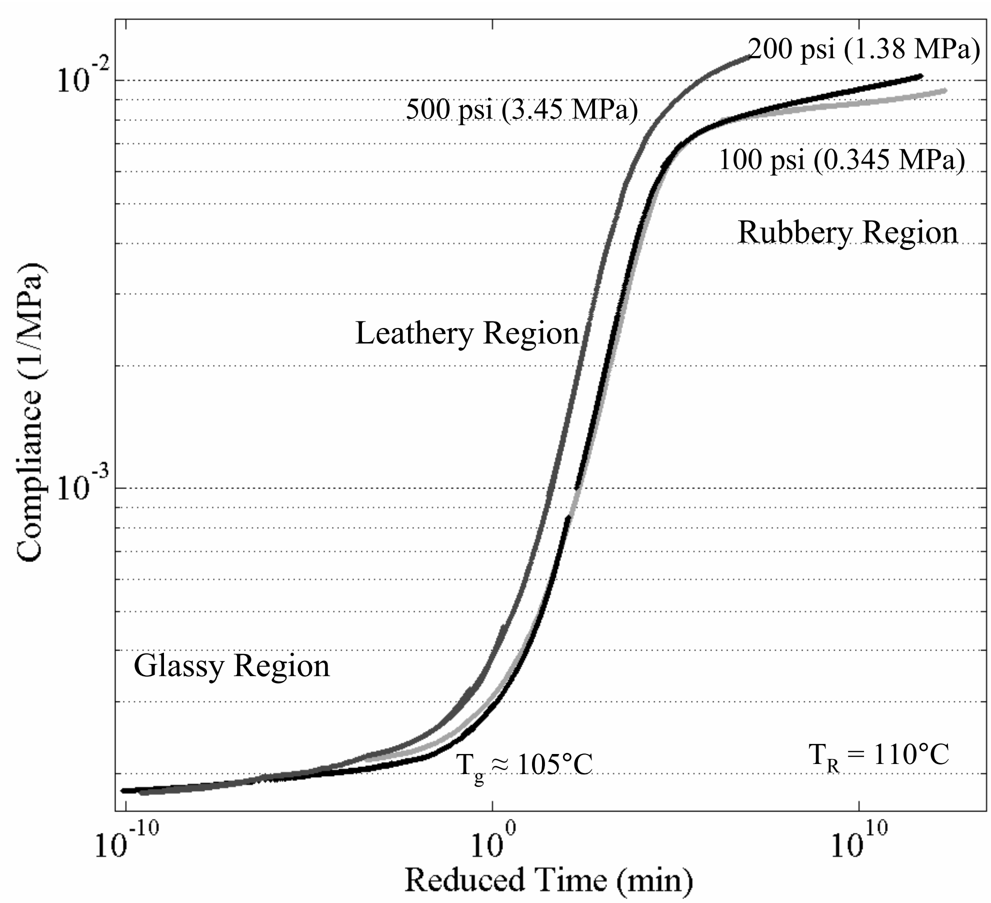

Figure 6: Typical temperature master-curves for V324/Derakane 510A – 40.

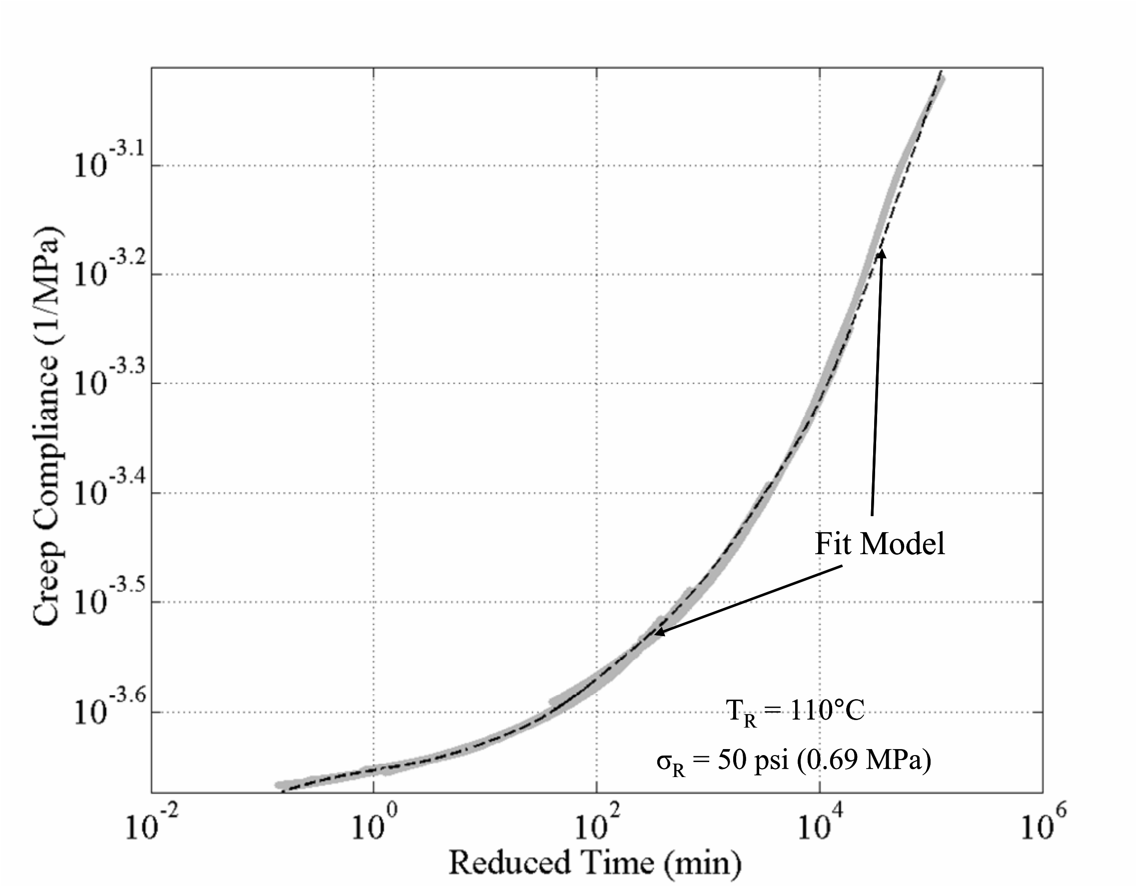

Figure 7: Stress master-curve at 90°C with fit model (dashed line).

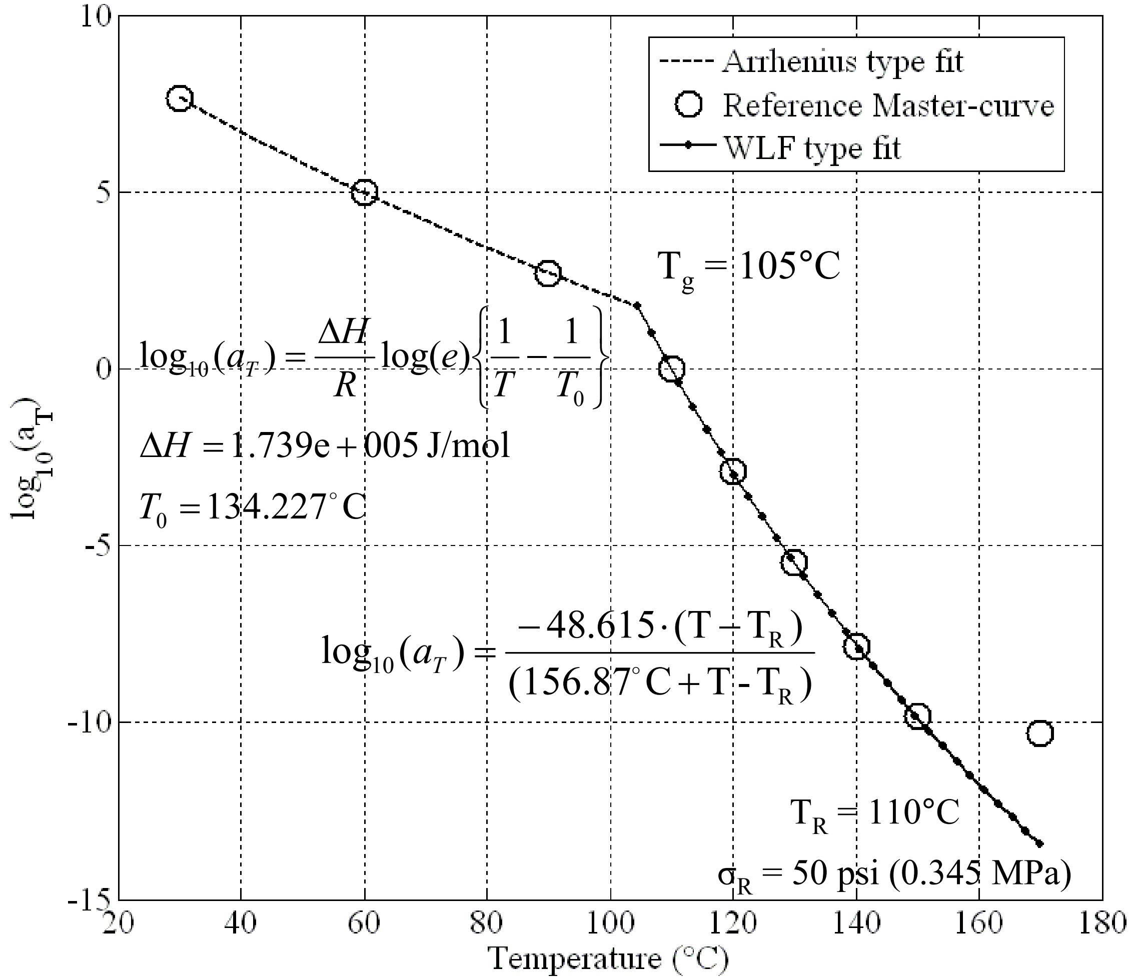

Figure 8: Temperature shift factor a_T for the reference master-curve.

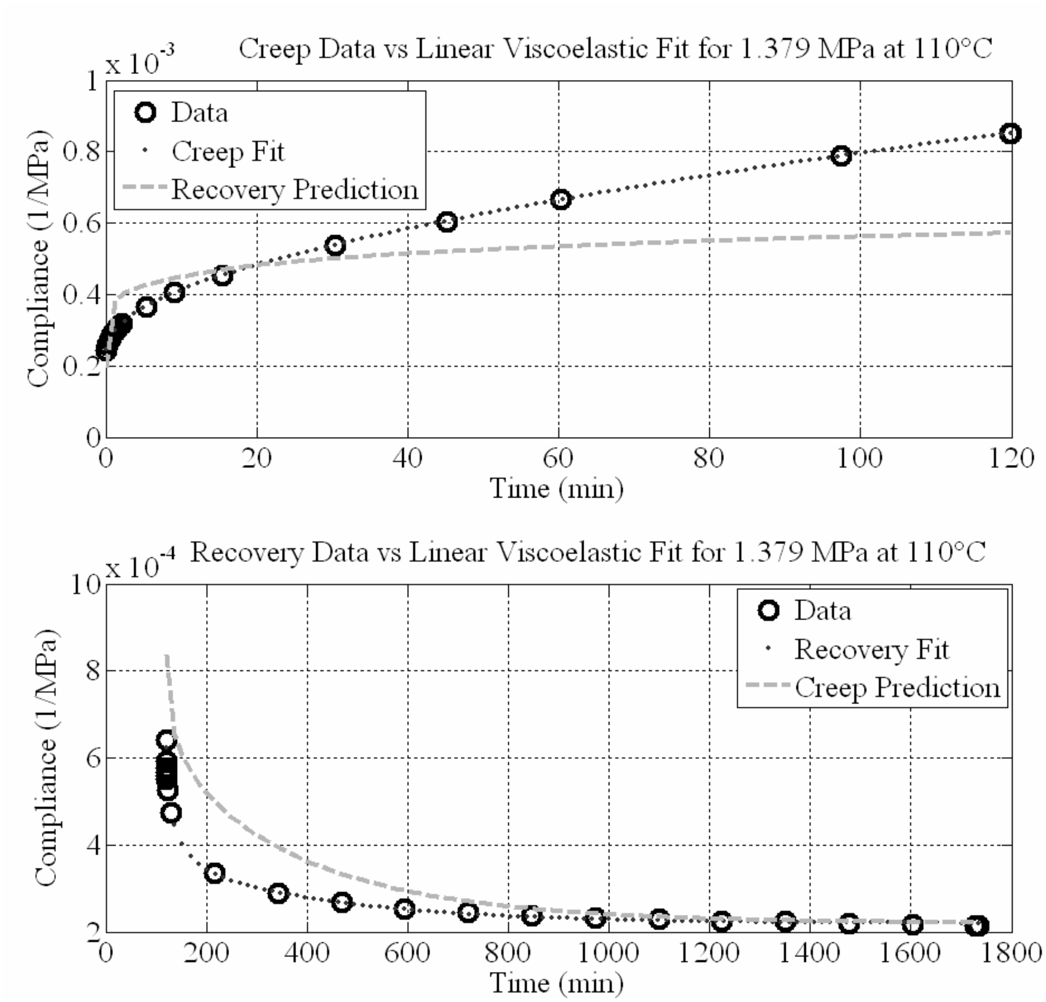

Figure 9: Low stress creep and creep recovery data at 110°C together with corresponding predictions from linear viscoelastic theory.

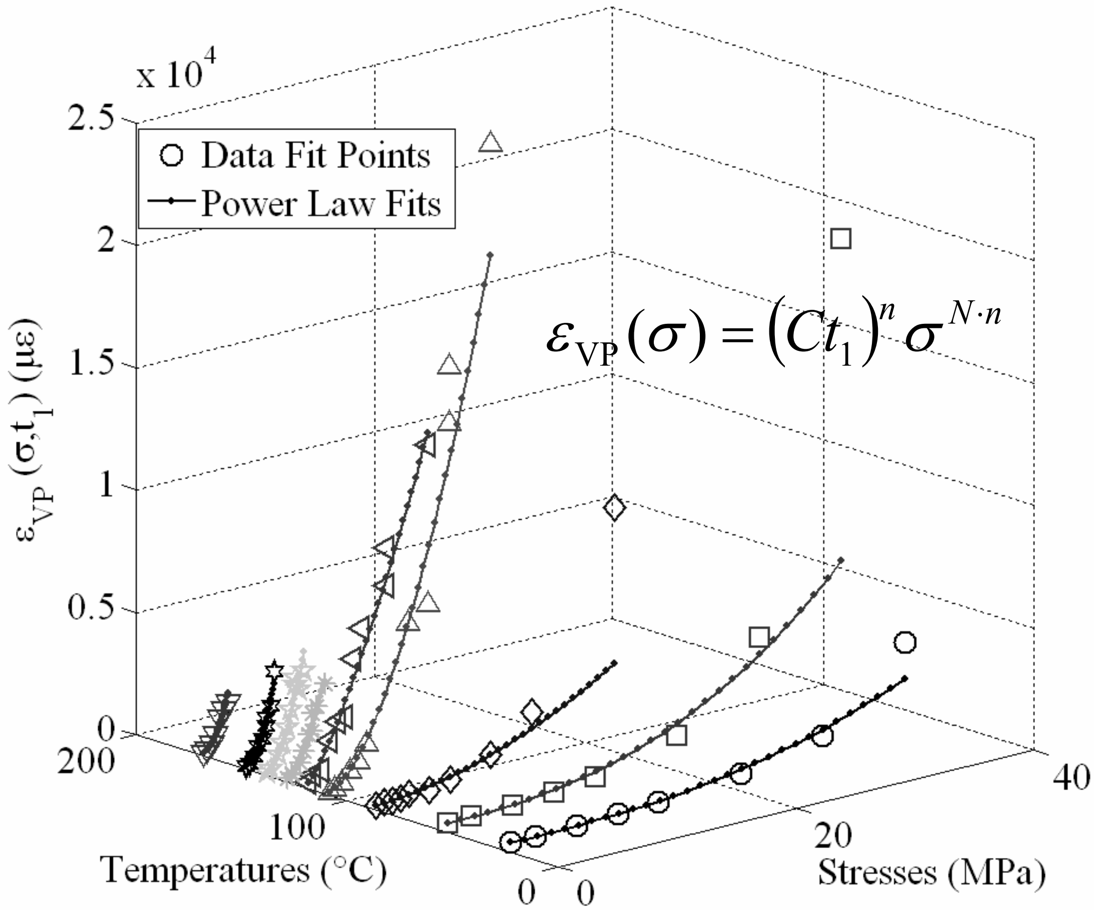

Figure 10: The viscoplastic permanent sets versus temperature and stress together with the power law predictions (Note the dramatic increase in the leathery and rubbery regions).

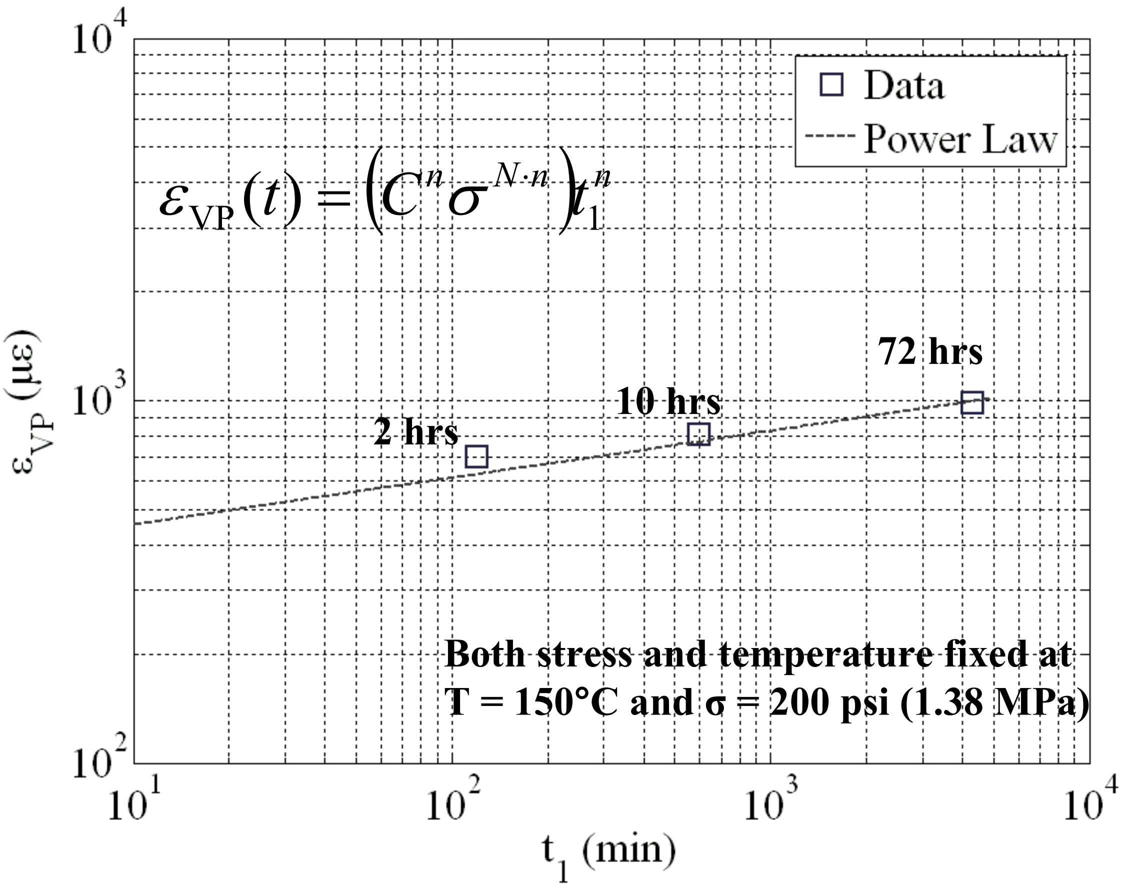

Figure 11: The viscoplastic permanent set versus varying creep times at 150°C and σ = 200 psi (1.38 MPa) (This fit is interdependent with the elevated stresses at t_1 = 120 min).

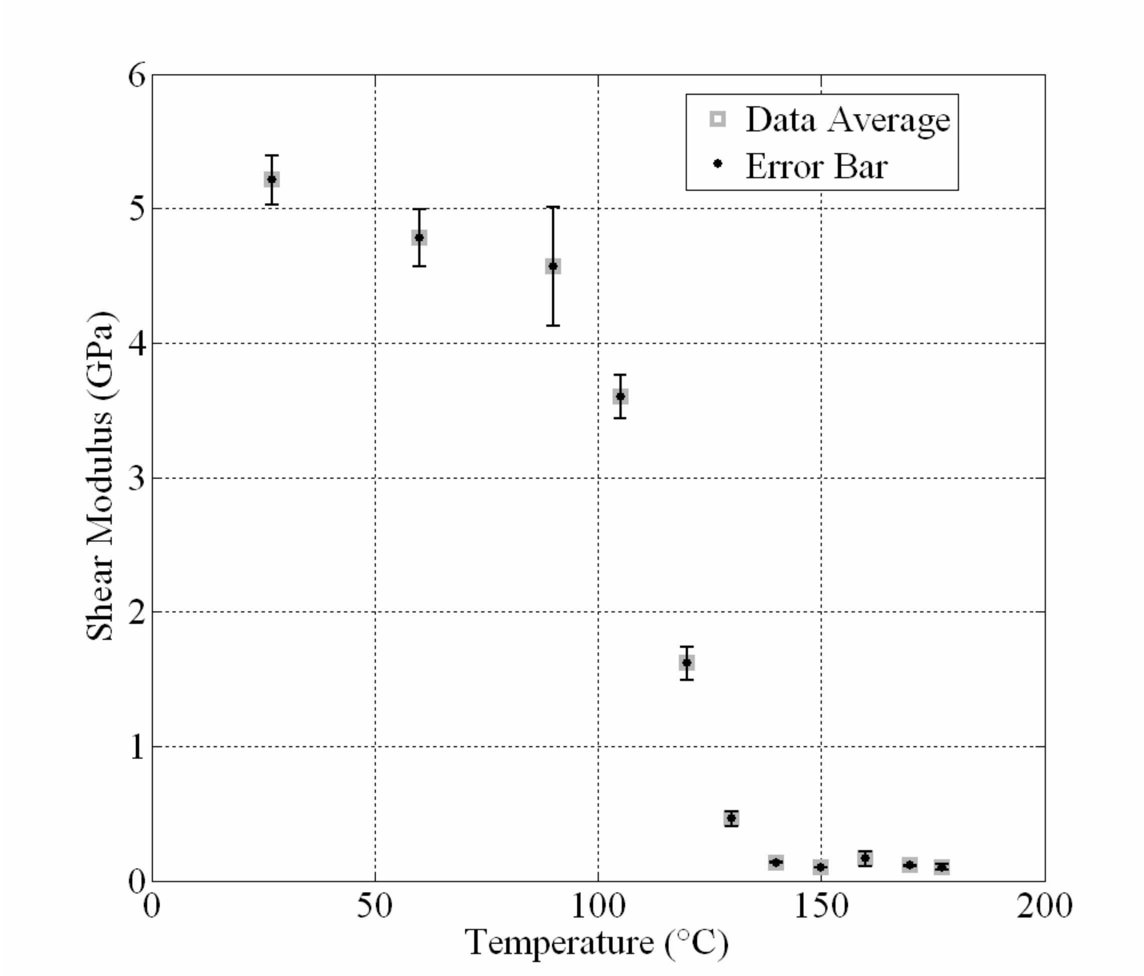

Figure 12: The shear modulus G_{12} versus temperature for V324/Derakane 510A – 40.

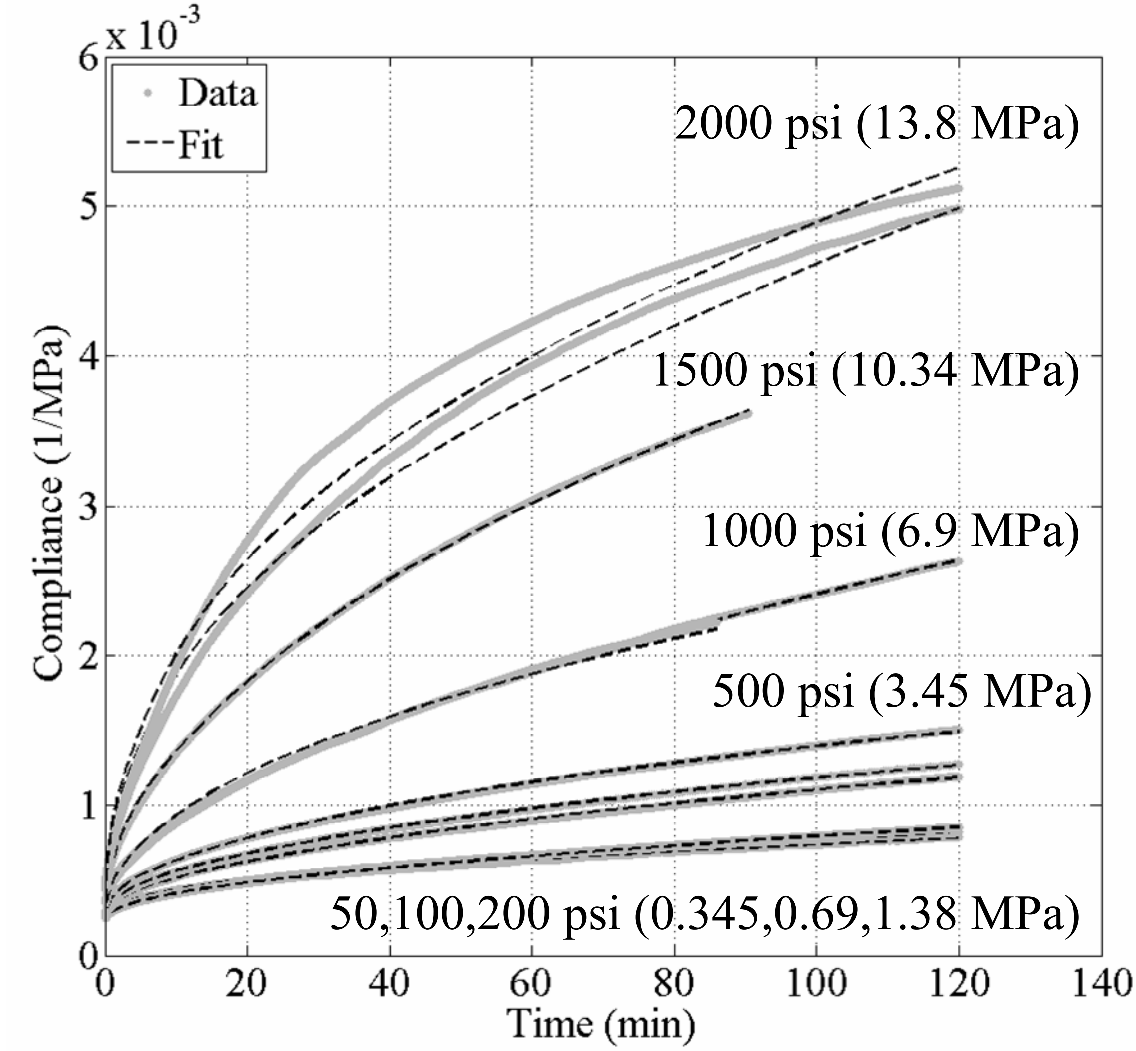

Figure 13: Typical creep data for 110°C (fit model is represented by the dashed lines).

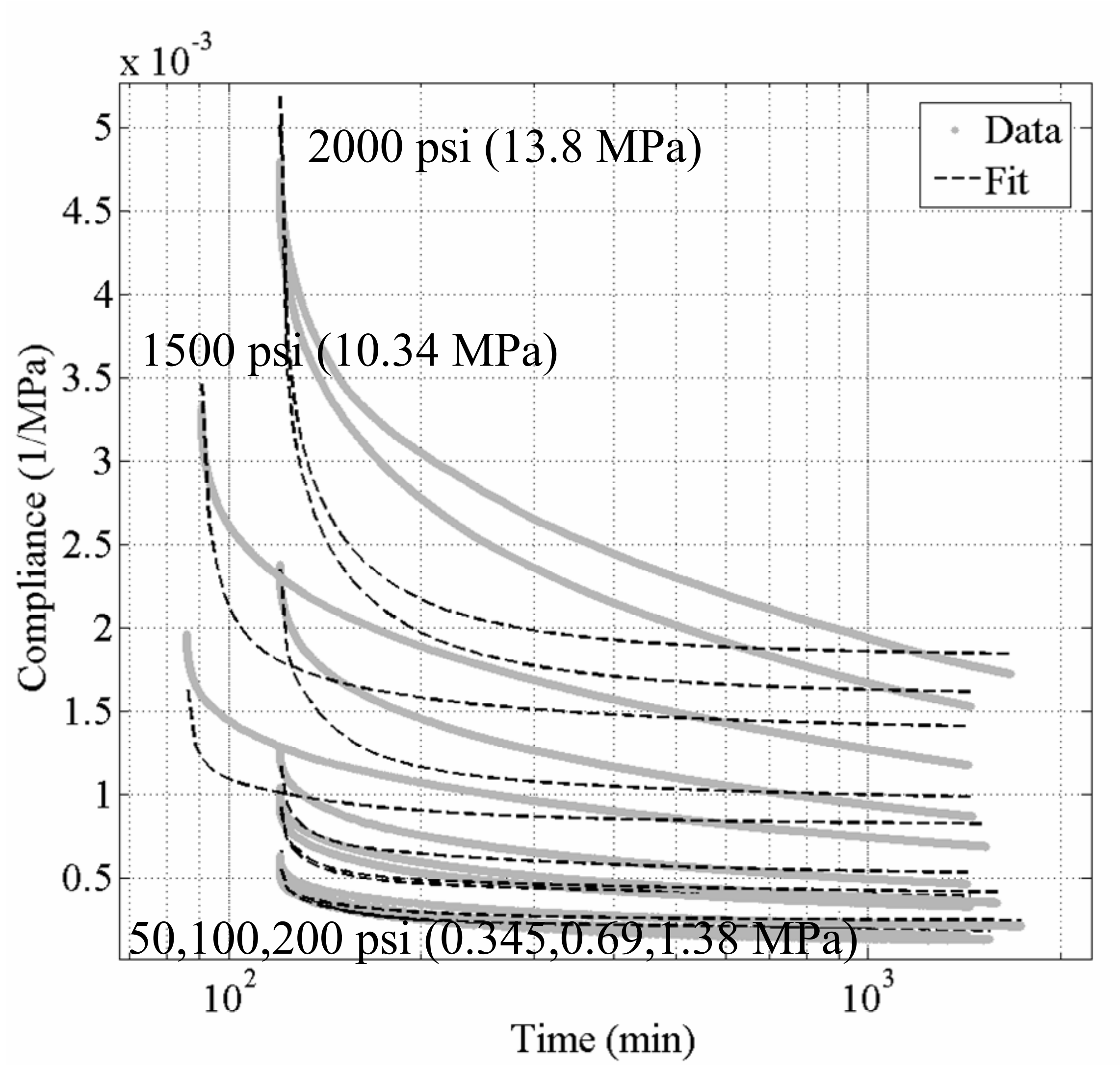

Figure 14: Typical recovery data at 110°C (fit model is represented by the dashed lines).

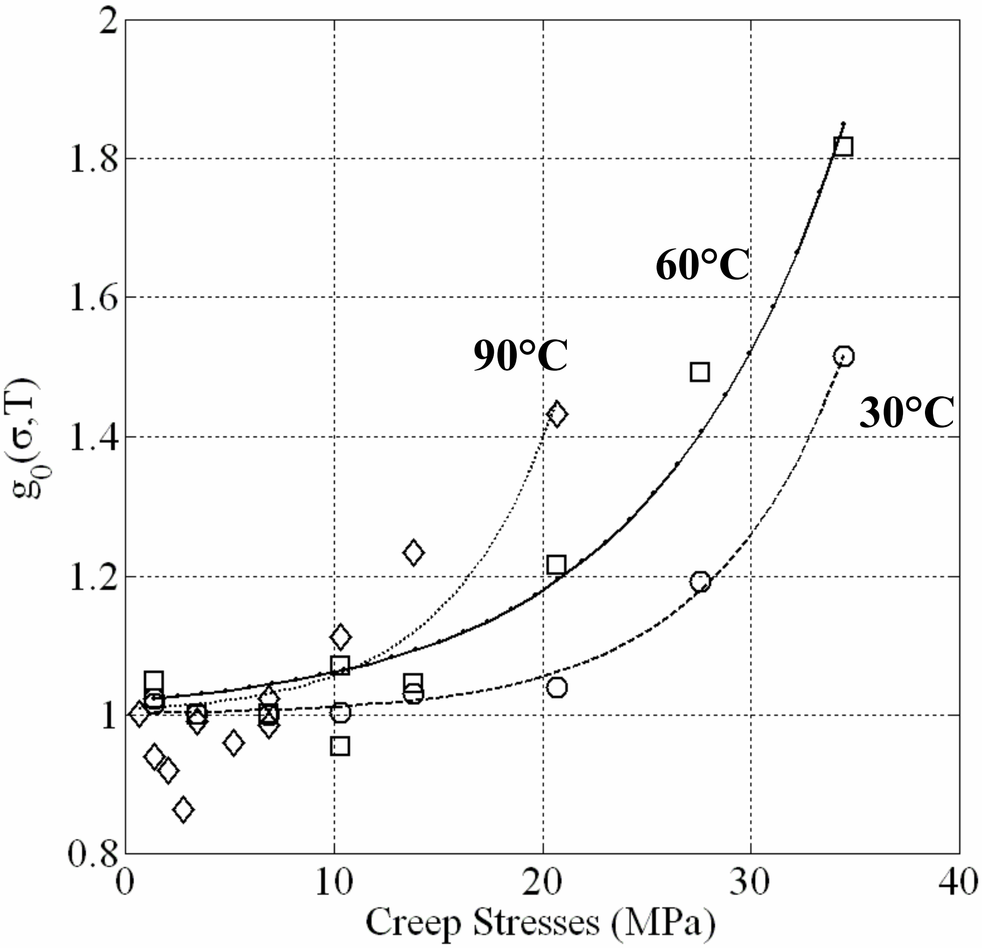

Figure 15: Schapery nonlinear parameter g_0 versus stress in the glassy region.

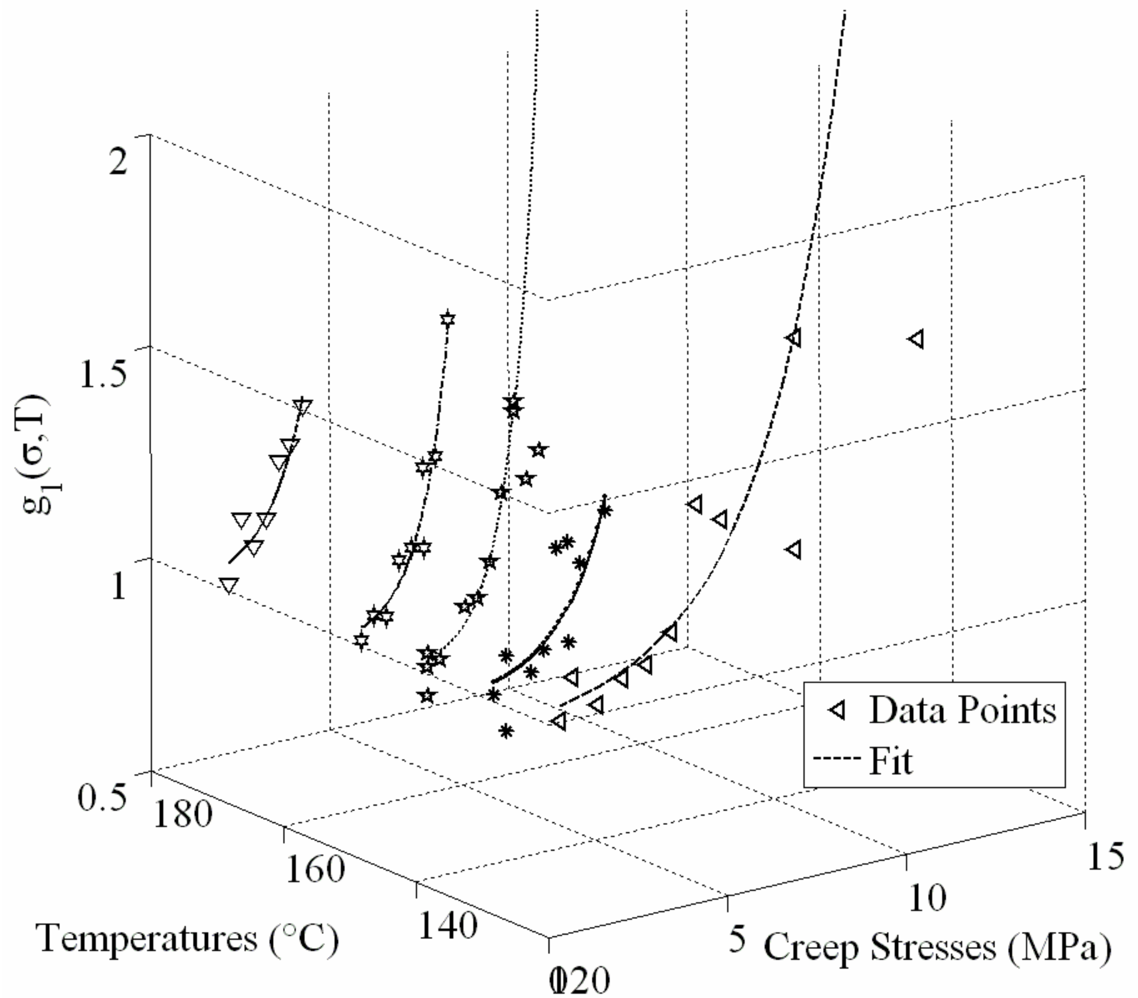

Figure 16: Schapery nonlinear parameter g_1 versus stress and temperature in the leathery to rubbery regions.

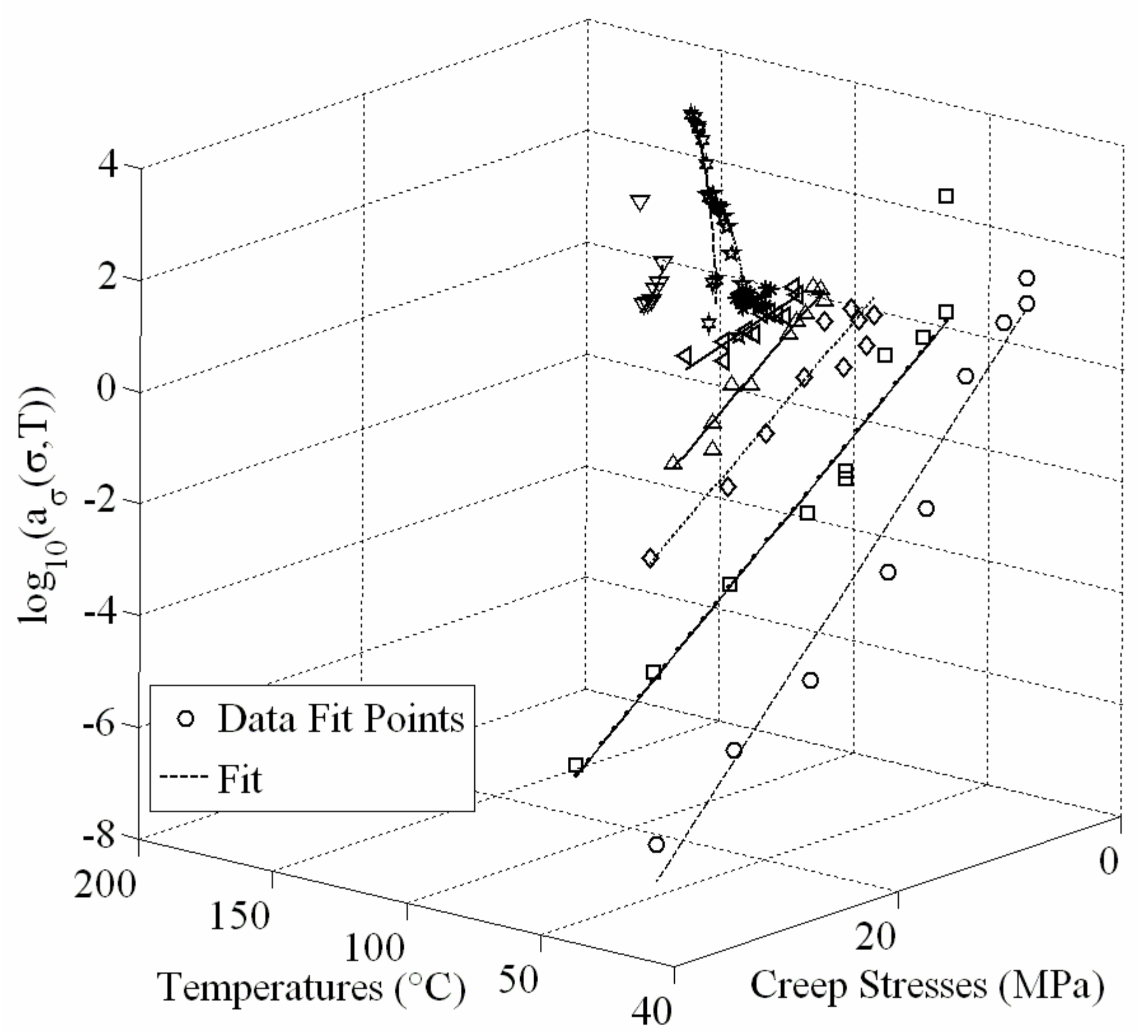

Figure 17: The stress shift factor a_σ versus stress and temperature.

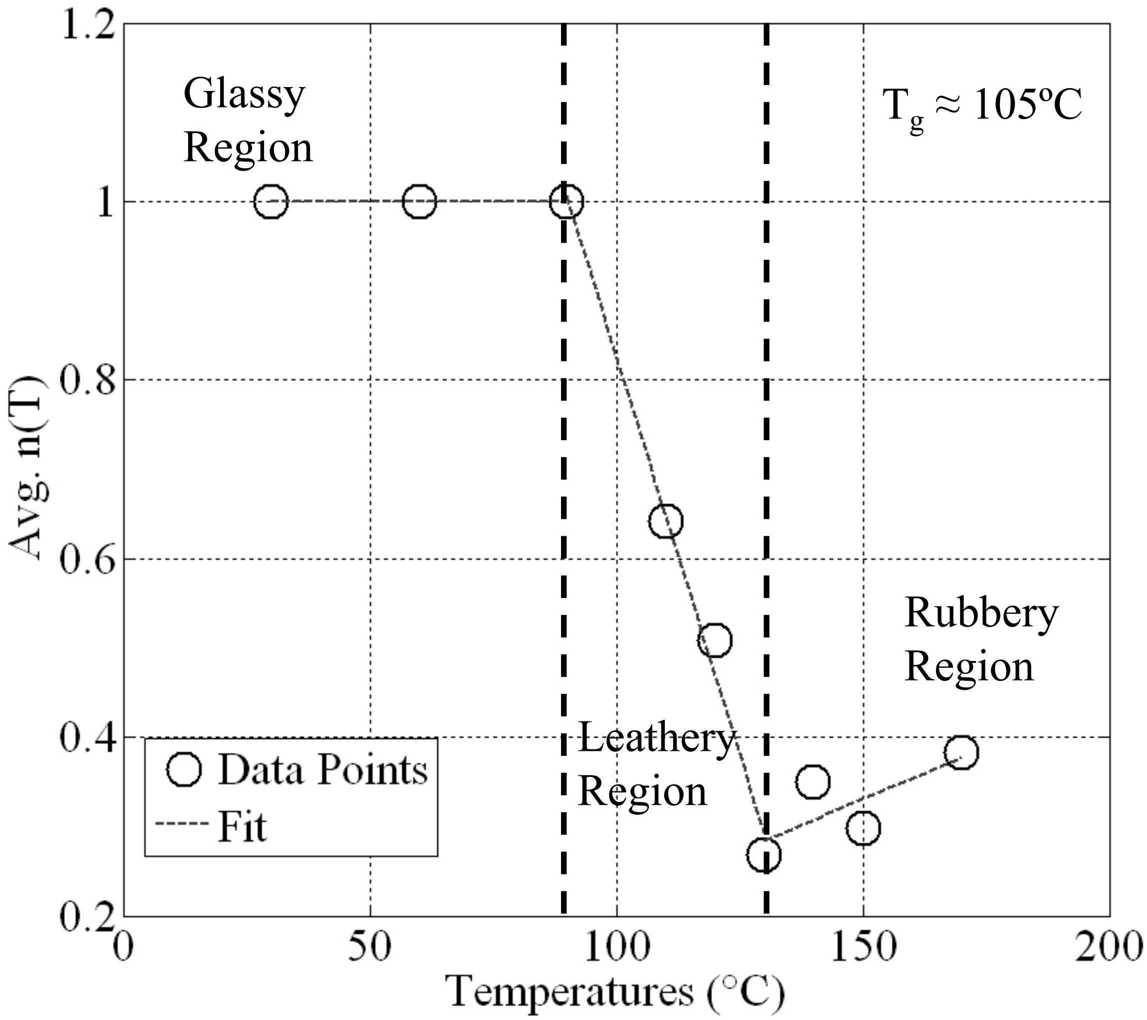

Figure 18: The average value of Zapas - Crissman parameter *n* versus temperature.

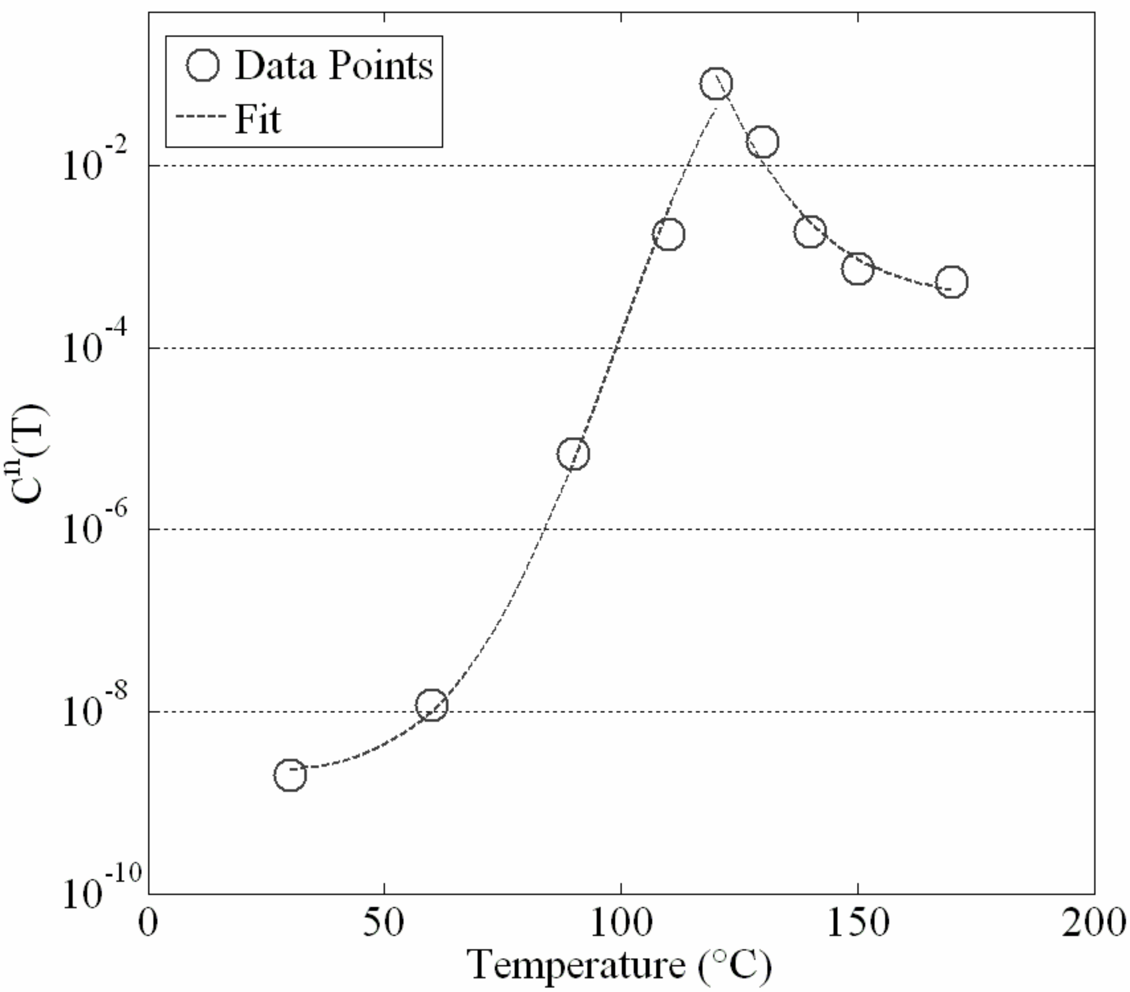

Figure 19: The Zapas - Crissman coefficient C^n versus temperature.

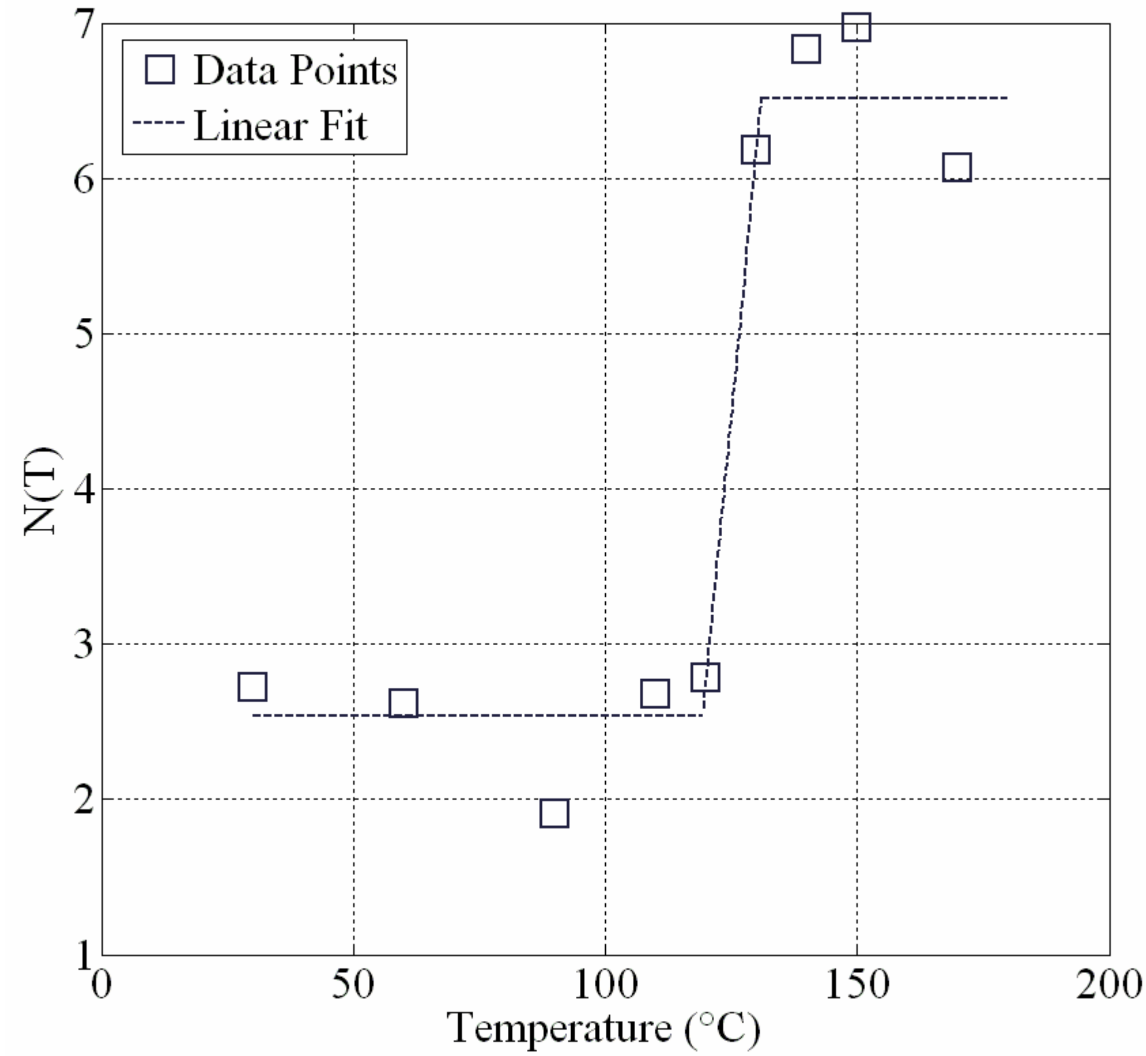

Figure 20: The Zapas - Crissman exponent *N* versus temperature.

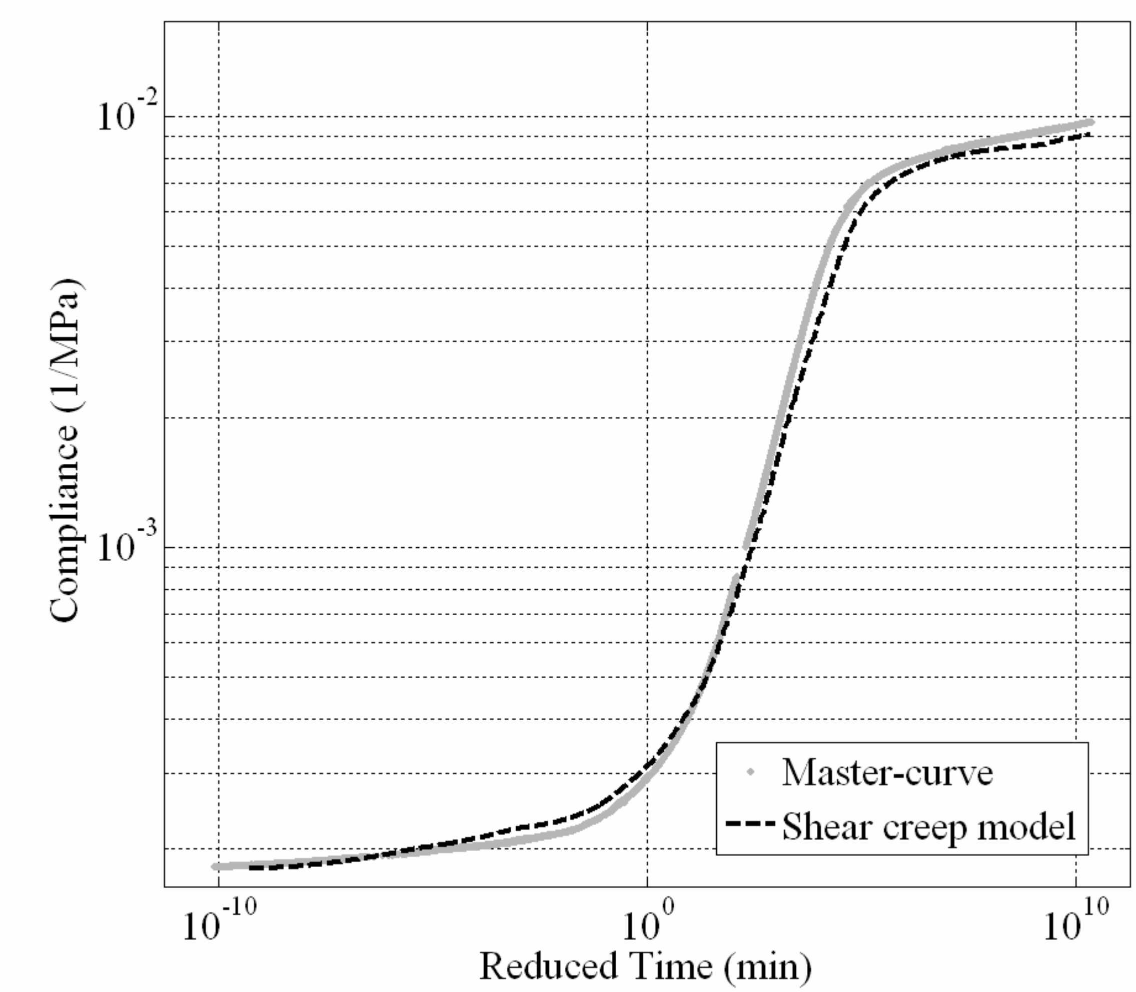

Figure 21: The temperature master-curve for σ = 200 psi (1.38 MPa) with fit model (dashed line).

Chapter 3: Compression Creep Rupture Behavior of a Glass/Vinyl Ester Composite Subject to Isothermal and One-sided Heat Flux Conditions[2]

3.1 Abstract

Given the expanding applications of polymer matrix composites to civil infrastructure, the marine industry, and the military, we examine the compression creep rupture behavior of a glass/vinyl ester composite subject to combined load and one sided heating simulating fire exposure. We focus on *reversible* non-linear viscoelastic effects which dominate delayed failure at lower temperatures in the vicinity of the glass transition temperature. A compression strength model which predicts local compression failure due to micro-buckling is extended to include viscoelasticity. Times to failure under combined mechanical load and one sided heating are estimated to within an order of magnitude.

Keywords: A. Polymer Matrix Composites, B. Creep, C. Analytical Modeling, Fire.

3.2 Introduction

Polymer matrix composites (PMC's) are growing in popularity as a replacement to conventional materials in civil infrastructure, construction, and marine applications. Many navies as well are exploring the possibility of applying glass/polyester and glass/vinyl ester systems to the construction of topside structures such as radar/communications mast, helicopter hangers, and structural bulkheads and flooring on larger naval ships and as structures on patrol boats and mine hunting vessels. PMC's offer benefits over conventional materials due to their high specific strength, excellent

[2] Boyd SE, Lesko JJ, Case SW. Compression Creep Rupture Behavior of a Glass/Vinyl Ester Composite Subject to Isothermal and One-sided Heat Flux Condition. Submitted to Composites, Part A: Applied Science and Manufacturing 2006.

corrosion resistance, low electromagnetic signature, overall improved operational performance and low heat conductivity. The United States Navy is currently investigating Vetrotex 324/Derakane 510A – 40, an E-glass/vinyl ester system, for use in topside structures on its naval vessels.

Before PMC's can be implemented on board naval and marine ships, questions regarding the fire performance and structural integrity of the organic polymer matrix with fire exposure must be investigated. To this point much research has been performed to characterize the flammability, toxicity and fire resistance of PMC's with fire exposure [2-4]; however, an understanding of the structural response of sandwich structures and laminates under combined mechanical load and fire is still largely unavailable. As the PMC is exposed to fire, it first undergoes *reversible* changes to its properties in the vicinity of the glass transition temperature T_g such as a precipitous drop in stiffness. At these elevated temperatures the structural integrity is compromised due to thermal softening which could lead to compression failure and possible collapse even though the polymer matrix has not been degraded.

The main goal of the modeling effort to characterize the structural response under fire loading conditions is to develop analytical models and finite element analysis methods and tools to predict laminate level limit state variables such as deflection, local and global buckling, thermo-mechanical evolution of properties with temperature including estimated times to failure. Given the importance of compressive loading at elevated temperatures in the structural fire response of composite structures, we focus on:

(d) Characterizing the nonlinear creep response of the E-glass/vinyl ester composites at and above the glass transition temperature.

(e) Describing compression strength mechanics as a function of fire (resulting in a non-uniform temperature profile) and mechanical loading based on a micromechanics model (Budiansky and Fleck [77]). This model is extended to include viscoelasticity.

(f) Integrating the viscoelastic characterization into the compression strength model to predict times to failure.

As mentioned much work has been done in the area of quantifying the smoke, toxicity and flammability of an organic matrix composite subject to fire exposure ([2-4] and flame spread and smoke density standard ASTM E 84). However, relatively little work has been done that evaluates the structural response and residual properties and strength of a composite structure compromised by fire exposure. Of the work that is currently available, Henderson and Wiecek [88], McMannus and Springer [29], and Gibson et al. [31] have lead in developing a thermodynamic polymer decomposition model that estimates degraded composite properties and residual strength as a function of thermal exposure. Their collective work has focused on laminate property degradation at temperatures well over the glass transition temperature T_g high enough to cause thermal decomposition of the matrix. Gibson et al. [18, 34] and Seggewiß [32, 33] have also done work in the area of developing models and methods that mechanistically estimate the structural performance and residual properties of fire damaged composites. Gibson et al. has developed a two-layer laminate mechanics model for estimating the post fire response and lifetimes of glass/polyester systems subject to a heat flux simulating fire exposure up to 75 kW/m^2. Seggewiß has shown a comparison of the tensile and compressive lifetimes for carbon/polyester systems in their principle orientations with heat fluxes up to 280 kW/m^2.

Most of these studies have been concerned with the very high temperature response of glass or carbon fiber reinforced composites subject to fire exposure. These high temperatures (heat fluxes greater than 50 – 75 kW/m^2) cause *irreversible* damage to the composite in the form of thermal decomposition of the matrix and typically a quick temperature controlled failure. As a continuation of the overall work to characterize the structural response under fire loading conditions, the current research effort seeks to study *reversible* phenomena that typically occur with lower heat fluxes (5 – 20 kW/m^2) and temperatures in the vicinity of T_g where viscoelastic creep and creep rupture effects control delayed failure.

Many researchers over the years have developed methods and models to predict delayed failure of general laminated composite systems at elevated temperatures where a viscoelastic process is the dominant factor for failure. The two most relevant to the current research are given by Miyano et al. [68-70] and Dillard et al. [73]. Miyano et al. have forwarded models predicting creep rupture behavior based purely on time-temperature equivalence. Miyano collected rupture times at different temperatures and stresses and shifted the data to form temperature master-curves. The resulting shift factors were modeled using an Arrhenius relationship and corresponding activation energies calculated. Miyano then used the master-curves to successfully predict rupture strengths. Dillard et al. utilized an elevated temperature viscoelastic characterization and extended the Tsai – Hill failure criterion to include viscoelastic effects to successfully predict delayed failure of carbon reinforced epoxy laminates. These models have been successfully applied to glass and carbon fiber reinforced composites to predict tensile creep rupture behavior in the vicinity of T_g.

The work presented in this manuscript builds on previous work that characterizes the nonlinear thermo-viscoelastic response of a E-glass/vinyl ester composite [81]. Isothermal creep and recovery tests were conducted on shear coupons ($[\pm 45^o]_{2S}$) and the results indicated that the nonlinear thermo-viscoelastic response of the composite was dominated by temperature and was significant at and above T_g and in the area of yield for a given temperature. In an effort to simulate the structural fire response of composites, Bausano et al. [83] conducted one-sided heat flux compression creep rupture tests on a pultruded nearly quasi-isotropic laminate of Vetrotex 324/Derakane Momentum 411-350 ($[0^o/90^o/\pm 45^o/CSM]_S$). Bausano et al. used thermally modified micromechanics together with classical lamination theory (CLT) and ANSYS to predict the rupture times which were found to be controlled by the glass transition temperature T_g of the matrix. Bausano et al. was also the first to demonstrate that the basic Budiansky and Fleck model could be extended to successfully predict compression failures in pultruded PMC's with a weave reinforcing phase.

The structural model presented here is similar to the work of Bausano et al. but includes thermoviscoelasticity. The compression strength model developed here is based on the Budiansky and Fleck model but is extended to include nonlinear viscoelasticity (replacing G with the in-plane shear relaxation modulus G_{12}) and is applied to woven roving reinforced composite. An average laminate compression strength is calculated as a function to time and temperature and used to predict laminate compression failure due to local micro-buckling in unidirectional composites subject to both isothermal conditions and one sided heating.

3.3 Experimental and Materials

Prediction of compression creep rupture times to failure occurred in successive steps. First quasi-static strength tests were performed on shear coupons at temperature (as defined in ASTM standard D3518/D3518M – 94(2001)) to determine necessary compression strength model parameters. Then isothermal compression rupture tests were performed on warp aligned coupons to validate the accelerated characterization framework in the viscoelastic model. Finally, one-sided heat flux tests (more accurately simulating fire exposure) were conducted on unidirectional coupons and rupture lifetimes predicted. The unique aspect of these tests is that they are not burn through tests but are performed at low heat fluxes and temperatures in the vicinity of T_g where viscoelasticity controls delayed failure.

3.3.1 Materials

The composite coupons consisted of a brominated vinyl ester resin (Ashland Derakane 510A – 40) reinforced with a 24 oz woven roving E-glass (Vetrotex 324). All coupons were manufactured at Virginia Tech using the vacuum assisted resin transfer method (VARTM). The cure package used was based on information from the Dow Chemical Company and consisted of 1.25% per total resin volume of Norox MEKP-925H (peroxide initiator), 0.2% Cobalt Naphthenate catalyst, and 0.05% 2,4 Pentanedione 99% (retarder). All coupons were post-cured in three stages; a procedure which was verified here at Virginia Tech [89] to increase the degree of cure and the glass transition temperature. First, the room temperature processed panel was post-cured at 2°C/min ramp to 130°C followed by a 2 hour hold in order to remove much of the remaining styrene. Second, the panel was cut into coupons and strain gages adhered with

Measurements Group 610A high temperature adhesive (which requires an elevated temperature cure). The coupons were clamped and post-cured with a 10°C/min ramp to 130°C followed by a 2 hour hold. Finally, the coupons were post-cured between glass plates (to maintain flatness) with a 10°C/min ramp to 200°C followed by a 2 hour hold and gradual cool down.

Compression strength tests and creep rupture tests were conducted on warp and weft aligned coupons and tension shear strength tests on shear coupons of Vetrotex 324/510A – 40 at various temperatures. The warp and weft coupons consisted of 10 layers of the Vetrotex woven roving with each layer having 55% (warp) or 45% (weft) of the E-glass reinforcement longitudinally aligned. Shear tests were conducted by applying tensile loads to coupons consisting of 8 layers of the woven roving aligned at ±45° with respect to the longitudinal axis. The dimensions of the coupons were nominally 23 cm x 2.5 cm for the shear coupons and 15 cm x 2.5 cm for the warp and weft coupons.

3.3.2 Isothermal Experimental Set-Up

The compression strength, tension shear strength and isothermal compression creep rupture coupons were all gaged back-to-back with Measurements Group CEA-06-500UW-350 gages and thermal strains compensated using the dummy gage technique. All tests were conducted on an MTS servo-hydraulic closed loop frame equipped with an environmental chamber (see Figure 22). Load data was provided by a 407 MTS controller and strain data was recorded using a Wheatstone bridge, a Measurements Group 2310 strain amp, and a National Instruments DAQ card and software. The tests were conducted over a wide temperature range from the glassy region of the polymer matrix into the leathery and rubbery regions. Tension shear strength tests were conducted to 180°C while the compression warp and weft tests only to 130°C. Coupon temperature was not recorded but was monitored using an Omega HH-21 digital thermometer by taping a K-type thermocouple to the coupon during testing.

3.3.3 One-sided Heat Flux Experimental Set-up

Compression creep rupture tests subject to a one-sided heat flux coupons were gripped longitudinally in a servo–hydraulic testing frame operated in load control, exposing a 50 mm gage length (less than the room temperature Euler buckling length). After the compressive load was ramped to the target constant value, an IR strip heater (manufactured by Research Inc.) was employed to apply a constant heat flux to one side of the sample as depicted in Figure 23. The IR heater uses a quartz lamp and a parabolic reflector to produce an approximately uniform heat flux. The coupons were painted with a high temperature black manifold paint in an attempt to achieve a uniform level of absorptivity. The applied heat flux was monitored and recorded using a Vatell HFM7-E/H heat flux gage that was mounted flush with the lamp side of the sample. To achieve a constant applied heat flux, the gage was monitored during each run, with a typical standard deviation of ±0.3 kW/m^2.

Front (side exposed to the heat flux) and back side temperatures were recorded using glass insulated 36 AWG K-type thermocouples that were bonded to the surface using a dot of a standard epoxy. The strains on the back side of the sample were measured with a non-contact laser extensometer manufactured by Fiedler Optoelektronik GmbH of Germany, over a gage length of approximately 40 mm. The laser extensometer used two reflective strips placed on the sample as references for the strain measurement. A standard 89 kN load cell was used to monitor the applied mechanical loads. All data channels were wired into a National Instruments SCXI Multiplexor Data Acquisition System which allowed for the real time monitoring of the variables and storage of the data.

3.4 Analytical Modeling

The developed compression strength model which includes thermoviscoelasticity is based on the Budiansky and Fleck model. The model requires various plasticity analysis parameters such as the material's strain hardening parameter, the nominal shearing stress and strain yield, and an estimate of the initial misalignment angle of the fiber reinforcement. However the most important input to the analytical model is a viscoelastic representation of the in-plane laminate shear modulus as a function of time, temperature, and stress. The analytical modeling method is described here by first presenting the necessary component inputs, the shear plasticity analysis, the accelerated characterization scheme on which the viscoelastic model is based, and the visoelastic form of the shear modulus. Then the compression strength model is presented with predictions of times to failure for both isothermal and one-sided heat flux compression rupture tests.

3.4.1 Ramberg – Osgood Plasticity Model

A plasticity analysis of the Ramberg – Osgood type was conducted on shear coupons in order to determine the nominal yielding shear strain and stress and the strain hardening parameter. Shear coupons ($[\pm 45°]_{2S}$) are used to characterize the in-plane laminate shear properties of laminated composites (ASTM Standard D3518/D3518M – 94(2001)) and give expected ductile and viscoelastic behavior, especially at temperature as shown in Figure 24 and Figure 25. Quasi-static tension strength tests were conducted on shear coupons to 180°C and the results fit to the Ramberg – Osgood equation at each temperature,

$$\gamma = \frac{\tau}{G}\left(1+\frac{3}{7}\left(\frac{\tau}{\tau_Y}\right)^{n-1}\right) \quad \mathrm{T} \leq 130^{\circ}\mathrm{C} \tag{12}$$

Here G is the composite shear modulus, τ_Y is the nominal yielding shear stress and n is the strain hardening index. The shear stress – strain data was fit for n and τ_Y with the shear modulus G determined graphically as the slope of the linear region for temperatures up to 130°C. The higher temperature shear stress – strain data was also fit using a variation of eq. (12) which included three parameters n, τ_Y and γ_Y substituting in τ_Y/γ_Y for G; however, these fits did not give reliable results. Figure 26 (a) – (d) illustrates the Ramberg – Osgood fits at various temperatures and Figure 27 (a) – (d) the temperature dependence of the shear modulus, shearing stress, strain, and strain hardening parameter.

3.4.2 Time-Temperature and Time-Stress Superposition

The idea of accelerated characterization is quite useful and convenient for extending the results of short-term testing to a representation of the long-term response. The shift factors, used to construct master-curves in temperature and stress, work to stretch or compress the actual time over which the short-term testing was performed into a reduced time,

$$\psi = \psi(t, T, \sigma) = \int_{0^-}^{t} \frac{d\xi}{a_T(T)\, a_\sigma(\sigma, T)} \tag{13}$$

Temperature and stress shift factors were found through a data reduction of tension shear creep data and are presented in Figure 28 and Figure 29 as they were modeled over stress and temperature. The experimental and theoretical work from Miyano et al. [68-70] has demonstrated that the temperature shift factor and thus time-temperature equivalence can be applied successfully to predict not only creep strengths, but also static and fatigue strengths as well in which temperature is the accelerating factor for the viscoelastic relaxation. The validity of this approach was verified for this research effort and the time-temperature and time-stress shift factors found from tension creep data worked well enough to shift the compression rupture data into a reasonably smooth master-curve. The resulting master-curve of compression creep rupture times is presented in Figure 30 (*a*) and the combined shifts used to form the curve in Figure 30 (*b*). The master-curve is especially smooth in the leathery and rubbery regions of the matrix material ($T > 105°C$).

3.4.3 Viscoelastic Shear Relaxation Modulus Representation

Non-fiber reinforced orientations in a laminate are the major contributors to observed viscoelastic behavior and significantly impact the elevated temperature response of the laminate. Since Vetrotex 324 is a woven roving with two fiber reinforcing orientations, the time – dependent behavior and response of the composite is expected to be confined to the in-plane shear properties. A detailed set of tension creep data [90] and a data reduction [81] using the time-temperature-stress superposition principle (TTSSP) is available for this composite and gives a direct expression for the in-plane shear creep compliance S_{66}. Once the in-plane shear creep compliance S_{66} is known, the in-plane shear relaxation modulus G_{12} is calculated through a method of interconversion involving Laplace transforms and is briefly described here.

The nonlinear thermo-viscoelastic and viscoplastic representation of the shear creep compliance $S_{66}(t,T,\sigma)$ is given as a combination of the Schapery model for the nonlinear elastic and viscoelastic part and the Zapas – Crissman model (see Tuttle et al. [54] and Zapas and Crissman [64]) for the viscoplastic part,

$$
\begin{aligned}
S_{66}(t,T,\sigma) = & \underbrace{g_0(T,\sigma)S_0(\sigma_{\text{Ref}})}_{\text{Nonlinear Elastic}} \\
& + \underbrace{g_1(T,\sigma)g_2(T,\sigma)\sum_{k=1}^{m} S_k(\sigma_{\text{Ref}})\left(1-e^{-t/a_T(T)a_\sigma(T,\sigma)\tau_k}\right)}_{\text{Nonlinear Viscoelastic}} \\
& + \underbrace{C^n(T)\sigma^{N(T)\cdot\bar{n}(T)-1}t^{\bar{n}(T)}}_{\text{Viscoplastic}}
\end{aligned}
\tag{14}
$$

Here, the nonlinear parameters g_0, g_1, and g_2 are the vertical shifts of the Schapery theory, a_T and a_σ are horizontal shifts representing the relevant accelerating factors of temperature and stress within the time-temperature and time-stress superposition principles (TTSSP), C^n, N, and $\bar{n}$ the viscoplastic parameters of the Zapas – Crissman model, and S_0, S_k, and τ_k the compliance coefficients and retardation times. Using Eq. (14) the shear compliance can be calculated and plotted versus the reduced time of Eq. (13) for any stress or temperature.

The modeling framework of TTSSP expressed in Eq. (14) is a convenient representation of the creep compliance; however, it departs from the experimental data due to the inherent averaging involved in determining model parameters over stress and temperature. In the event that experimental data for the master-curve is available (as shown in Figure 24), the shear creep compliance may be determined directly from the master-curve data using a Prony series of the generalized Kelvin – Voigt type,

$$
\begin{aligned}
S^{\text{MC}}(\psi(t,T)) &= S_0^{\text{MC}} + \sum_{k=1}^{m} S_k^{\text{MC}}\left(1-e^{-\psi(t,T)/\tau_k}\right) \\
\psi(t,T) &= \int_{0^-}^{t} \frac{d\xi}{a_{\sigma,T}(T)}
\end{aligned}
\tag{15}
$$

In this case the compliance coefficients S_0 and S_k are unique to the master-curve (as indicated by "*MC*") as well as the combined shift factor $a_{\sigma,T}$ whose temperature dependence is determined by an Arrhenius relationship in the glassy to leathery region of the matrix and a WLF relationship in the leathery to rubbery region. The approach of Eq. (15) is a stress independent approach which uses a *linear* viscoelastic expression to model the response as solely a function of time and temperature.

To obtain G_{12} from Eqs. (14) or (15) we use a method of interconversion involving Laplace transforms to relate the creep compliance to the relaxation modulus. From linear viscoelastic theory the Laplace transform of the creep compliance is related to the Laplace transform of the relaxation modulus by,

$$\overline{G} = \frac{1}{s^2 \overline{J}} \tag{16}$$

Where $\overline{G}$ is the Laplace transform of the relaxation modulus and $\bar{J}$ is the Laplace transform of the creep compliance and s is the Laplace variable. It may be very difficult to obtain the exact Laplace transform of the creep compliance $\bar{J}$ from the creep compliance as represented by Eqs. (14) or (15), and then the inverse Laplace transform of the relaxation modulus from Eq. (16). Therefore, it is usually necessary to apply an approximate analytical method such as the one suggested by Leaderman [91] and described by Ferry [86] and Park and Schapery [92]. The conditions of the approximate method are satisfied by the shear compliance and Eq. (17) is used to calculate G_{12},

$$G_{12}(t,T,\sigma) = \begin{cases} \dfrac{\sin m\pi}{m\pi\, S_{66}(t,T,\sigma)} & 0 < m < 1 \\ \dfrac{1}{S_{66}(t,T,\sigma)} & m \approx 0 \end{cases} \tag{17}$$

where m is the local slope of $\log_{10}\left(S_{66}(t,T,\sigma)\right)$ versus $\log_{10}\left(\psi(t,T,\sigma)\right)$.

3.4.4 The Compression Strength Model with Viscoelasticity

The Budiansky and Fleck model is a post micro-buckling, mechanistic model which combines the plasticity of the matrix material (through shear deformation) with the effects of kinking kinematics in the buckled region in order to estimate the residual compression strength of unidirectional fiber reinforced composites. A detailed derivation of the theoretical results and expressions for static kinking strength and matrix plasticity can be found in Budiansky and Fleck [77]; however, this study focuses on the expression for the composite compression strength as derived for a state of pure compression loading,

$$\sigma_C = G\left[1 + n\left(\frac{3}{7}\right)^{\frac{1}{n}}\left(\frac{\bar{\phi}/\gamma_Y}{n-1}\right)^{\frac{n-1}{n}}\right]^{-1} \tag{18}$$

Here G is the elastic shear modulus, n is the strain hardening parameter, γ_Y is the nominal shearing strain at yield, and $\bar{\phi}$ is the initial fiber misalignment angle. From the form of Eq. (18) the portion in brackets can be viewed as a knockdown factor solely dependent on the matrix strain hardening parameter n and fiber imperfection ratio ($\bar{\phi}/\gamma_Y$). The knockdown factor however is more sensitive to the fiber imperfection ratio than the strain hardening index as demonstrated by Budiansky and Fleck (see Figure 4 in [77]). Further calculations involving Eq. (18) will also demonstrate that the value of the shearing strain at yield (γ_Y) has less impact than G and $\bar{\phi}$ which dominate the compression strength estimation.

The compression strength model developed here is based on the Budiansky and Fleck model is a suitable choice for modeling the compression behavior of the glass/vinyl ester composite considered due to the initial fiber misalignment angle coupled with compressive loading and in-plane viscoelastic shear relaxation in the matrix at temperature. In order to estimate the compression strength under fire loading conditions, it is necessary to extend Eq. (18) to reflect the temperature range over which the rupture data is taken and the viscoelasticity of the matrix. Figure 27 (c) and (d) show the temperature dependence of the strain hardening parameter and the shearing strain at yield. While the temperature dependence of n and γ_Y are appreciable in the vicinity of T_g (≈ 105°C), the effect on the compression strength results of Eq. (18) are not very significant. Therefore a decision was made to fix both n and γ_Y at their room temperature fit values given the expectation that the initial misalignment angle $\bar{\phi}$ and the temperature dependence of G would dominate Eq. (18). The initial fiber misalignment was determined by microscopy (see Figure 31) as approximately 10°. For the most part the time, temperature, and stress dependence of the compression strength is entirely contained within the viscoelastic shear relaxation modulus (G replaced by G_{12}) with $\bar{\phi}$ controlling the value of the knockdown factor.

3.4.5 Isothermal Compression Strength Estimation and Times to Failure

Isothermal compression creep rupture data was taken over a temperature range of 90°C to 130°C within a test window of 0.1 to 10,000 minutes. The shearing stress, τ, used in the calculation of G_{12} is determined by noting that shearing stress inputs into the creep model of 0.345 MPa to 3.45 MPa (50 psi to 500 psi) have little effect on the life predictions of Figure 32 and Figure 34. Since a complete experimental master-curve is available for 1.38 MPa (200 psi) (see Figure 24), G_{12} is determined directly from the data using the linear viscoelastic expression Eq. (15) instead of the non-linear model of Eq. (14). The compression strength model (Eq. (18)) then becomes,

$$
\begin{aligned}
X_C(t,T) &= G_{12}^{\mathrm{MC}}(t,T)\left[1+n\left(\frac{3}{7}\right)^{\frac{1}{n}}\left(\frac{\bar{\phi}/\gamma_Y}{n-1}\right)^{\frac{n-1}{n}}\right]^{-1} \\
n &= 5.3 \\
\gamma_Y &= 0.59\% \\
\bar{\phi} &\approx 10^{\circ}
\end{aligned}
\tag{19}
$$

The compression strength prediction of Eq. (19) is plotted versus the shifted isothermal compression creep rupture data in Figure 32.

3.4.6 Time – Temperature Profile Determination in ANSYS

Under realistic fire conditions the composite will not be subject to isothermal conditions but to a temperature profile that will be hottest on the face toward the fire exposure and coolest on the face away. For this reason we have conducted one-sided heat flux compression creep rupture tests and used the resulting time – temperature profile as input into the model. Thermocouples adhered to the coupon surfaces recorded temperatures on the front face (face toward the IR lamp; hot side) and the back face (cool side). These temperature readings were used as boundary conditions in a transient 2D thermal analysis in ANSYS 9.0. A 50 mm by 6 mm area that corresponds to a cross-section of the gage length of a coupon was meshed with plane 55 elements. The resulting element mesh consisted of one column of elements for each laminate layer. The recorded front and back temperatures were applied to the front and back faces, while the top and bottom surfaces were assumed to be insulated. The code solved for the time – temperature profile through thickness of the composite coupon giving a temperature at each layer interface for a total of nine temperature estimates and two readings (interfaces for 10 layers, front face and back face as illustrated in Figure 33 for warp coupon #2a).

3.4.7 One-sided Compression Strength Estimation and Times to Failure

Once the time – temperature profile was known, Eq. (19) was applied at all eleven points and the average laminate compression strength for the composite coupon was calculated using Simpson's rule. Failure is predicted when the average laminate compression strength X_C is less than the applied laminate compressive stress.

$$\begin{aligned} \sigma_{\mathrm{C}}^{k}(t,T_k) &= G_{12}^{\mathrm{MC}}(t,T_k)\left[1+n\left(\frac{3}{7}\right)^{\frac{1}{n}}\left(\frac{\bar{\phi}/\gamma_Y}{n-1}\right)^{\frac{n-1}{n}}\right]^{-1} \\ X_{\mathrm{C}} &= \frac{1}{H}\int_{-H/2}^{H/2}\sigma_C^k\,dz \\ X_{\mathrm{C}} &< \sigma_{\mathrm{applied}}^{\mathrm{C}} \end{aligned} \tag{20}$$

The average laminate compression strength was used to indicate laminate failure because it avoids issues regarding discount criteria in individual layers and stress redistribution in the laminate. In cases where the predicted life was longer than the experimental value, the time – temperature profile was extended by calculating the average through thickness temperatures over the last 10% of the test and keeping those values constant until failure was predicted to occur. Figure 34 shows the experimental versus predicted failure times for the three sets of one-sided heat flux tests; the preliminary tests used to adjust the experimental set-up, those which had a fixed front face temperature of 130°C, and those which had a fixed front face temperature of 135°C.

3.5 Results and Discussion

3.5.1 Isothermal Results

A master curve was formed from the isothermal creep rupture test data using the temperature and stress shift factors obtained from the non-linear viscoelastic data reduction and is presented in Figure 30 (*a*) and Figure 32. The isothermal rupture data analysis provided an opportunity to validate the inclusion of thermoviscoelasticity within the compression strength model and its ability to predict the rupture times. The ability to form a master-curve from the isothermal rupture data indicates that the appropriate relaxation mechanism of the compression failure process (viscoelastic shear relaxation) is correctly modeled. Indeed the results of the shifting clearly indicate that the dominant relaxation mechanism, elevated temperature through the glass transition of the matrix, is controlling the viscoelastic behavior and the failure time predictions.

Several issues that are apparent from the master-curve of Figure 32 include the smoothness of the shifting and an under-prediction of rupture times especially in the rubbery region. Smoothness of the shifting heavily depends on the shift factors used and the values for the shift factors can be significantly altered by underlying variations in the creep compliance data used to form the master-curve. Variations in the underlying shear creep data (see reference [81]) and variations in the compression rupture data (an order of magnitude) will both significantly affect the smoothness of the shifting and the apparent "goodness" of the predictions. The shifting is best above the glass transition temperature T_g indicating that temperature and not stress is dominating the viscoelastic relaxation. However, the predictions severely fall off into the rubbery region versus the data. This consequence has nothing to do with the shifting but illustrates that the tension shear creep compliance is more compliant with temperature than the compression creep rupture data indicates. Despite these issues, the inclusion of thermoviscoelasticity within the compression strength model adequately predicts the isothermal compression rupture data and validates the modeling effort.

3.5.2 One-sided Heat Flux Results

The compression strength model with viscoelasticity was successful overall in predicting the compression creep times to failure of the warp aligned coupons (see Figure 34). However, the predicted lifetimes were susceptible to either under or over prediction of the experimental lifetimes depending on various parameter inputs and manner in which the time – temperature profiles were calculated. Most of the tests showed some cooling of the back half of the coupon during the test. For some tests this was explained by a simple thermal overshoot and gradual equilibrating of the through thickness temperatures. For other tests the cooling off of the back face was more severe (a gradient -8°C to -15°C from front to back face) suggesting that wrinkles due to kinking and delaminations had formed through thickness and where causing an insulating effect; an effect for which the time – temperature profile did not account.

When the cooling was significant, this created a severe problem for cases (such as coupon #5) in which the model with an extended time – temperature profile severely over predicted the experimental failure time. In other cases of over prediction the feasibility of extending the time-temperature profile was very problematic due to the failure of the coupon during the warm up (such as coupons #6 and #11). For these cases it is difficult to project the time – temperature profile because the coupon did not survive long enough to experience a temperature equilibration through thickness and provide an observable temperature trend.

For tests that were under predicted (such as coupons #4 and #5a), the problem may be how the time – temperature profile is determined. The temperature profile through thickness does not account for delaminations that form when layers kink. These delaminations are suspected of causing an insulating effect that would propagate through thickness and decrease temperatures in each layer toward the back side of the coupon. This would increase the residual average compression strength and the predicted lifetime of the coupon. A more sophisticated determination of the time – temperature profile which takes into account a possible insulating barrier may be needed. Considering the way in which the compression strength is determined (as an average through thickness), a better time – temperature profile may have a limited influence to sway the results. Closer inspection of Figure 34 reveals that the hotter front face temperature group (coupons #6 - #13) experienced slightly better predictions, but there is an even division of under versus over predicted lifetimes regardless the front side temperature. Despite these issues, the one-sided compression strength model predictions are better than expected falling within plus or minus a decade of time of the experimental lifetimes.

3.6 Conclusions

Compression creep rupture tests are performed on unidirectional laminates of an E-glass/vinyl ester (Vetrotex 324/Derakane 510A – 40) subject to a combined compressive load and one sided heating. A compression strength model based on the Budiansky and Fleck model for unidirectional laminates is developed to describe local failure due to micro-bucking. The model is unique in that it implements a characterization of the non-linear thermoviscoelasticity of the matrix within a compression mechanics model that describes compression failure as a function time and temperature. The compression model also accounts for compression failures in woven roving reinforced laminates where kink formation due to compressive loading and initial fiber undulations play a significant role in predicting the time to failure. The results indicate convincingly that the correct relaxation mechanism, elevated temperature shear viscoelasticity, is adequately modeled and is dominating delayed failure in the vicinity of the glass transition temperature. Results are considered to be good predicting the experimental results to within an order of magnitude and the modeling approach validated.

Future work will include refining the structural modeling approach and extending it to a general laminate lay-up and performing a viscoelastic stress analysis with prediction of laminate failure under combined mechanical load and one sided heating. A more accurate time – temperature profile calculation will be required for this especially for extending the profile. Application of the thermoviscoelastic constitutive relation to other composite systems which are not composed of an amorphous, cross-linked polymer matrix or subject to the same types of relaxation mechanisms will have to be investigated. Also, since the temperature is overwhelmingly the dominate accelerating factor for the viscoelastic response, the current approach of ignoring the stress dependence and modeling the viscoelastic response as linear will have to justified for a general laminate. Finally, the average laminate compression strength approach to predicting failure will be further investigated.

3.7 Acknowledgments

The authors acknowledge the support of the Office of Naval Research Code 334, Award # N00014-04-1-0195. John Bausano and Dan Villareal are acknowledged for taking experimental data relevant to this work.

3.8 Figures

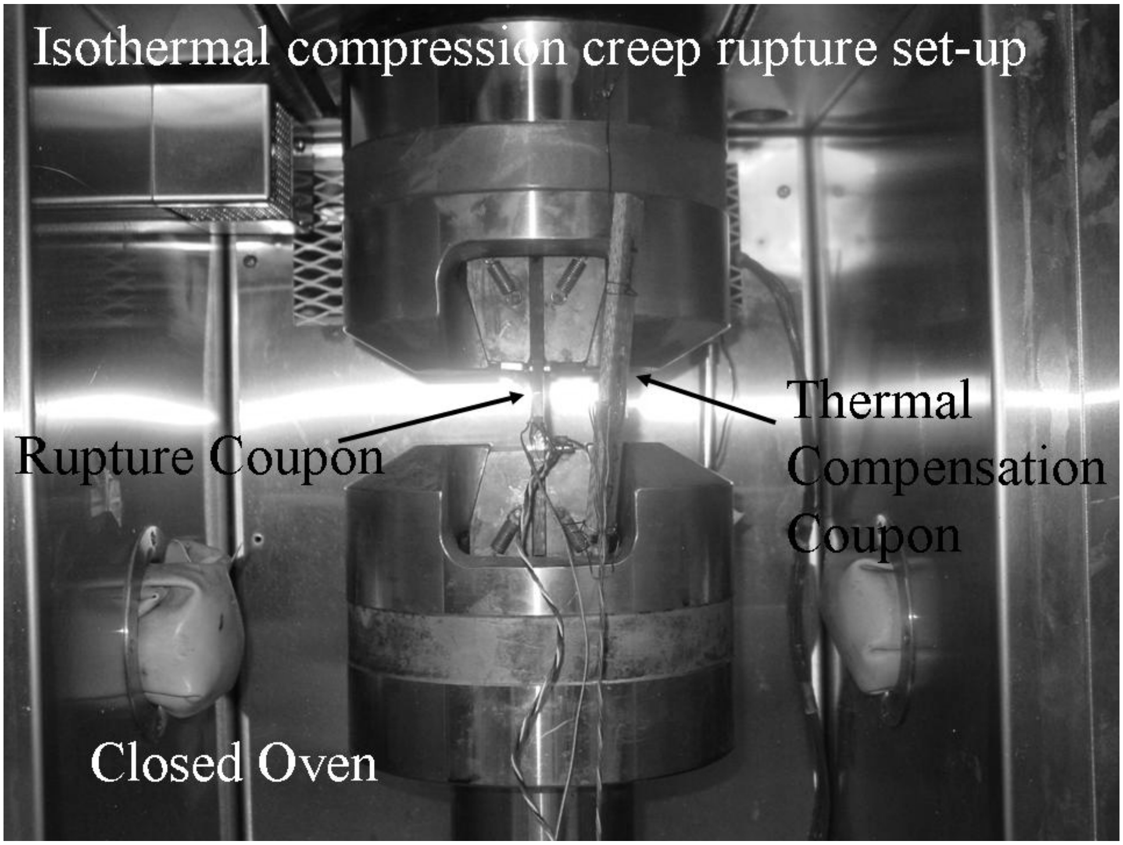

Figure 22: Isothermal, compression creep rupture experimental set-up.

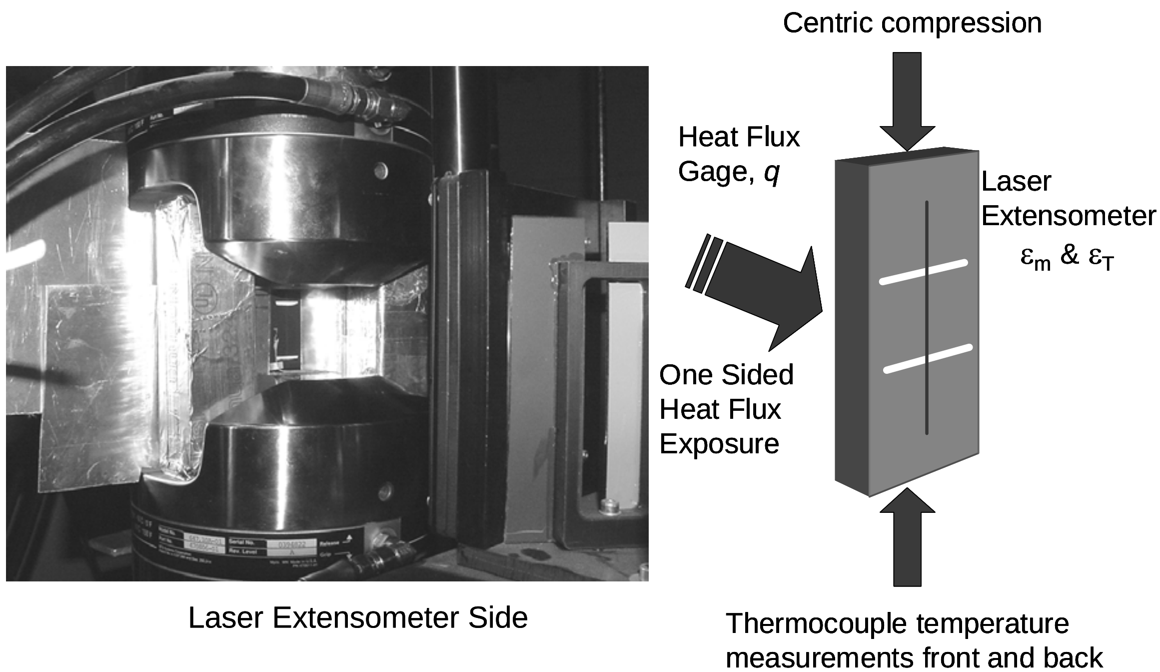

Figure 23: Combined centric compression loading and one sided heat flux exposure tests set-up and diagram.

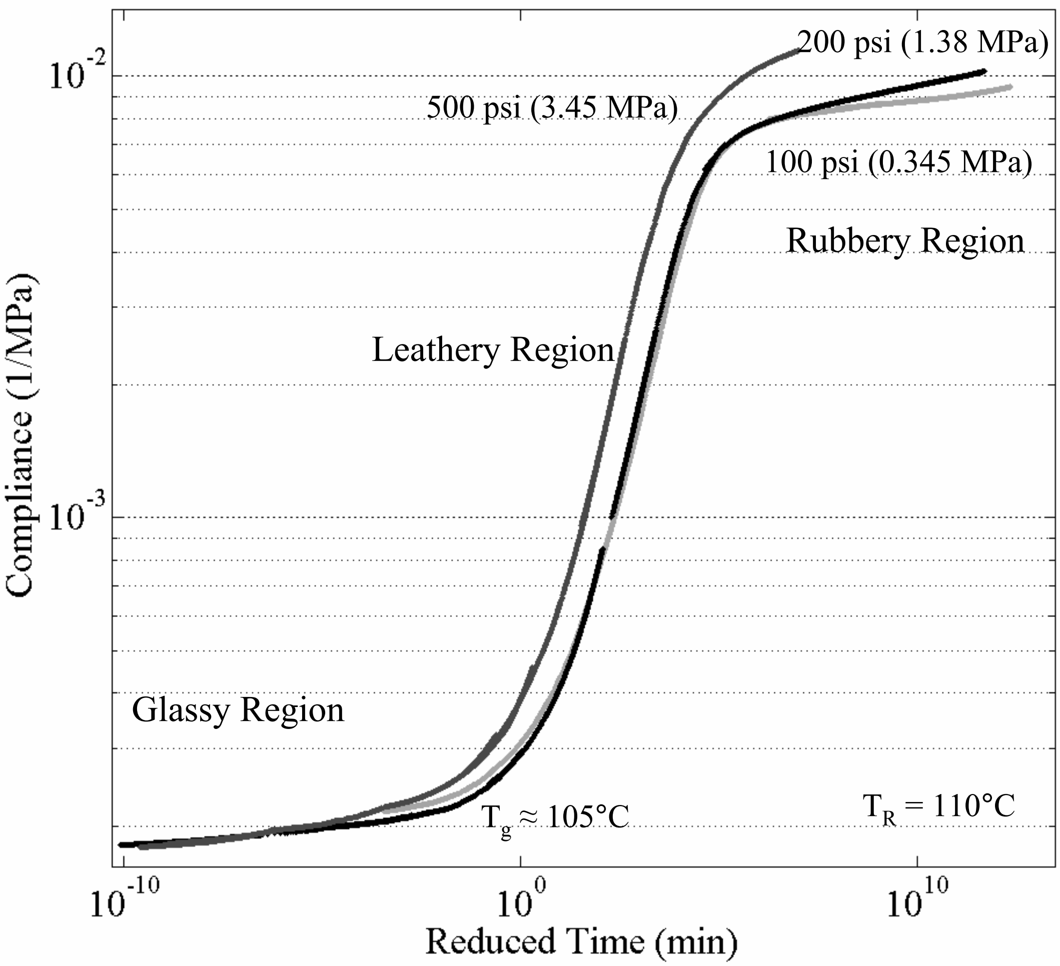

Figure 24: Temperature master-curves for Vetrotex 324/Derakane 510A – 40 at various stress levels.

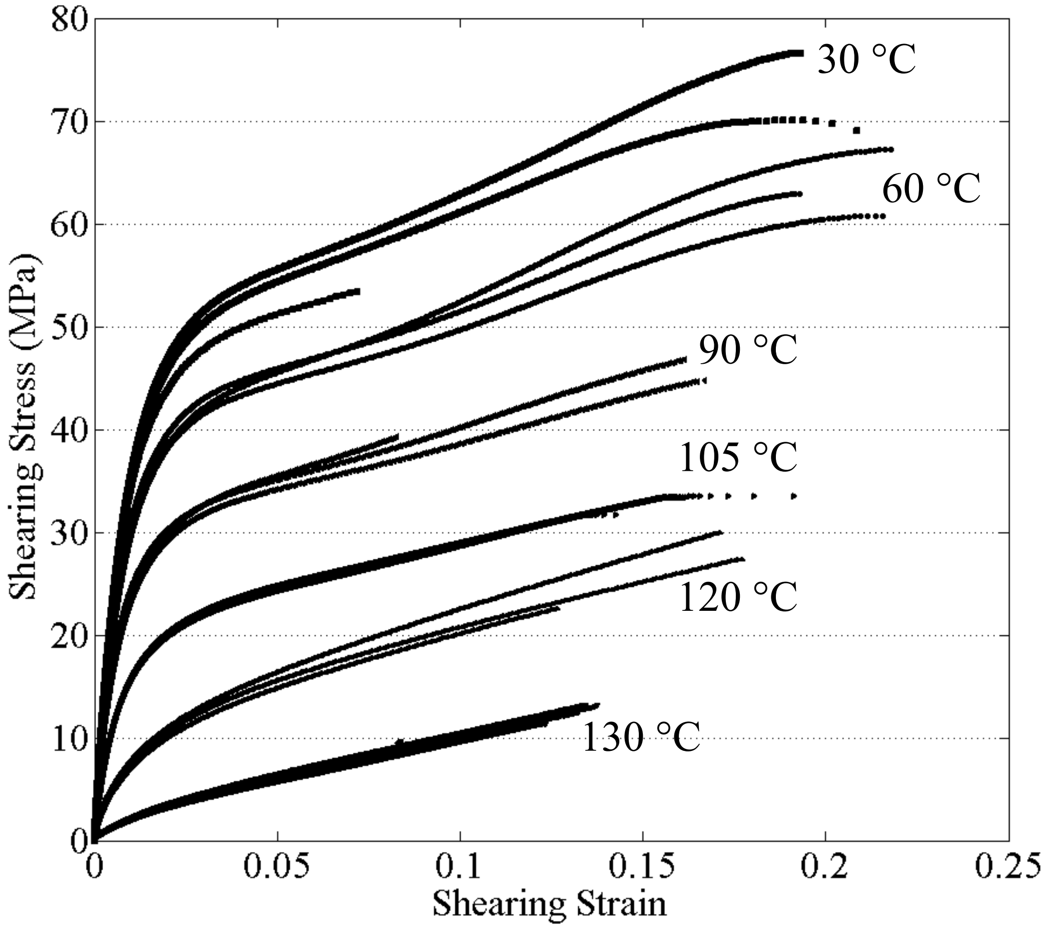

Figure 25: Tensile strength data for Vetrotex 324/Derakane 510A – 40 at temperature (T_g ≈105°C).

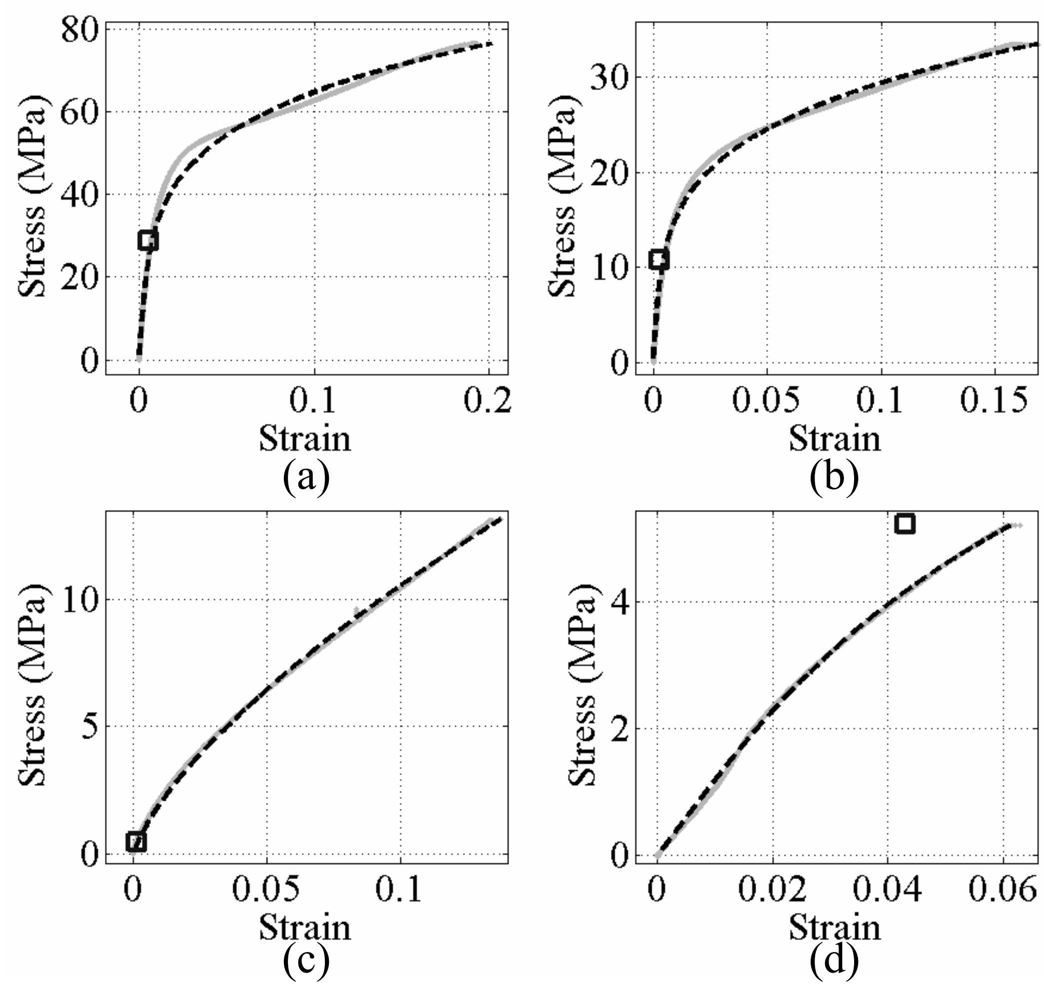

Figure 26: Results for Ramberg – Osgood fits to four tests at (a) 30°C, (b) 90°C, (c) 130°C, and (d) 160°C (the dashed line is the fit and the square indicates the yielding shearing strain and stress).

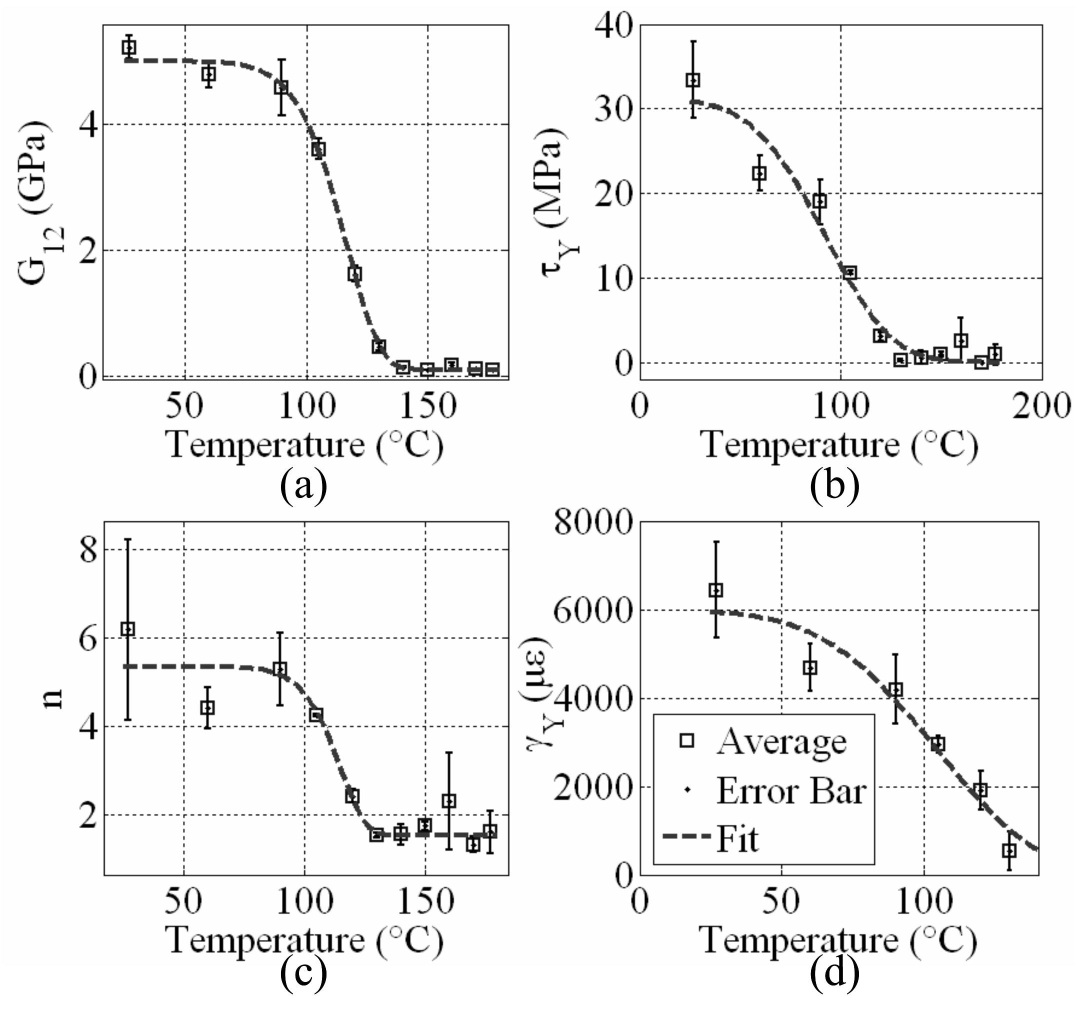

Figure 27: Summary of the Ramberg – Osgood fits to tensile strength data for (a) the shear modulus, (b) and (d) yielding shear stress and strain, and (c) the strain hardening with temperature (error bars indicate standard deviation at each temperature and dashed lines are stretched exponential fits).

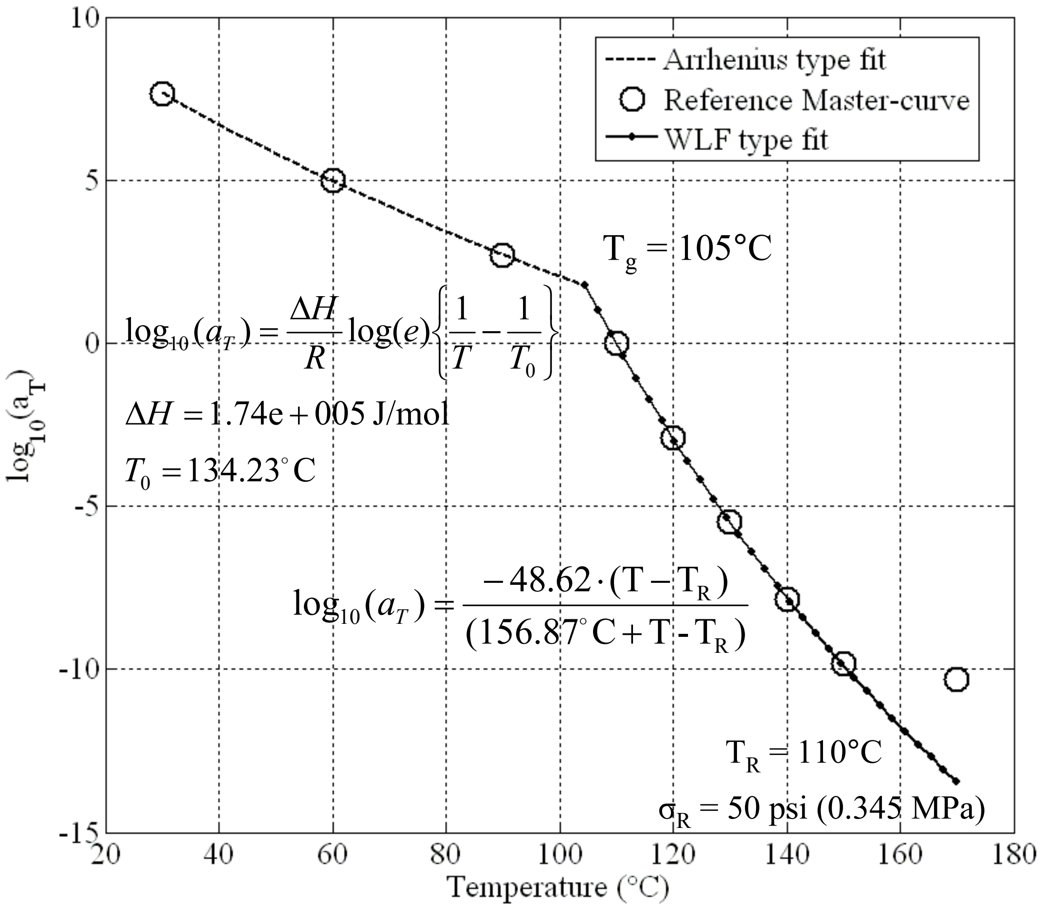

Figure 28: Temperature shift factor from the tensile shear creep data reduction of shear coupons of Vetrotex 324/Derakane 510A – 40.

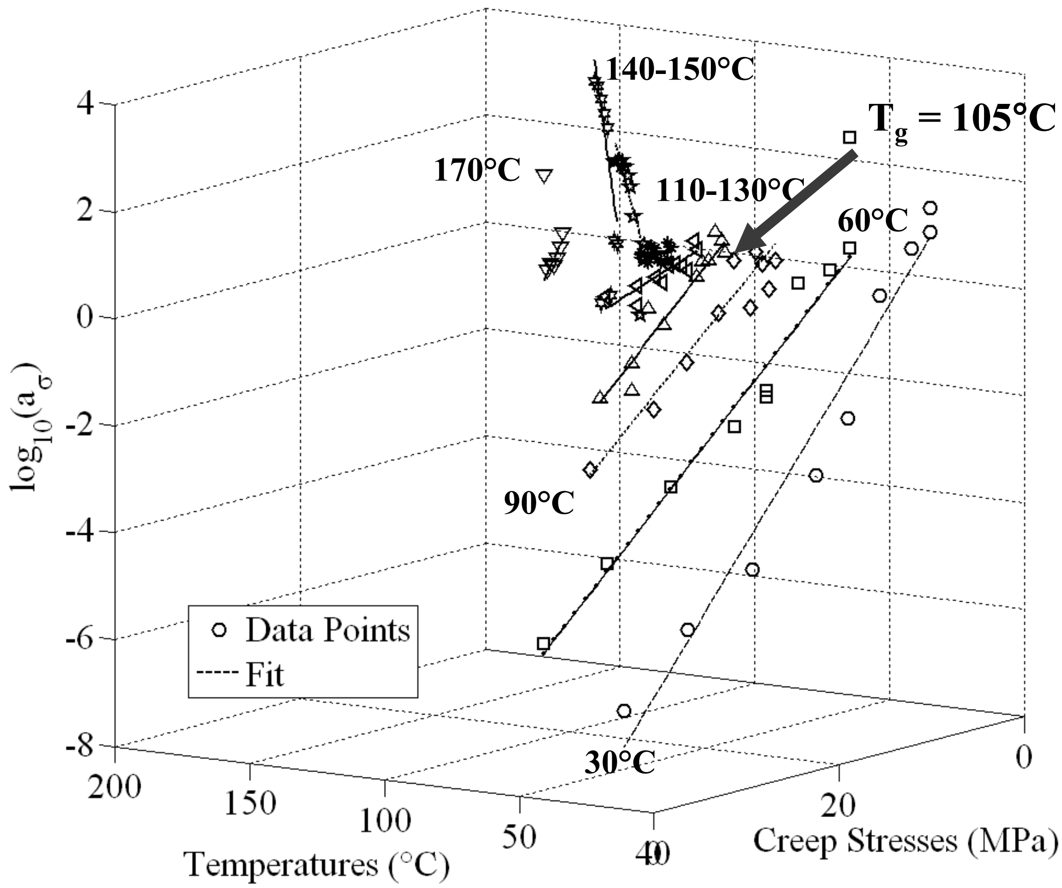

Figure 29: Stress shift factor in stress and temperature from the tensile shear creep data reduction of shear coupons of Vetrotex 324/Derakane 510A – 40.

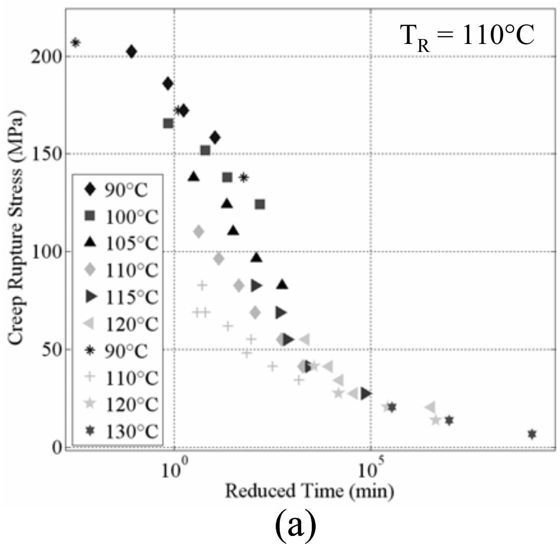

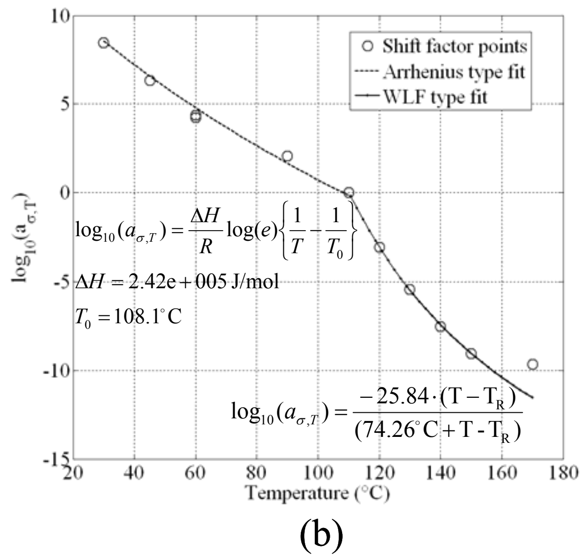

Figure 30: (*a*) The isothermal compression creep rupture data shifted using a (*b*) combined shift factor from the 1.38 MPa (200 psi) experimental master-curve. Note that the shifting is especially good above T_g (105ºC).

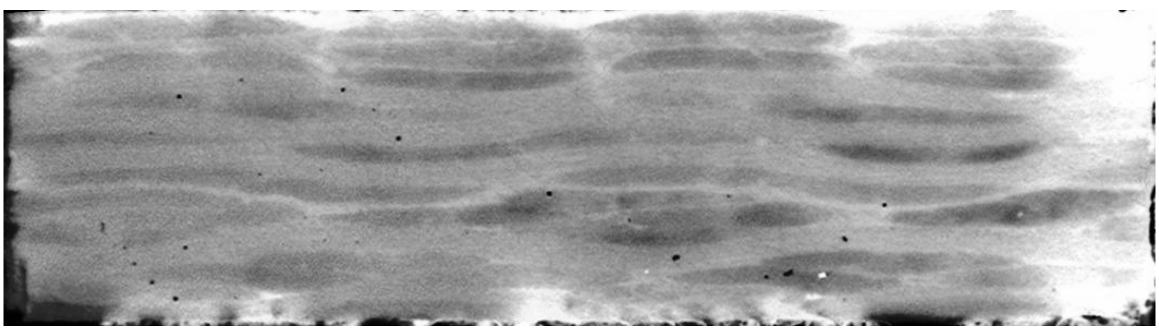

Figure 31: Polished cross-section of a shear coupon (8 layers) of Vetrotex 324/Derakane 510A – 40 used to determine the initial misalignment angle for the compression strength model.

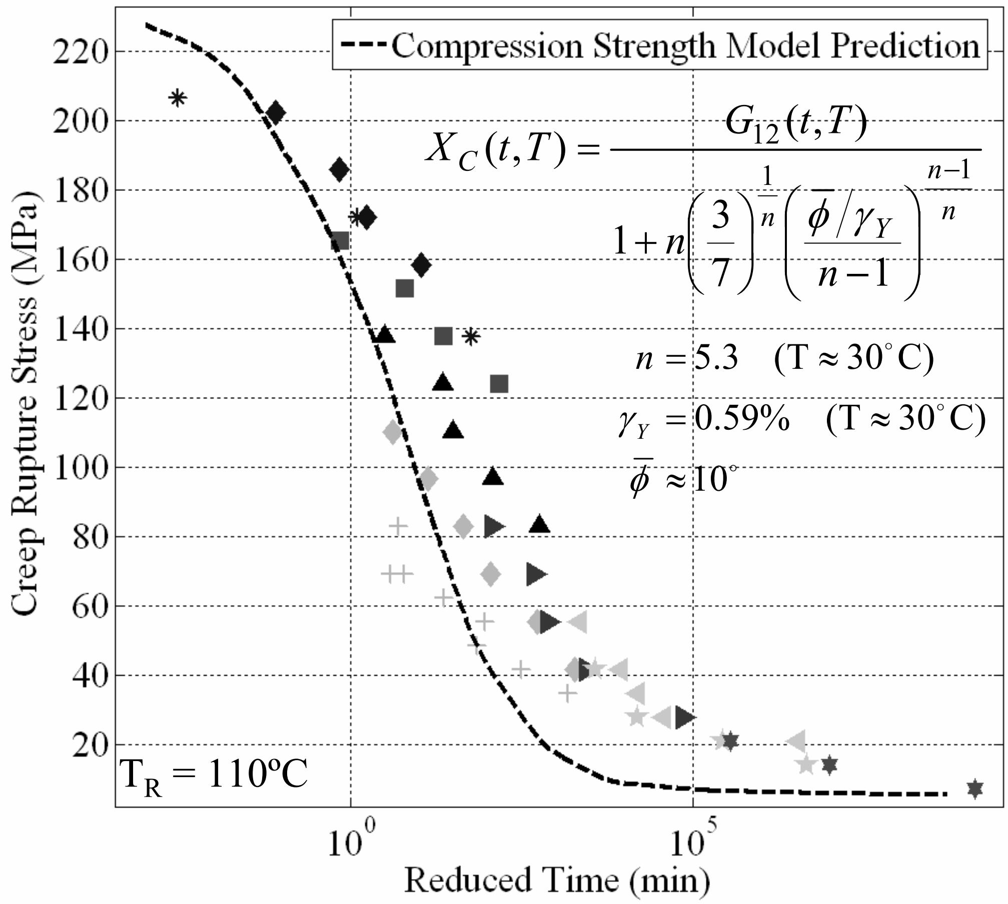

Figure 32: Shifted isothermal compression creep data of warp and weft coupons of Vetrotex 324/Derakane 510A – 40 with compression strength model prediction.

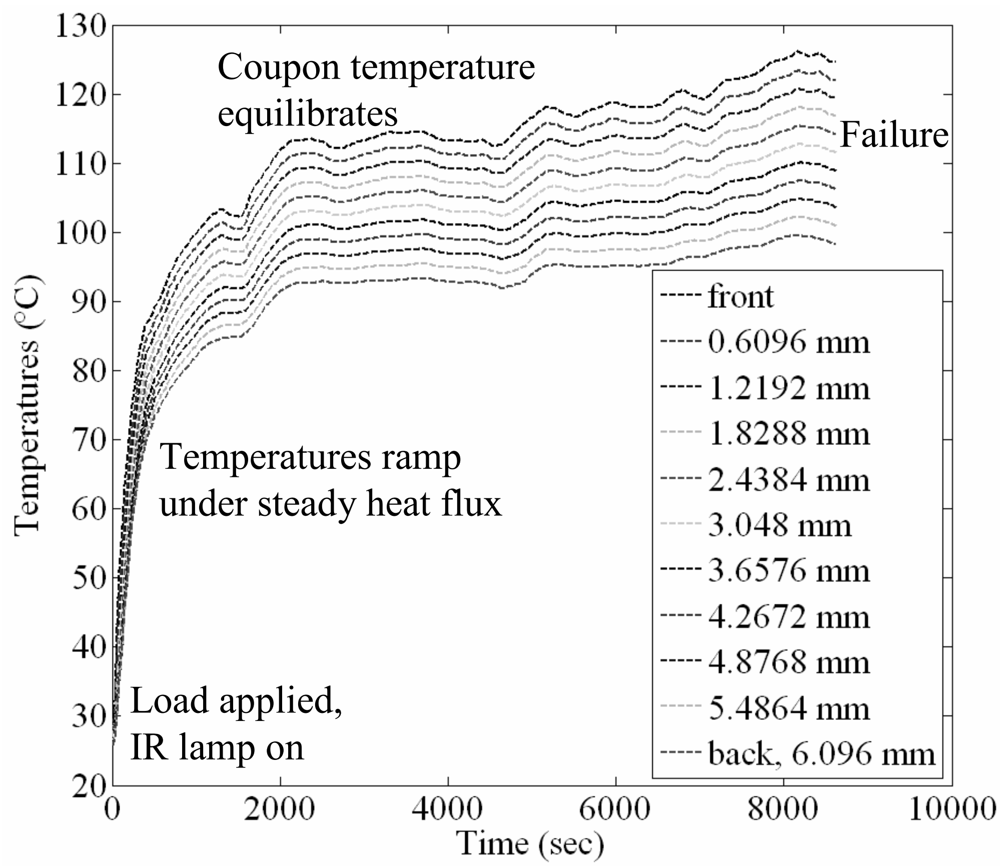

Figure 33: One-sided heat flux test for warp coupon #2a showing the time-temperature profile to failure. The front and back face temperatures are thermocouple readings and the interface temperatures were calculated by ANSYS.

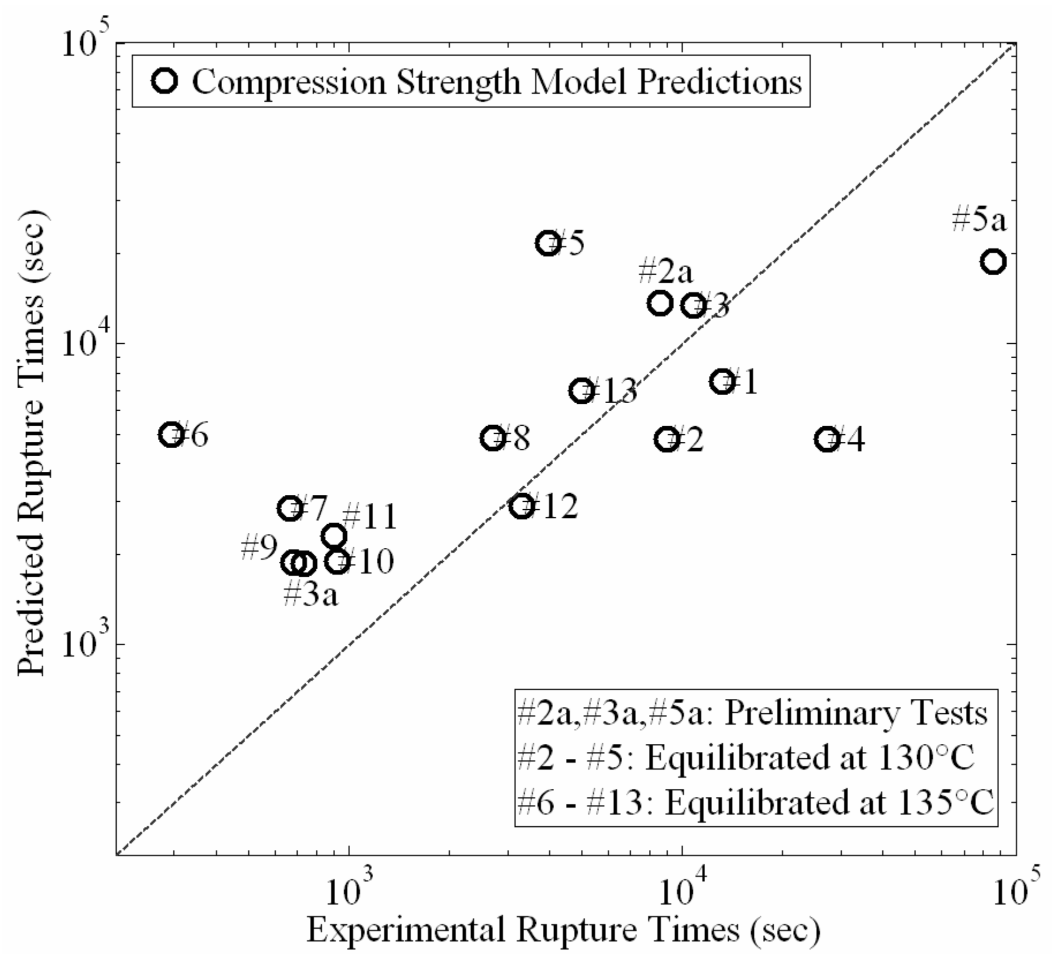

Figure 34: Predicted times to failure versus rupture times for one-sided heat flux tests on warp coupons of Vetrotex 324/Derkane 510A – 40 using the compression strength model.

Chapter 4: Compression Creep Rupture Behavior of a Glass/Vinyl Ester Composite Laminate Subject to Fire Loading Conditions[3]

4.1 Abstract

The growing use of polymer matrix composites on USN ships provides the impetus for examining in detail their structural performance and durability under combined mechanical and fire loading. A viscoelastic stress analysis using classical lamination theory is conducted on an E-glass/vinyl ester composite. The analysis includes a characterization of the non-linear viscoelastic behavior at temperature and its inclusion into the compression strength model for the prediction of laminate failure under combined compressive load and temperature profile simulating fire exposure. Model validation is achieved by successfully predicting one sided heating tests with constant heat flux exposure for a $[0/+45/90/-45/0]_S$ laminate.

Keywords: A. Polymer Matrix Composites, B. Creep, C. Analytical Modeling, Fire.

4.2 Introduction

Many navies are currently developing applications for polymer matrix composites in the construction of non-armored, supporting topside structures such as radar/communications masts, helicopter hangers, and structural bulkheads and flooring on larger naval ships and as structures on patrol boats and mine hunting vessels. Composites are beneficial due to their high specific strength, long fatigue life, excellent resistance to water corrosion, and low electromagnetic signature. However, their poor

---

[3] Boyd SE, Lesko JJ, Case SW. Compression Creep Rupture Behavior of a Glass/Vinyl Ester Composite Laminate Subject to Fire Loading Conditions. A more condensed version of this manuscript has been submitted to Composite Science and Technology 2006.

impact resistance, high cost, low rigidity, and joining problems are impediments to their full application. One major impediment that must be removed if polymer matrix composites are to see a wider application to topside structures is their performance under fire conditions. Although the rate of heat conduction for polymer matrix composites is low and may prevent fire from spreading quickly from one compartment to another, the overall performance of composites versus metals in fire is still worse due to the softening of the organic matrix reducing strength and increasing buckling risk and matrix decomposition releasing heat, smoke, soot, and toxic gases. Before these composites can be implemented on board naval ships, questions regarding the fire resistance, flammability, toxicity, and structural integrity of the organic polymer matrix must be investigated. Though much research has been performed to characterize and improve the flammability and fire resistance of these composite systems [2-4], relatively few efforts are undertaken to characterize the structural response of sandwich type structures and laminate panels under fire conditions.

A model of the structural response of a glass reinforced vinyl ester composite under fire loading conditions is developed. The model predicts laminate level variables, global buckling, residual strength, and times to failure using classical lamination theory (CLT) and finite element analysis to model the stress state. The overall goal is to develop an integrated tool for structural analysis of composite systems subject to fire which includes the following:

(g) Characterization of the non-linear viscoelastic/viscoplastic response of the E-glass/vinyl ester composites at and above the glass transition temperature T_g (see Boyd et al. [81]).

(h) Description of the compression mechanics as a function of stress and temperature using a compression strength model (based on the Budiansky and Fleck model [77]) extended to include viscoelasticity (see Boyd et al. [82]).

(i) Integrating the material characterization and failure criterion into CLT and a finite element analysis code.

To date the first two objectives have been completed along with a CLT implementation; however, the FE code development is still underway.

As mentioned, relatively few works have been conducted that evaluate the residual strength and times to failure of a composite structure compromised by fire exposure. Of the work that is available, Henderson and Wiecek [88], McMannus and Springer [29], and Gibson et al. [31] have lead in developing a thermodynamic polymer decomposition model that estimates degraded composite properties and residual strength as a function of thermal exposure. Their collective work has focused on laminate property degradation at temperatures well over the glass transition temperature T_g high enough to cause thermal decomposition of the matrix. Gibson et al. [18, 34] and Seggewiß [32, 33] have also done work in the area of developing models and methods that mechanistically estimate the rupture times fire damaged composites. Gibson et al. has developed a two-layer (char + composite) thermal softening model (progressive stiffness discount as a function of temperature) and a buckling failure criterion using laminate plate mechanics for estimating the post fire response and lifetimes of glass/polyester systems subject to one sided heating. Seggewiß has shown a comparison of the tensile and compressive lifetimes for carbon/polyester systems in their principle orientations with heat fluxes up to 280 kW/m^2. Most of these studies have been concerned with the very high temperature response of glass or carbon fiber reinforced composites subject to fire exposure. These high temperatures (heat fluxes greater than 50

– 75 kW/m^2) cause irreversible damage to the composite in the form of thermal decomposition of the matrix and typically a quick temperature controlled failure (approximately 10^2 seconds).

As a continuation of this overall work, the current research effort seeks to study reversible phenomena that typically occur with lower heat fluxes (5 – 20 kW/m^2) and temperatures in the vicinity of T_g where viscoelastic and viscoplastic effects dominate delayed failure behavior. Additionally, we present a laminate model and micromechanical failure criterion which have both been extended to include thermo-viscoelasticity and viscoplasticity in the structural analysis. Implementation of a viscoelastic constitutive model in to the conventional CLT algorithm to predict long term viscoelastic response and delayed failures began with Dillard et al. [78, 79] and Tuttle et al. [42] for carbon fiber/epoxy laminates subject to isothermal temperatures. This same algorithm was modified to include a viscoplasticity by Ha and Springer [52, 53] who predicted the response of carbon fiber/epoxy laminates subject to a cyclic temperature history, Tuttle et al. [54] who predicted the response of carbon fiber/epoxy laminates subject to a cyclic stress and temperature history, and Guedes et al. [56] who investigated other types of viscoelastic processes such as relaxations and flexural loading in beams. As with all numerical procedures, the forward explicit CLT algorithm is only conditionally stable and susceptible to poor convergence, oscillations, restricted to small time step size and divergence. To overcome these issues Gramoll et al. [47] developed an implicit CLT algorithm which had better convergence properties and never oscillated or diverged regardless of time step size. Initially the explicit CLT algorithm of Dillard et al. was implemented; however, due to the large strains encountered at high temperatures and the aggressive time – temperature profile of the one-sided heating tests, the method always diverged and after much effort to improve convergence was abandoned and replaced by the implicit CLT method. The implicit CLT algorithm is applied to the time – temperature profile to estimate the ply level state of stress which is then input to the viscoelastic and viscoplastic constitutive models. A numerical iteration is carried out until the compression strength model predicts laminate failure.

4.3 Experimental and Materials

Compression creep rupture tests subject simulated fire exposure were performed in two ways. As is standard in the literature, the tests were performed through the control of the one-sided heat flux made constant at 5, 10, 15, and 20 kW/m^2 (see Figure 35). This particular approach to control caused numerous problems for the proposed model mostly related to obtaining a stable time – temperature profile. Also, some of the tests simply became too hot considering the focus of the proposed model is to predict failure at temperatures in the vicinity of T_g (105°C) where delayed failure is due to non-linear viscoelastic effects and not irreversible thermal decomposition of the matrix. As a result a second set of tests were conducted maintaining front face temperatures at 125°C, 130°C, and 135°C. The second set of tests typically gave much more stable time – temperature profiles.

4.3.1 Materials

Large composite panels of a 24 oz E-glass woven roving (Vetrotex 324) in a brominated vinyl ester matrix (Ashland Derakane 510A – 40) were manufactured by Seemans Composites, Inc. using the vacuum assisted resin transfer method (VARTM) and delivered to Virginia Tech pre-cut into 48 in by 48 in panels. The composite panels were then post-cured according to a multi-step procedure which was verified here at Virginia Tech [89] to increase the degree of cure and the glass transition temperature. First, the panel was post-cured at 2°C/m ramp to 130°C followed by a 2 h hold in order to remove much of the remaining styrene. Finally, the panels were post-cured between glass plates with a 10°C/m ramp to 200°C followed by a 2 h hold and gradual cool down.

One-sided compression creep rupture tests were conducted on pseudo-isotropic coupons of Vetrotex 324/510A – 40 ($[0/+45/90/-45/0]_S$) at various exposed heat fluxes and front face temperatures. The coupons consisted of 10 layers of the Vetrotex woven roving with each layer having 55% (warp) or 45% (weft) of the E-glass reinforcement longitudinally aligned. The 0° orientation was regarded as the warp direction and the 90° orientation as the weft direction. The laminate was laid up by orienting the warp direction at either 0°, 90°, or ±45° with respect to the a set direction. Once the panels were fully cured, coupons were cut to the approximate dimensions of 6 in x 1 in (15 cm x 2.5 cm) with a thickness of 0.24 in (6.1 mm).

Material properties where found as a function of temperature whenever possible. Stiffnesses E_{11} and E_{22} and major Poisson's ratio ν_{12} were found by conducting compression strength tests at temperature on warp and weft coupons as illustrated in Figure 36. The coefficients of thermal expansion α_1 and α_2 were estimated by gaging a thick section of the composite with warp and weft direction gages and heating the sample under a controlled temperature ramp. The resulting thermal strains were recorded and plotted versus temperature as shown in Figure 37. Plasticity parameters relevant to the Budiansky and Fleck failure criterion were found as a function of temperature by conducting tensile strength tests on shear coupons ($[\pm45°]_{2S}$). The strain hardening parameter and the yielding shearing strain are illustrated in Figure 38. All relevant material properties are summarized in Table 2.

4.3.2 One-sided Heat Flux Experimental Set-up

Compression creep rupture tests subject to a one-sided heat flux (see Figure 39) were gripped longitudinally in a servo–hydraulic testing frame operated in load control, exposing a 2 in (50 mm) gage length (less than the room temperature Euler buckling length). After the compressive load was ramped to the target constant value, an IR strip heater (manufactured by Research Inc.) was employed to apply a constant heat flux to one side of the sample. The IR heater uses a quartz lamp and a parabolic reflector to produce an approximately uniform heat flux. For the heat flux controlled tests, the applied heat flux was monitored and recorded using a Vatell HFM7-E/H heat flux gage that was mounted flush with the lamp side of the coupon. To achieve a constant applied heat flux, the gage was monitored during each run, with a typical standard deviation of $\pm0.3\ kW/m^2$. Front (side exposed to the heat flux) and back side temperatures were recorded using glass insulated 36 AWG K-type thermocouples that were bonded to the surface using a dot of a standard epoxy. The data acquisition and control system could also be set up to maintain a target front face temperature. A standard 89 kN load cell was used to monitor the applied mechanical loads. All data channels were wired into a National Instruments SCXI Multiplexor Data Acquisition System which allowed for the real time monitoring of the variables and storage of the data.

4.4 Analytical Modeling

Prediction of times to failure for isothermal and one sided heat flux data for warp coupons of Vetrotex 324/Derakane 510A – 40 is described in detail in Boyd et al. [82]. The described approach is extended in this paper to account for the orthotropic symmetry of a laminate using CLT. Besides the restrictions imposed by the key assumptions of CLT, using CLT proved to be more difficult than expected because the numerical implementation of the Dillard et al. [78] explicit algorithm exhibited convergence issues and had to be abandoned for the more stable implicit algorithm of Gramoll et al. [47]. The shear modulus G in the compression strength model is accepted as the in-plane relaxation modulus G_{12} as calculated with the state of stress given by CLT and is used to predict laminate failure under a sustained compressive load and temperature profile [81]. What follows here is a brief review of the laminate constitutive equation, the time – temperature profile estimation and extension, application of viscoelasticity in the Budiansky and Fleck model and a detailed development of the viscoelastic and viscoplastic strain recursion formulas and their implementations within the stable numerical iteration of the implicit CLT algorithm.

4.4.1 Laminate Constitutive Model

The constitutive model for the inclusion of creep into the structural response of Vetrotex 324/Derakane 510A – 40 will briefly be presented here. This methodology is identical to that presented in other papers such as Guedes et al. [57], Tuttle, Pasricha, and Emery [54] and Tuttle, Mescher, and Potocki [87] except that the laminate will be subject to a non-uniform temperature profile. Since Vetrotex 324 is a woven roving with two fiber reinforced directions, we assume that a negligible amount of creep is occurring in either the warp ("1") or weft ("2") directions. Therefore each layer k will experience this principal coordinate total strain when subject to a given stress history,

$$\begin{Bmatrix} \varepsilon_1(t) \\ \varepsilon_2(t) \\ \gamma_{12}(t) \end{Bmatrix}_k = \begin{bmatrix} S_{11} & S_{12} & 0 \\ S_{12} & S_{22} & 0 \\ 0 & 0 & g_0^k\left(T^k, {}_k\tau_{12}(t)\right) S_0 \end{bmatrix} \begin{Bmatrix} \sigma_1(t) \\ \sigma_2(t) \\ \tau_{12}(t) \end{Bmatrix}_k + \begin{Bmatrix} \alpha_1 \\ \alpha_2 \\ 0 \end{Bmatrix}_k \Delta T^k + \begin{Bmatrix} 0 \\ 0 \\ \gamma_{12}^{\mathrm{VE}}(t) \end{Bmatrix}_k + \begin{Bmatrix} 0 \\ 0 \\ \gamma_{12}^{\mathrm{VP}}(t) \end{Bmatrix}_k \quad (21)$$

The total strain is a combination of elastic, thermal, viscoelastic, and viscoplastic strain components. Only the matrix dominated shear compliance S_{66} is time dependent; the fiber dominated terms S_{11}, S_{12}, and S_{22} are *assumed* to be time independent. The shear strains in the k^{th} ply induced by the stress history are given by the following general expressions utilizing the Schapery non-linear hereditary integral [85] and the Zapas – Crissman viscoplastic functional [63],

$$\begin{aligned} {}_k\gamma_{12}^{\mathrm{VE}}(t, T^k, {}_k\tau_{12}^t) &= {}_k g_1^t(T^k, {}_k\tau_{12}^t) \int_{0^-}^{t} \Delta S_{66}(\psi - \psi') \frac{d}{ds}\left\{ {}_k g_2^t(T^k, {}_k\tau_{12}^t)\ {}_k\tau_{12}(s) \right\} ds \\ {}_k\gamma_{12}^{\mathrm{VP}}(t, T^k, {}_k\tau_{12}^t) &= \left(C(T^k) \int_{0^-}^{t} {}_k\tau_{12}^{N(T^k)}(s)\, ds \right)^{\bar{n}(T^k)} \end{aligned} \quad (22)$$

Here, ${}_k g_1^t$ and ${}_k g_2^t$ are non-linear parameters of the Schapery model in the k^{th} ply at time t and C, N, and $\bar{n}$ are temperature dependent parameters of the Zapas – Crissman model. The thermal strain of Eq. (21) is distinguished from the familiar thermal strain in CLT by temperature profile ΔT^k. The expressions for the principal coordinate viscoelastic and viscoplastic shearing strains of Eq. (22) must be evaluated iteratively by recursion formulas reflecting changes in the strain corresponding changes in stress and temperature history. Details regarding the development of recursion formulas for both strains are given later in the paper.

4.4.2 Time – Temperature Profile Determination

Front and back temperature readings recorded during each tests were used as boundary conditions in a 1D numerical solution of the heat equation. The 1D heat equation was discretized using the forward time, centered space (FTCS) method with a fully implicit Euler step for stability and solved through the thickness of the coupon,

$$\begin{aligned} \frac{\partial T}{\partial t} &= \alpha \frac{\partial^2 T}{\partial z^2} \\ \frac{T_i^t - T_i^{t-\Delta t}}{\Delta t} &= \alpha \left\{ \frac{T_{i+1}^t - 2T_i^t + T_{i-1}^t}{(\Delta z)^2} \right\} \end{aligned} \tag{23}$$

where i is the node number and the temperatures are evaluated at time t and previous time $t - \Delta t$ (The Crank – Nicolson approach may used instead of backward Euler if more accuracy is desired; however, care must be taken when larger time steps are desired). The recorded front and back temperatures were applied to the front and back faces as boundary conditions and the thermal diffusivity was assumed constant with a value of $\alpha = 1.4 \times 10^{-7}\ \mathrm{m^2/s}$.

$$T\left(t, -H/2\right) = T_f \qquad\qquad T\left(t, +H/2\right) = T_b \tag{24}$$

Eleven nodes were selected (nine interior and two surface) and eleven temperatures produced. These temperatures were averaged to give ten temperature readings which were used in the calculation of the strain components within the CLT algorithm.

In the event that failure was not predicted to occur within the experimental failure time, the time – temperature profile was extended in a manner which best replicates the conditions of the test. The boundary conditions for both types of tests changed to, Constant front face Temperature, T_f

$$T\left(t,-H/2\right)=T_f$$
$$-k\left.\frac{\partial T}{\partial z}\right|_{z=H/2}=h_{\text{conv}}\left(T_\infty-T_b\right)$$

Constant incident heat flux, q_0

$$-k\left.\frac{\partial T}{\partial z}\right|_{z=-H/2}=q_0+h_{\text{conv}}\left(T_\infty-T_f\right)$$
$$-k\left.\frac{\partial T}{\partial z}\right|_{z=H/2}=h_{\text{conv}}\left(T_\infty-T_b\right) \tag{25}$$

With the convection loss coefficients given as $h=30\,\text{W}/(\text{m}^2\cdot\text{C})$ and $T_\infty\approx 28^\circ\text{C}$ which were both estimated as a best fit to the data time – temperature profiles. Figure 40 and Figure 41 show two examples of how the time – temperature profiles were extended using this approach.

4.4.3 The Compression Strength Model with Viscoelasticity

As mentioned, a detailed development of the compression strength model based on the Budiansky and Fleck model is given in [82]. Viscoelasticity within the individual laminate layers is included in the compression strength model by substituting in the in-plane relaxation modulus G_{12}^k to estimate the average compression strength of the composite subject to a state of pure compression loading,

$$\sigma_C^k=G_{12}^k(t,T^k,{}_k\tau_{12}^t)\left[1+n\left(\frac{3}{7}\right)^{\frac{1}{n}}\left(\frac{\bar{\phi}/\gamma_Y(T^k)}{n-1}\right)^{\frac{n-1}{n}}\right]^{-1} \tag{26}$$

Here the superscript k refers to the fact that the average compression strength must be calculated for each ply in the laminate since the in-plane shear relaxation modulus G_{12}^k is dependent on the temperature T^k and the shear stress ${}_k\tau_{12}^t$ in each ply. The knockdown factor values of the strain hardening parameter n (estimated as 5.3) and the fiber imperfection ratio as a function of temperature $\bar{\phi}/\gamma_Y$ (with $\bar{\phi}\approx 10^\circ$) were found from a Ramberg – Osgood analysis of strength data for shear coupons ($[\pm 45^\circ]_{2S}$).

4.4.4 Determination of the Viscoelastic, Viscoplastic Shear Modulus

In a previous paper [82] the in-plane shear relaxation modulus G_{12}^{k} was calculated through an approximate interconversion method first suggested by Leaderman [91] and described by Ferry [86] and Park and Schapery [92]. The expression is simply stated as,

$$G_{12}^{k}(t,T^{k},{}_{k}\tau_{12}^{t})=\begin{cases}\dfrac{\sin m^{k}(t)\pi}{m^{k}(t)\pi\, S_{66}^{k}(t,T^{k},{}_{k}\tau_{12}^{t})} & 0<m^{k}(t)<1\\ \dfrac{1}{S_{66}^{k}(t,T^{k},{}_{k}\tau_{12}^{t})} & m^{k}(t)\approx 0\end{cases} \tag{27}$$

The shear compliance is calculated as,

$$S_{66}^{k}(t,T^{k},{}_{k}\tau_{12}^{t})=g_{0}^{k}(T^{k},{}_{k}\tau_{12}^{t})S_{0}+\frac{{}_{k}\gamma_{12}^{\mathrm{VE}}(t,T^{k},{}_{k}\tau_{12}^{t})+{}_{k}\gamma_{12}^{\mathrm{VP}}(t,T^{k},{}_{k}\tau_{12}^{t})}{{}_{k}\tau_{12}^{t}}=\frac{{}_{k}\gamma_{12}^{t}}{{}_{k}\tau_{12}^{t}} \tag{28}$$

where ${}_{k}\gamma_{12}^{t}$ is given by Eq. (21). The local slope m^k in each ply is given by the expression,

$$m^{k}(t)=\frac{\log_{10}\left(S_{66}^{k}(t,T_{t}^{k},{}_{k}\tau_{12}^{t})\right)-\log_{10}\left(S_{66}^{k}(t-\Delta t,T_{t-\Delta t}^{k},{}_{k}\tau_{12}^{t-\Delta t})\right)}{\log_{10}\left(\psi^{k}(t,T_{t}^{k},{}_{k}\tau_{12}^{t})\right)-\log_{10}\left(\psi^{k}(t-\Delta t,T_{t-\Delta t}^{k},{}_{k}\tau_{12}^{t-\Delta t})\right)} \tag{29}$$

The reduced time $\psi^{k}(t,T^{k},{}_{k}\tau_{12}^{t})$ in Eq. (29) is represented by the following integral,

$$\begin{aligned}\psi^{k}&=\psi^{k}(t,T^{k},{}_{k}\tau_{12}^{t})=\int_{0^-}^{t}\frac{d\xi}{{}_{k}a_{T}^{t}(T^{k})a_{\sigma}^{t}(T^{k},{}_{k}\tau_{12}^{t})}\\ \psi^{t}&=\psi^{t-\Delta t}+\Delta\psi^{t}\\ \Delta\psi^{k}(t,T^{k},{}_{k}\tau_{12}^{t})&\cong\frac{1}{2}\left(\frac{1}{{}_{k}a_{T}^{t}(T_{t}^{k})\,{}_{k}a_{\sigma}^{t}(T_{t}^{k},{}_{k}\tau_{12}^{t})}+\frac{1}{{}_{k}a_{T}^{t-\Delta t}(T_{t-\Delta t}^{k})\,{}_{k}a_{\sigma}^{t-\Delta t}(T_{t-\Delta t}^{k},{}_{k}\tau_{12}^{t-\Delta t})}\right)\Delta t\end{aligned} \tag{30}$$

and is updated recursively using the trapezoidal formula. Though this interconversion method worked well in a previous paper [82], fluctuations in the temperature data T^k caused up and down fluctuations in the shear compliance $S_{66}^{k}(t,T^{k},{}_{k}\tau_{12}^{t})$ in time. As a result the local slope m^k of Eq. (29) did not obey the restrictions of Eq. (27) and the interconversion method was abandoned in favor of the reciprocal relationship. This of course will give a relaxation modulus estimate larger than the exact value; however, it should only introduce a 5% to 10% error in the leathery temperature region (the vicinity of T_g) and should not have a profound effect on the model's ability to predict compression rupture lifetimes.

4.4.5 The Viscoelastic and Viscoplastic Recursion Formulas

The expressions for the non-linear viscoelastic and viscoplastic strains represented in Eq. (22) are easily evaluated if the stress history is given as a constant creep stress even with varying temperatures. However, in practice the state of stress in a laminate will vary continuously in time. Therefore the integrals of Eq. (22) must be evaluated under conditions of a continuously varying stress history. The non-linear viscoelastic hereditary integral is the most difficult to evaluate and several methods will be presented to approximate it. The non-linear viscoplastic integral is not a hereditary integral and may be evaluated in the same manner as the reduced time of Eq. (30).

There are a number of ways to evaluate the non-linear Schapery hereditary integral of Eq. (22). All involve approximating a continuously varying stress history as a series of discrete steps where the state of stress is considered constant over a time $t - \Delta t$ to t. Dillard et al. [79] and Tuttle and Brinson [42] derived a recursion formula based on a power law form for the transient compliance function. Since the power law kernel function requires the stress history to be stored for all subsequent time step evaluations, this type of kernel function has been replaced by a generalized Kelvin or Prony series which only requires knowledge of the previous time step stress and viscoelastic strain. Henriksen [93], using the Schapery's non-linear viscoelastic hereditary integral (Eq.

(22)), developed a recursion formula based on a Prony series representation of the transient compliance which has since been used by Roy and Reddy [94], Pasricha et al. [55], Lai and Bakker [95], and more recently in Haj-Ali and Muliana [96] (Guedes et al. [56] also has an alternate derivation of what is essentially the same approach). Another recursion formula was developed by Zienkiewicz et al. [58] and extended by Gramoll et al. [47] for non-linear orthotropic materials and is based on approximating the exact solution to the basic non-linear differential equation governing a Kelvin – Voigt element.

The derivation of Henriksen's recursion formula may be found in [93] and supplemented by [94] and is stated for application to an individual ply *k* as,

$$ {}_k\gamma_{12}^{\mathrm{VE}}(t, T^k, {}_k\tau_{12}^t) = {}_k g_1^t(T^k, {}_k\tau_{12}^t)\, {}_k g_2^t(T^k, {}_k\tau_{12}^t) \sum_l^m S_l\, {}_k\tau_{12}^t + {}_k g_1^t(T^k, {}_k\tau_{12}^t) \sum_l^m S_l\, {}_k q_l^t \quad (31) $$

Again ${}_k\tau_{12}^t$ is the current shearing stress for time *t* and S_l are the compliance coefficients for the Prony series. The hereditary strains for each ply are contained in ${}_k q_l^t$ which is updated by the following recursion formula,

$$ {}_k q_l^t = e^{-\lambda_l \Delta\psi_k^t}\, {}_k q_l^{t-\Delta t} + \left({}_k g_2^t(T^k, {}_k\tau_{12}^t)\, {}_k\tau_{12}^t - {}_k g_2^{t-\Delta t}(T^k, {}_k\tau_{12}^{t-\Delta t})\, {}_k\tau_{12}^{t-\Delta t} \right) {}_k\Gamma_l^t \quad (32) $$

where ${}_k\Gamma_l^t$ is the relaxation coefficient for the l^{th} term in the hereditary strain series and is calculated as,

$$ {}_k\Gamma_l^t = \frac{\left(1 - e^{-\lambda_l \Delta\psi_k^t}\right)}{\lambda_l \Delta\psi_k^t} \quad (33) $$

Here $\Delta\psi_k^t$ is the change in the reduced time over the current time step and is given by Eq. (30) and λ_l is the reciprocal of the retardation times τ_l. Equations (31) through (33) provide a concise set of equations for evaluating the non-linear viscoelastic strain for a given shear stress ${}_{k}\tau_{12}^{t}$, time t, and temperature T^k in each ply.

Another method for evaluating the non-linear viscoelastic strain was presented by Zienkiewicz et al. [58] for linearly viscoelastic isotropic materials and extended by Gramoll et al. [47] to non-linear, orthotropic materials. The method involves approximating the differential equation of a Kelvin – Voigt element. The derivation presented in Gramoll et al. of the recursion formula started with a linear viscoelastic Kelvin – Voigt element; however, in order to derive a recursion formula which is more relevant to the current non-linear viscoelastic analysis, we will start with a non-linearized Kelvin – Voigt element. The spring and dashpot of Figure 42 are made non-linear by the two functions α and β which are both functions of applied stress and temperature. Requiring equilibrium for a single stressed non-linear Kelvin – Voigt element and substituting in corresponding constitutive equations for the spring and dashpot gives,

$$\begin{aligned} \sigma_{\text{Spring}} + \sigma_{\text{Dashpot}} &= \sigma \\ \alpha(T,\sigma)E\varepsilon + \beta(T,\sigma)\eta\dot{\varepsilon} &= \sigma \end{aligned} \tag{34}$$

Equation (34) can be rearranged to yield the governing differential equation,

$$\dot{\varepsilon} = \frac{1}{\beta(T,\sigma)\eta}\sigma - \frac{\alpha(T,\sigma)E}{\beta(T,\sigma)\eta}\varepsilon \tag{35}$$

which has the exact solution given by,

$$\varepsilon(t,T,\sigma) = \frac{\sigma}{\alpha(T,\sigma)E}\left(1 - e^{-\frac{\alpha(T,\sigma)E}{\beta(T,\sigma)\eta}t}\right) \tag{36}$$

If there are a series of non-linear Kelvin – Voigt elements as in Figure 43, the solutions of Eq. (36) can be summed to yield the total strain,

$$\varepsilon_{\text{Total}}(t,T,\sigma)=\frac{1}{\alpha(T,\sigma)}\sum_{l}^{m}S_l\left(1-e^{-\frac{\alpha(T,\sigma)}{\beta(T,\sigma)}\lambda_l t}\right)\sigma \tag{37}$$

where S_l is the reciprocal of E_l and λ_l is the reciprocal of the retardation times τ_l and σ, α and β are the same for each Kelvin element of the generalized Kelvin or Prony series. The non-linear functions α and β may now be recast in terms of their Schapery model equivalents (*refer to next section for a special note regarding this step*),

$$\begin{aligned}\frac{1}{\alpha(T,\sigma)}&\equiv g_1(T,\sigma)\\ \frac{\alpha(T,\sigma)}{\beta(T,\sigma)}&\equiv\frac{1}{a_T(T)a_\sigma(T,\sigma)}\end{aligned} \tag{38}$$

Returning to the differential equation Eq. (35) for a single non-linear Kelvin – Voigt element *l*,

$$\dot{\varepsilon}_l=\frac{g_1(T,\sigma)\lambda_l S_l}{a_T(T)a_\sigma(T,\sigma)}\sigma-\frac{\lambda_l}{a_T(T)a_\sigma(T,\sigma)}\varepsilon_l \tag{39}$$

A recursive solution to Eq. (39) may be developed by approximating the derivative of the strain and casting the equation as an implicit backward Euler step [97],

$$\begin{aligned}\dot{\varepsilon}_l&\approx\frac{\varepsilon_l^t-\varepsilon_l^{t-\Delta t}}{\Delta t}\\ \underbrace{\frac{\varepsilon_l^t-\varepsilon_l^{t-\Delta t}}{\Delta t}}_{\frac{y^{i+1}-y^i}{h}}&\approx\underbrace{\frac{g_1(T,\sigma^t)\lambda_l S_l}{a_T(T)a_\sigma(T,\sigma^t)}\sigma^t-\frac{\lambda_l}{a_T(T)a_\sigma(T,\sigma^t)}\varepsilon_l^t}_{f(t_{i+1},y^{i+1})}\end{aligned} \tag{40}$$

Equation (40) is an approximation to the exact solution of Eq. (36) and represents an implicit (unconditionally stable) first order recursive formula for calculating the viscoelastic strain. If more accuracy is required, Eq. (40) may be replaced by a higher order implicit method such as the modified Euler method (which is still unconditionally stable); however, care must be taken to make certain that the linear approximation of the trapezoidal formula to the function remains valid for a given time step size. Rearranging terms in Eq. (40) and solving for the current viscoelastic strain,

$$
\begin{aligned}
\varepsilon_l^t &= \frac{\Delta t\ g_1^t}{(\mu_l^t + \Delta t)} S_l\,\sigma + \frac{\mu_l^t}{(\mu_l^t + \Delta t)} \varepsilon_l^{t-\Delta t} \\
\mu_l^t &= \frac{a_T(T) a_\sigma(T, \sigma^t)}{\lambda_l}
\end{aligned}
\tag{41}
$$

where μ_l^t is introduced for convenience. In order to calculate the total non-linear viscoelastic strain to time *t*, the individual strain contributions of Eq. (41) need only be summed together to yield,

$$
{}_t\gamma_{12}^{\mathrm{VE}} = \sum_l^m \frac{\Delta t\ g_1^t}{(\mu_l^t + \Delta t)} S_l\,\tau_{12}^t + \sum_l^m \frac{\mu_l^t}{(\mu_l^t + \Delta t)}\, {}_{t-\Delta t}^{\quad l}\gamma_{12}^{\mathrm{VE}} \tag{42}
$$

Equation (42) is an alternate method to Henriksen (Eqs. (31) - (33)) for calculating the viscoelastic strain and may be generalized to account for the orthotropic symmetry of a laminate for application in CLT. Equation (42) is also used in Eq. (28) for calculating the shear creep compliance $S_{66}^k(t, T^k, {}_k\tau_{12}^t)$.

In contrast the evaluation of the non-linear viscoplastic strain is relatively straight forward. The viscoplastic Zapas – Crissman model was first used by Tuttle et al. [54] and more recently by Guedes et al. [56, 57] to model non-linear viscoplastic effects. The recursion formula presented by Tuttle et al. [54], however, is unsuitable for our application and a slightly different formula was derived for the integral of Eq. (22) using the trapezoidal formula,

$$
\begin{aligned}
{}_k\gamma_{12}^{\mathrm{VP}}(t,T^k,{}_k\tau_{12}^t) &= \left(\underbrace{\int_{0^-}^{t} C(T^k)\,{}_k\tau_{12}^{N(T^k)}(s)ds}_{{}_kf_t^{\mathrm{VP}}} \right)^{\bar{n}(T^k)} \\
{}_kf_t^{\mathrm{VP}} &= {}_kf_{t-\Delta t}^{\mathrm{VP}} + {}_k\Delta f_t^{\mathrm{VP}} \\
{}_k\Delta f_t^{\mathrm{VP}} &\cong \frac{1}{2}\left(C(T_t^k)\left({}_k\tau_{12}^t\right)^{N(T_t^k)} + C(T_{t-\Delta t}^k)\left({}_k\tau_{12}^{t-\Delta t}\right)^{N(T_{t-\Delta t}^k)} \right)\Delta t
\end{aligned}
\tag{43}
$$

The only complication in Eq. (43) is that the value of $\bar{n}$ may depend on temperature; however, this is usually circumvented by understanding that the temperature dependence is not very strong and that $\bar{n}$ may be averaged for the given temperatures in each ply. By using a single average value $\bar{n}$ in Eq. (43) the viscoplastic strain will always increase with increasing stress and temperature and never appear to decrease or recover. The viscoplastic strain of Eq. (43) is directly substituted into Eq. (28) to calculate the shear creep compliance $S_{66}^k(t,T^k,{}_k\tau_{12}^t)$.

4.4.6 Comparison of the Viscoelastic Recursion Formulas

There are two recursion methods presented in this paper for the non-linear viscoelastic strain. Both have their advantages and disadvantages but the key difference between them was found to be stability related. As briefly mentioned the explicit CLT algorithm of Dillard et al. [79, 80] with Henriksen suffered insurmountable stability issues and was abandoned. The backward stepping approach of Gramoll et al. [47] proved to be more successful and is adopted for the current study. In their paper Gramoll et al. claim that Henriksen's formula represents an explicit forward step which is only conditionally stable (i.e. time step size is limited) and is a key culprit in the instability and/or eventual divergence of the explicit CLT method of Dillard. An additional problem we observed with Henriksen's formula centers on the evaluation of the relaxation coefficient of Eq. (33). This expression suffers from finite precision error for very small values of the change in the reduced time $\Delta\psi_k^t$ and the reciprocal of the retardation times λ_l such that for some of the l components the computational program is forced to evaluate,

$$\begin{aligned} &\lambda_l \Delta\psi_k^t \approx 0^+ \\ &{}_k\Gamma_l^t \approx \frac{\left(1-e^{-\lambda_l \Delta\psi_k^t}\right)}{\lambda_l \Delta\psi_k^t} \approx \frac{1-1}{(\approx 0^+)} \end{aligned} \tag{44}$$

where the superscript "+" indicates that the number is close to zero but not negative. This consequence was found to occur at temperatures below the reference temperature T_R (110°C) and Eq. (33) inadvertently zeroed some of the l terms in ${}_k\Gamma_l^t$ and Henriksen (and also Guedes et al. [56]) gave incorrect results whenever a change in stress history was encountered. This problem was not seen in the backward Euler method proposed by Zienkienwicz et al. [58] and Gramoll et al. [47]; however, care must be taken with this approach to make it compatible with a non-linear data reduction using the Schapery model. Equations (34) through (42) do ***not*** represent a rigorous derivation of a recursion formula for the Schapery viscoelastic strain using the backward Euler method especially noticing the absence of vertical shift g_2. The equations worked for this study because we modeled only creep and not creep recovery behavior and therefore g_2 was set to one for all temperatures and stresses. The remaining parameters g_0, g_1, and a_σ are adequate for representing the non-linear viscoelastic strain whose recursion formula is conveniently given by Eq. (42). If g_2 is acting, a more rigorous derivation of Eq. (42) is necessary or simply use Henriksen's method.

4.4.7 The Implicit CLT Algorithm

The main goal of current work is to develop a mechanistically based model based on first principles to characterize the non-linear viscoelastic behavior and predict delayed failure of a glass reinforced vinyl ester composite subject to fire loading conditions. For an orthotropic laminate subject to a constant compressive load and a temperature profile, knowledge of both the time – temperature profile, an estimation of the state of stress in each ply, and application of these two inputs to the Budiansky and Fleck failure criterion are required to solve the problem. A finite element implementation will eventually be developed to solve the structural problem; however, CLT gives a simple, straight forward method for calculating the state of stress for now and validating the modeling approach.

A CLT based approach for calculating the long term viscoelastic response and delayed failure of polymer matrix composites was developed here at Virginia Tech by Dillard and Brinson [78]. A detailed description of this forward explicit CLT algorithm may be found in Dillard [78-80] and Tuttle and Brinson [42]. Dillard et al. used the non-linear Findley model with a viscoelastic recursion based on a power law kernel within CLT to predict long term viscoelastic response and delayed failure of a graphite/epoxy composite. Tuttle and Brinson performed a similar analysis except used the Schapery model to describe the non-linear viscoelastic behavior. Ha and Springer [53] used the Schapery model with a Prony series kernel and a viscoplastic strain within CLT to predict the response of a graphite epoxy composite under conditions of changing stress and temperature. Tuttle et al. [54], Pasricha [98] and Guedes et al. [56, 57] continued with this approach except used the Zapas – Crissman model for the viscoplastic strain component.

Dillard [79] was the only author to mention stability problems with the forward explicit CLT algorithm. Dillard reported that the convergence characteristics of the algorithm depended on the time-step size, the type of laminate considered (worse for two angle laminates), convergence to the correct state of stress was required if stresses changed significantly through the laminate (such as loading or discounting a ply), and on modifying the stress inputs to the non-linear viscoelastic functions using a pseudo-central difference technique. Gramoll et al. [47] continued the work of using CLT to calculate the long term viscoelastic response of polymer matrix composites, but had similar problems with the forward explicit CLT algorithm and eventually developed an implicit method (the non-linear differential equation method – NDEM) which is unconditionally stable and allows modeling of laminate strain and stress out to very long times regardless of time step size. The implicit CLT algorithm is simple and can easily be adapted to orthotropic laminates. The stress – strain equations of CLT and the equilibrium equations are not solved using the A-B-D matrix, but are solved with the Newton – Raphson method which has better convergence properties. The method of Gramoll et al. was applied to the time – temperature profile and was successful; the CLT algorithm converged and produced results. We now present some key steps in the solution method including modification of the backward Euler method for orthotropic laminates, development of the non-linear system of equations, the Newton – Raphson method, and application of the Budiansky and Fleck failure criterion (for additional information on stability issues and a verification of the implicit method see Gramoll et al [47]).

4.4.8 Prediction of Laminate Failure using Implicit CLT

The non-linear system of equations for CLT consists of the stress – strain relations of Eq. (21), the Kirchhoff hypothesis, and the force and moment equilibrium equations (see Figure 44 for a flowchart of the solution method). The total strain in global coordinates for each ply is related to the mid-plane strains and curvatures for the laminate,

$$\begin{Bmatrix} \varepsilon_x^0(t) \\ \varepsilon_y^0(t) \\ \gamma_{xy}^0(t) \end{Bmatrix} + \bar{z}_k \begin{Bmatrix} \kappa_x^0(t) \\ \kappa_y^0(t) \\ \kappa_{xy}^0(t) \end{Bmatrix} = \begin{Bmatrix} \varepsilon_x(t) \\ \varepsilon_y(t) \\ \gamma_{xy}(t) \end{Bmatrix}_k \tag{45}$$

where $\bar{z}_k$ is the location from the mid-plane of the laminate to the midpoint of each ply *k*. A transformation of Eq. (21) to global coordinates gives,

$$\begin{gathered} \begin{Bmatrix} \varepsilon_x(t) \\ \varepsilon_y(t) \\ \gamma_{xy}(t) \end{Bmatrix}_k = \overline{C}_k^t \begin{Bmatrix} \sigma_x(t) \\ \sigma_y(t) \\ \tau_{xy}(t) \end{Bmatrix}_k + \begin{Bmatrix} \alpha_x \\ \alpha_y \\ \alpha_{xy} \end{Bmatrix}_k \Delta T^k + \begin{Bmatrix} \varepsilon_x^{\mathrm{VE}}(t) \\ \varepsilon_y^{\mathrm{VE}}(t) \\ \gamma_{xy}^{\mathrm{VE}}(t) \end{Bmatrix}_k + \begin{Bmatrix} \varepsilon_x^{\mathrm{VP}}(t) \\ \varepsilon_y^{\mathrm{VP}}(t) \\ \gamma_{xy}^{\mathrm{VP}}(t) \end{Bmatrix}_k \\ \overline{C}_k^t = T_k^{\mathrm{T}} \begin{bmatrix} S_{11} & S_{12} & 0 \\ S_{12} & S_{22} & 0 \\ 0 & 0 & g_0^k\left(T^k, {}_k\tau_{12}^t\right) S_0 \end{bmatrix} T_k \end{gathered} \tag{46}$$

where the transformation matrix T_k and its transpose T_k^{T} is used to transform the strains and the instantaneous compliance matrix in the manner of Jones [99]. Additional simplification of Eq. (46) is required for the viscoelastic and viscoplastic terms since both are explicit functions of the current state of stress.

The non-linear viscoelastic recursion formula of Eq. (42) may be rewritten as a matrix equation in global coordinates,

$$
\begin{Bmatrix} {}_{t}\varepsilon_{xy}^{\mathrm{VE}} \\ {}_{t}\varepsilon_{xy}^{\mathrm{VE}} \\ {}_{t}\gamma_{xy}^{\mathrm{VE}} \end{Bmatrix}_k = \sum_{l}^{m} \frac{\Delta t \;\; {}_{k}g_{1}^{t}}{\left({}_{k}\mu_{l}^{t} + \Delta t\right)} {}_{k}\bar{S}_{l} \begin{Bmatrix} \sigma_{x}^{t} \\ \sigma_{y}^{t} \\ \tau_{xy}^{t} \end{Bmatrix}_k + \sum_{l}^{m} {}_{k}E_{l}^{t}
$$

$$
{}_{k}E_{l}^{t} = \frac{{}_{k}\mu_{l}^{t}}{\left({}_{k}\mu_{l}^{t} + \Delta t\right)} \begin{Bmatrix} {}_{t-\Delta t}^{\;\;\;l}\varepsilon_{x}^{\mathrm{VE}} \\ {}_{t-\Delta t}^{\;\;\;l}\varepsilon_{y}^{\mathrm{VE}} \\ {}_{t-\Delta t}^{\;\;\;l}\gamma_{xy}^{\mathrm{VE}} \end{Bmatrix}_k \tag{47}
$$

Here ${}_{k}E_{l}^{t}$ is introduced for convenience, the vector ${}_{t-\Delta t}^{\;\;\;l}\{\varepsilon\}_{k}^{\mathrm{VE}}$ are l components of the previous viscoelastic strain, and ${}_{k}\bar{S}_{l}$ is the transformed compliance matrix for the Prony series compliance coefficients and is an array of $3k \times 3$ matrices,

$$
{}_{k}\bar{S}_{l} = T_{k}^{\mathrm{T}} \begin{bmatrix} 0 & 0 & 0 \\ 0 & 0 & 0 \\ 0 & 0 & S_{l} \end{bmatrix} T_{k} \tag{48}
$$

(Note that the transformed compliance matrix is mostly sparse because only the shear compliance S_{66} is modeled as a Prony series; see Gramoll et al. [47] for a more general treatment). The non-linear viscoplastic strain is also an explicit function of the current state of stress; however, as illustrated in Eq. (43) the stress is the argument of an exponent nested within an integrand. Therefore, Eq. (43) was calculated for each time step and ply, transformed into global coordinates and merged into the vector of knowns as presented below.

Equations (45) through (47) may now be assembled into a non-linear system of equations together with the laminate equilibrium equations using a short hand notation "{}" to represent a vector quantity,

$$
\begin{gathered}
\left\{\varepsilon_0^t\right\}+\bar{z}_1\left\{\kappa_0^t\right\}-\left(\sum_l^m \frac{{}_1g_1^t \Delta t}{\left({}_1\mu_l^t+\Delta t\right)}{}_1\bar{S}_l+\bar{C}_1^t\right){}_1\left\{\sigma^t\right\}=\sum_l^m {}_1E_l^t+{}_1\left\{\varepsilon_{\mathrm{TH}}^t\right\}+{}_1\left\{\varepsilon_{\mathrm{VP}}^t\right\} \\
\left\{\varepsilon_0^t\right\}+\bar{z}_2\left\{\kappa_0^t\right\}-\left(\sum_l^m \frac{{}_2g_1^t \Delta t}{\left({}_2\mu_l^t+\Delta t\right)}{}_2\bar{S}_l+\bar{C}_2^t\right){}_2\left\{\sigma^t\right\}=\sum_l^m {}_2E_l^t+{}_2\left\{\varepsilon_{\mathrm{TH}}^t\right\}+{}_2\left\{\varepsilon_{\mathrm{VP}}^t\right\} \\
\vdots \\
\left\{\varepsilon_0^t\right\}+\bar{z}_k\left\{\kappa_0^t\right\}-\left(\sum_l^m \frac{{}_kg_1^t \Delta t}{\left({}_k\mu_l^t+\Delta t\right)}{}_k\bar{S}_l+\bar{C}_k^t\right){}_k\left\{\sigma^t\right\}=\sum_l^m {}_kE_l^t+{}_k\left\{\varepsilon_{\mathrm{TH}}^t\right\}+{}_k\left\{\varepsilon_{\mathrm{VP}}^t\right\} \\
\sum_k t_k\,{}_k\left\{\sigma^t\right\}=\{N\} \\
\sum_k t_k\bar{z}_k\,{}_k\left\{\sigma^t\right\}=\{M\}
\end{gathered} \tag{49}
$$

where t_k is the thickness of each ply and "TH" and "VP" indicate the thermal and viscoplastic components of the strain. Note here that the forward explicit CLT algorithm substitutes the stress – strain equations into the equilibrium equations to form the A-B-D matrix for the laminate and solves in the familiar way. However, the implicit CLT algorithm uses the Newton – Raphson method to converge upon the solution; a method which deals more effectively with the fact that so many of the coefficient terms in Eq. (49) depend on the current shear stress ${}_k\tau_{12}^t$.

The left hand side (LHS) of Eq. (49) may be recognized as a coefficient matrix $\mathbf{A}^t$ ($3k + 6 \times 3k + 6$) and the right hand side (RHS) as a vector of knowns $\underline{b}^t$ ($3k + 6 \times 1$) with the solution vector $\underline{x}^t$ given as,

$$
\underline{x}^t=\left\lfloor {}^t\varepsilon_x^0,{}^t\varepsilon_y^0,{}^t\gamma_{xy}^0,{}^t\kappa_x^0,{}^t\kappa_y^0,{}^t\kappa_{xy}^0,{}_1\sigma_x^t,{}_1\sigma_y^t,{}_1\tau_{xy}^t,{}_2\sigma_x^t,{}_2\sigma_y^t,{}_2\tau_{xy}^t,\cdots,{}_k\sigma_x^t,{}_k\sigma_y^t,{}_k\tau_{xy}^t\right\rfloor^T \tag{50}
$$

The non-linear system $\underline{F}^t$ is written in the form,

$$
\underline{F}^t=A^t\cdot\underline{x}^t-\underline{b}^t=0 \tag{51}
$$

A modified Newton – Raphson method is used to iteratively solve Eq. (51) with an initial guess for $\underline{x}^t$ (typically the last time step solution). The modified Newton – Raphson method described here follows that of Bathe [100] in which the Jacobian of the non-linear system is calculated by a central difference approximation only once for an accepted equilibrium state (i.e. the last solution) in the manner of,

$$
\begin{aligned}
\underline{F}_i^t &= A_i^t \cdot \underline{x}_i^t - \underline{b}_i^t \\
J_i^t &= \frac{\partial \underline{F}_i^t}{\partial \underline{x}_i^t} \\
J_a^t &= J_0^t \\
\underline{x}_{i+1}^t - \underline{x}_i^t &= -\left[J_a^t\right]^{-1} \cdot \underline{F}_i^t
\end{aligned}
\tag{52}
$$

The iterative procedure of Eq. (52) is repeated until an acceptable tolerance in $\underline{x}^t$ *and* $\underline{F}^t$ is satisfied. It should be noted here that both the coefficient matrix $\mathbf{A}^t$ and the vector of knowns $\underline{b}^t$ depend on the current solution vector $\underline{x}^t$. This could cause convergence issues for the Newton – Raphson method of Eq. (52) in which the iteration may diverge. Problems with convergence and how they were solved is discussed in more detail in the results and discussion section; however, for the most part a solution was always achieved.

Once a solution was achieved for a particular time step, the shear creep compliance $S_{66}^k(t, T^k, {}_k\tau_{12}^t)$ was calculated using Eq. (28) and the in-plane shear relaxation modulus $G_{12}^k(t, T^k, {}_k\tau_{12}^t)$ found by taking the reciprocal. The average compression strength was calculated in each ply by substituting the relaxation shear modulus $G_{12}^k(t, T^k, {}_k\tau_{12}^t)$ into Eq. (19). The failure criterion was applied to the laminate by integrating the compression strengths through thickness,

$$\sigma_C^k = G_{12}^k(t, T^k, {}_k\tau_{12}^t)\left[1 + n\left(\frac{3}{7}\right)^{\frac{1}{n}}\left(\frac{\bar{\phi}/\gamma_Y(T^k)}{n-1}\right)^{\frac{n-1}{n}}\right]^{-1}$$
$$X_{\text{Laminate}}^C = \frac{1}{H}\int_{-H/2}^{H/2} \sigma_C^k \, dz \tag{53}$$
$$X_{\text{Laminate}}^C < \bar{\sigma}_x \left(= N_x/H\right)$$

and comparing the average laminate compression strength to the applied compression stress. Failure was predicted to occur when the average laminate compression strength was less than the applied compression stress and the numerical iteration stopped. This method of predicting laminate failure using the average compression strength is simplest to implement and avoids issues regarding progressive discount of critical layers in the laminate. Focusing on individual layers using a more conventional discount approach is problematic because it is difficult to decide on an appropriate discount criterion for the discounted layer. Another more serious issue with conventional discount is that the resulting stress redistribution in the laminate will cause the non-linear solver to diverge. The predicted times to failure for the constant heat flux tests are presented in Figure 45 and Table 3 and the times to failure for the tests equilibrated at front face temperatures of 125°C, 130°C, and 135°C are given in Figure 46 and Table 4.

4.5 Results and Discussion

A previous paper by Bausano et al. [83] used CLT and finite element analysis (FEA) to predict the compression creep rupture of pultruded laminates of an E-glass/vinyl ester composite using progressive thermal softening to account for the change in material properties with elevating temperatures. The results largely under predicted the actual lifetimes, especially the lower heat flux tests. In this paper the combination of matrix viscoelasticity (a time dependent shear modulus) and progressive thermal softening (temperature dependencies of other time independent properties) corrected the short fall of the previous analysis. As can be seen in both Figure 45 and Figure 46, matrix viscoelasticity controls delayed failure of a glass/vinyl ester composite in the vicinity of T_g. However, at higher temperatures such as those encountered in the 15kW/m^2 and 20 kW/m^2 tests, thermal softening controls delayed failure.

Though the results of Figure 45 and Figure 46 are regarded as excellent, there are some limitations which include the effectiveness of the non-linear solver and problems with the time – temperature profiles. Although the Newton – Raphson method has robust convergence properties, the viscoelastic shear modulus and the temperature dependencies of the stiffnesses, thermal properties and the compression strength parameters exceeded the solvers ability to converge on a solution. To improve convergence many material properties were fixed at their room temperature values and the viscoplastic strain component was omitted. Although these decisions may compromise the analysis, it is apparent from the successful predictions that matrix viscoelasticity and thermal softening of the compression strength parameters control the elevated temperature delayed failure. Moreover, omitting some of the weak temperature dependencies for this temperature range is very reasonable and certainly simplifies the analysis. Some of these exclusions could possibly be corrected by adding line search/backtracking functionality, using an "accelerated" convergence scheme or replacing Newton – Raphson by a more sophisticated Broyden – Fletcher – Goldfarb – Shano (BFGS) method.

Issues with the time – temperature profiles are also discussed in a previous paper [82]. Some of these issues regarding extending the profiles are corrected in this paper with the 1D FTCS solutions to the heat equation which worked quite well. However, the main problems of reproducibility and thermocouple reliability persist. When performing replicate tests, the loading was replicated but the time – temperature profiles were often quite different. In the case of the higher heat fluxes front thermocouple failure or spurious readings resulted. Since the analysis is driven by elevated temperature, the tests which became sufficiently hot through thickness were the most likely to fail more quickly and be successfully predicted (such as the 130°C and 135°C tests) than the tests which stayed relatively cool (such as some of the 125°C tests). Use of a silicon resistance heater attached to the front surface with insulation on the back surface and sides of the coupon would provide better control and replication of the profile temperatures over the IR lamp. The more stable time – temperature profiles would undoubtedly provide better temperature profile data for model validation.

4.6 Conclusions

Compression creep rupture tests subject to one sided heating are successfully predicted for a constant heat flux and front face temperature. The modeling approach which includes both non-linear viscoelasticity and progressive thermal softening for the prediction of delayed failure is validated in the vicinity of T_g. The Budiansky and Fleck failure criterion is successful extended to include matrix viscoelasticity and plasticity to predict global failure. The state of stress in each ply is calculated by extending the implicit CLT algorithm of Gramoll et al. [47] to include laminate curvatures and the TTSSP accelerated characterization scheme. The implicit CLT algorithm is superior in this application due to the unconditionally stability of the viscoelastic recursion and the convergence properties of the Newton – Raphson method. Even though there are some limitations to the analysis, the structural model is validated by the one sided heating data and provides a useful tool for evaluating the structural performance of polymer matrix composites under fire loading conditions. Future work will involve implementing viscoelasticity and progressive thermal softening within a commercially available FEA code to predict structural limit states for a laminated structure.

4.7 Acknowledgements

The authors acknowledge the support of the Office of Naval Research, Code 334, Award # N00014-04-1-0195. We graciously thank Dave Dillard and Kurt Gramoll for providing their original computational codes for study and comparison. John Bausano and Brian Clements are recognized for coupon preparation and conducting the one-sided heat flux tests. We also thank Seemans Composites, Inc. for manufacturing the composite panels used in this study.

4.8 Figures

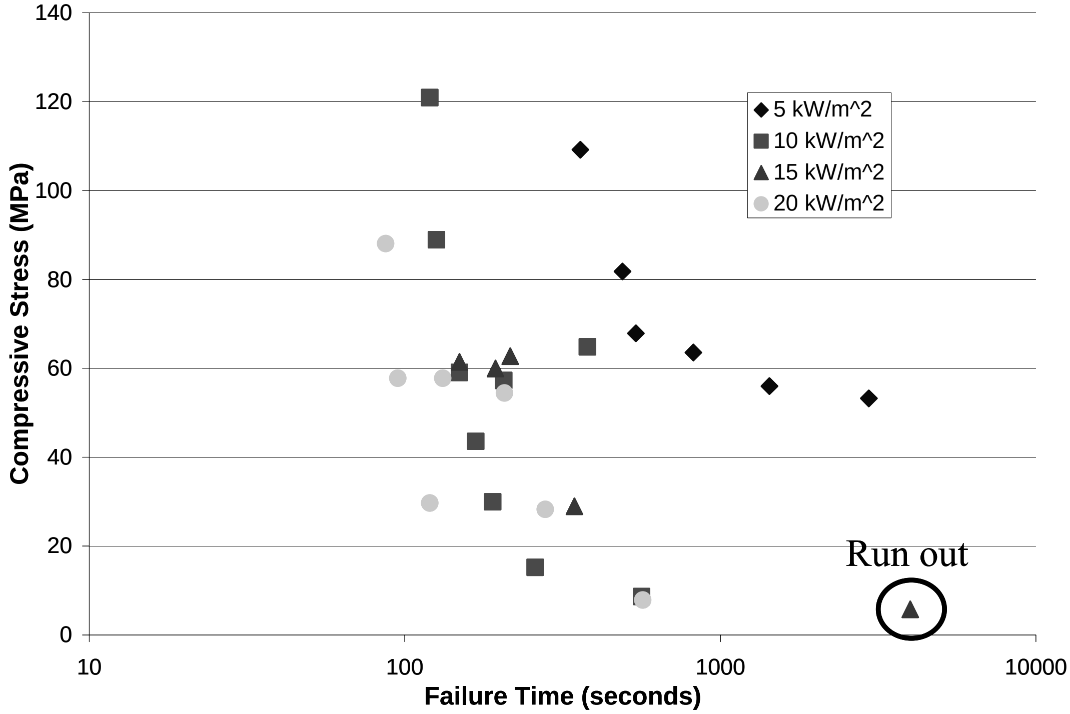

Figure 35: Compression creep failure of Vetrotex 324/Derakane 510A – 40 laminate ([0/+45/90/-45/0]$_S$) subject to a one sided constant heat flux

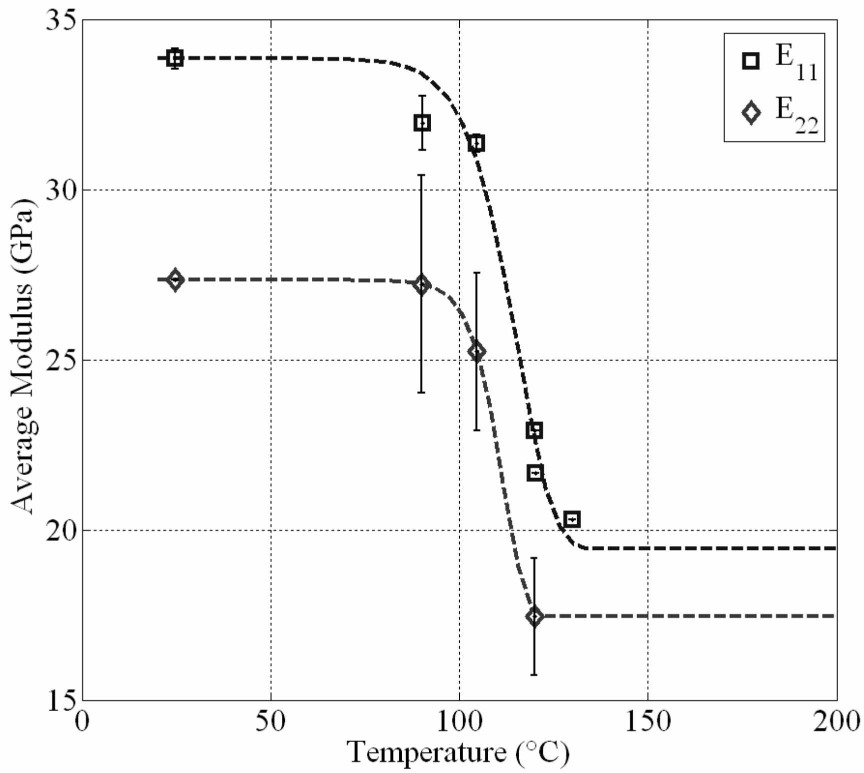

Figure 36: E_{11} and E_{22} as a function of temperature for Vetrotex 324/Derakane 510A – 40 (dashed lines are fits and error bars indicate the standard deviation).

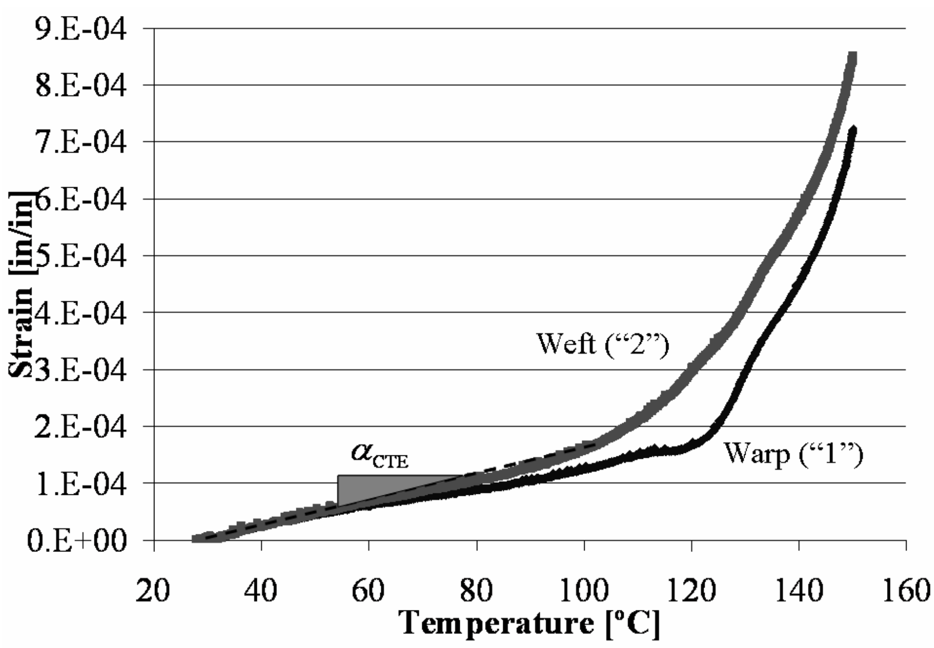

Figure 37: Thermal strain versus temperature for thick block sample of Vetrotex 324/Derakane 510A – 40.

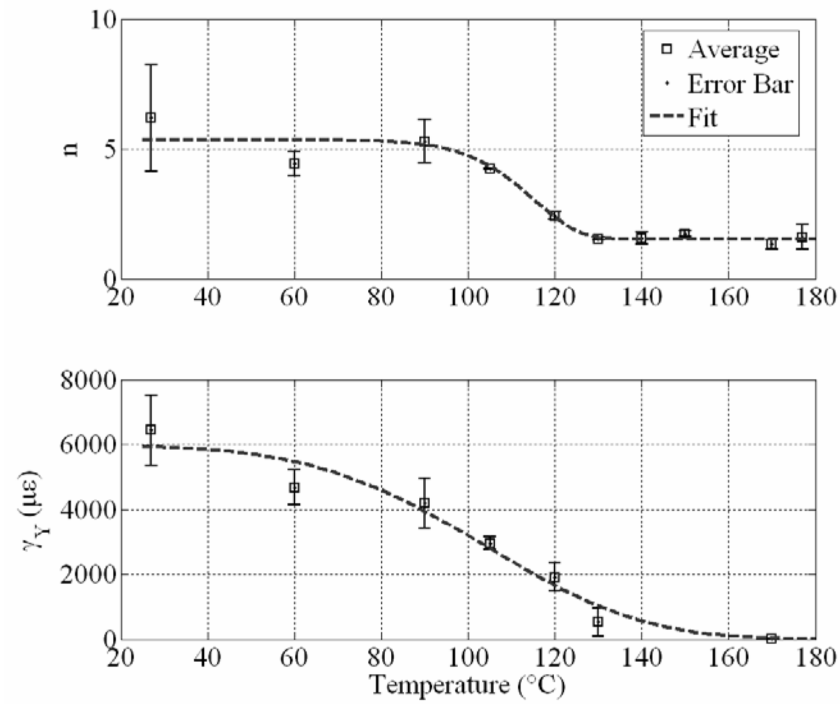

Figure 38: Strain hardening parameter and yield shearing strain versus temperature. Results from fits of the Ramberg – Osgood equation to stress – strain data for shear coupons of Vetrotex 324/Derakane 510A – 40.

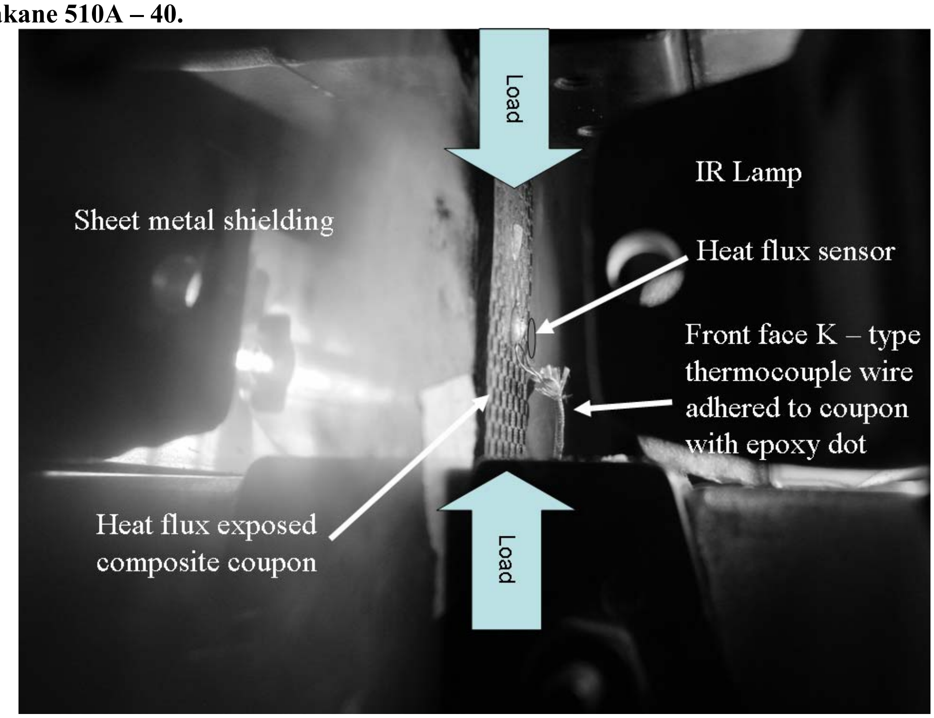

Figure 39: One sided heat flux experimental set-up. Image shows close-up view of a coupon seated in servo-hydraulic grips subject to heat flux from an IR lamp.

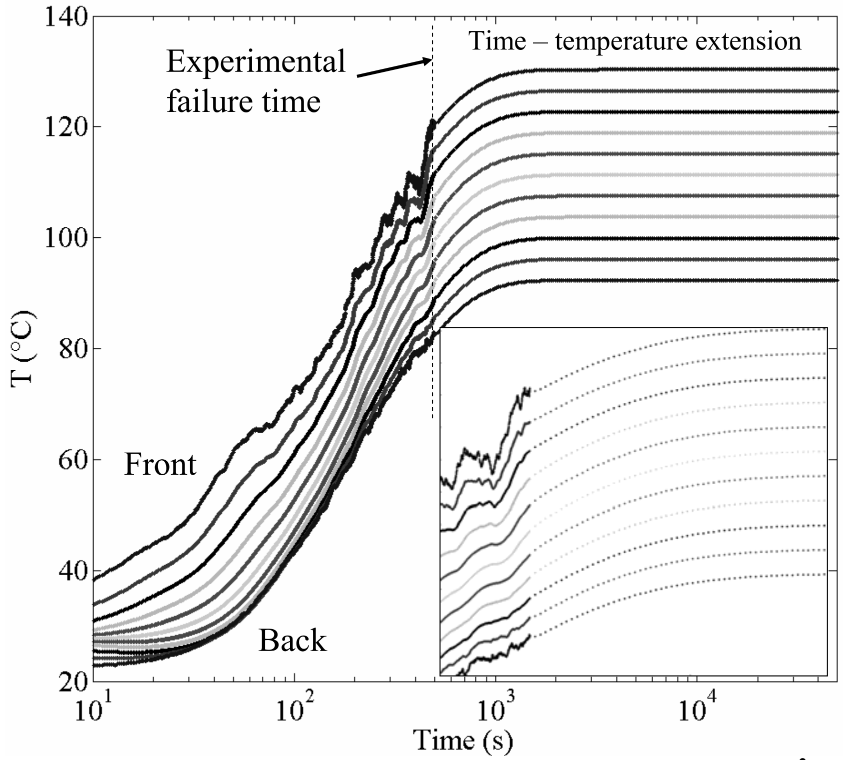

Figure 40: Time – temperature profile extension for constant heat flux test 5 kW/m^2 at a compressive load of 2800 lb.

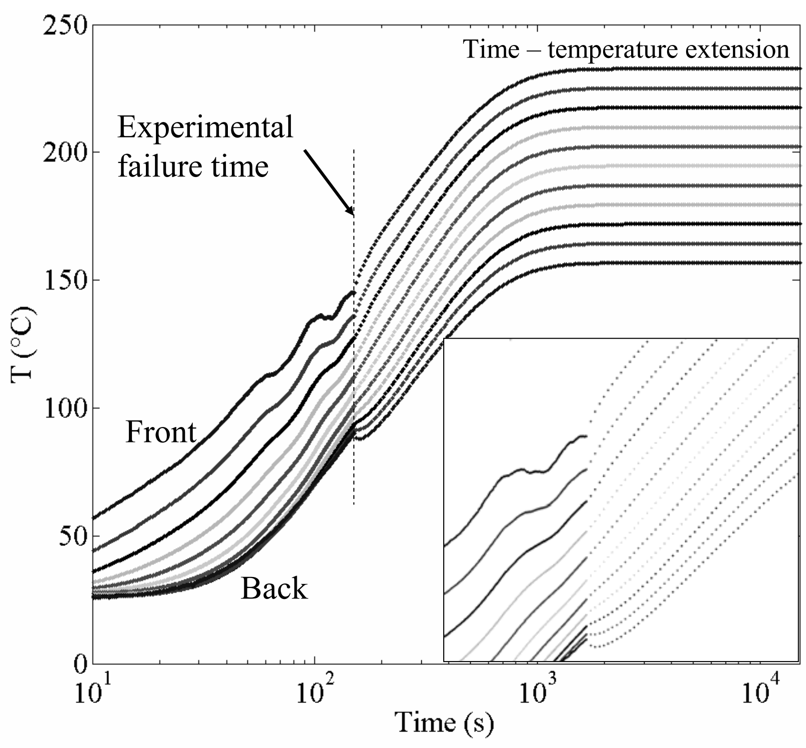

Figure 41: Time – temperature extension for a constant heat flux 10 kW/m^2 test at a compressive load of 3000 lb.

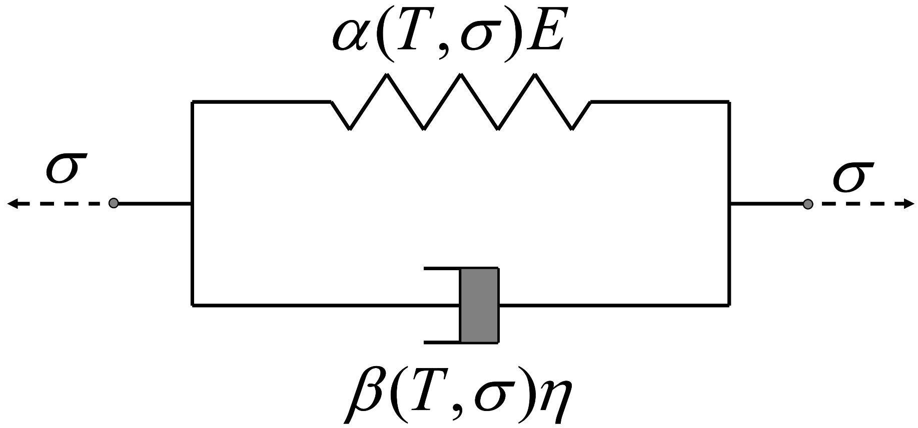

Figure 42: Non-linear Kelvin – Voigt element mechanical analog.

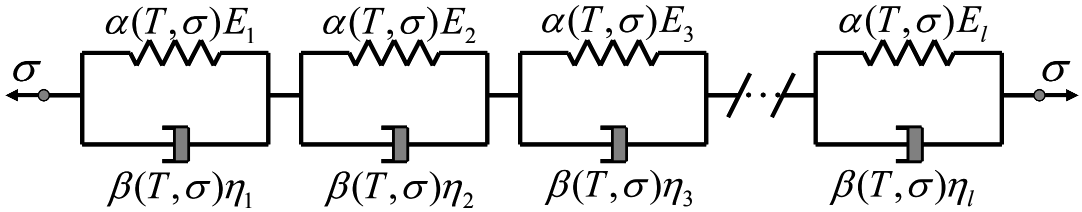

Figure 43: A series of *l* non-linear Kelvin – Voigt elements.

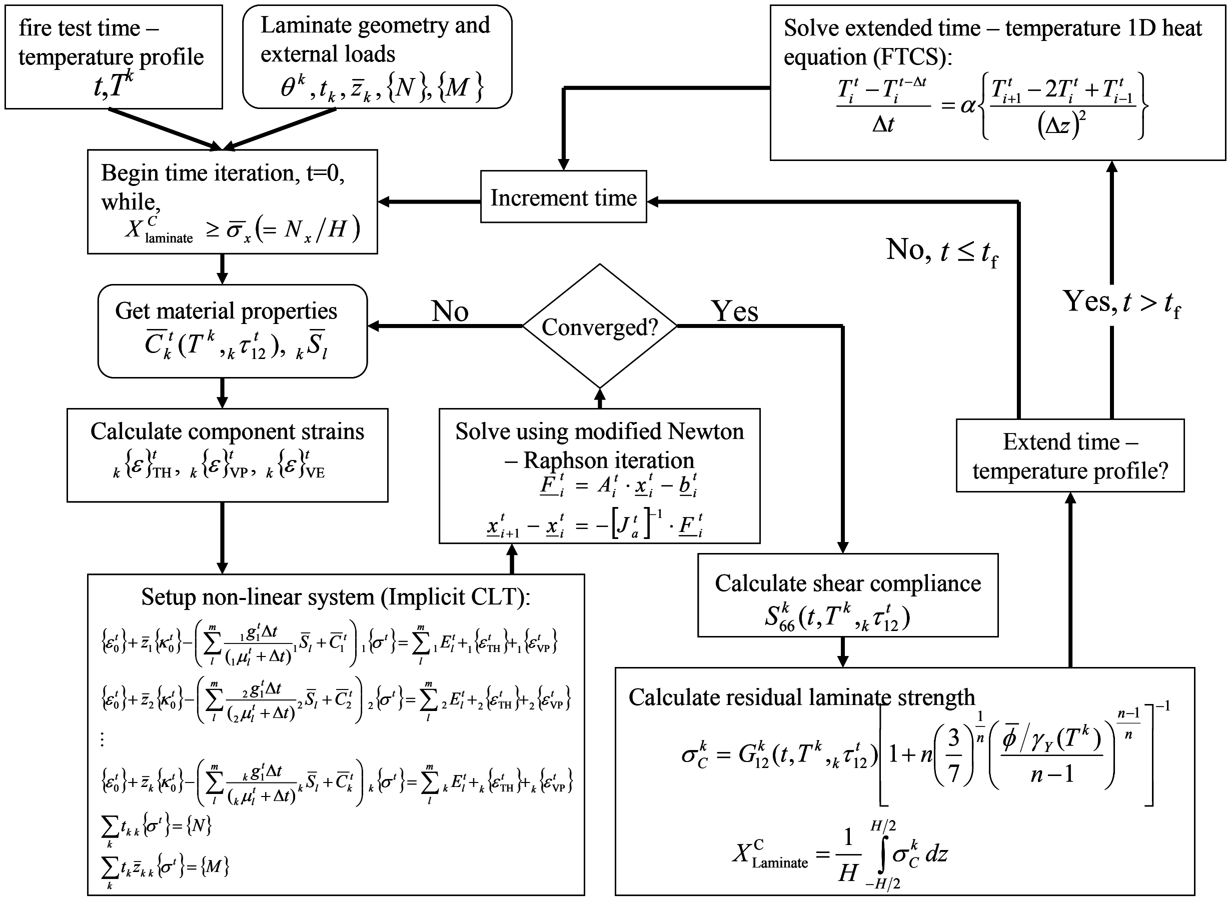

Figure 44: Flowchart of the solution method used in predicting times to failure for laminates of Vetrotex 324/Derakane 510A – 40.

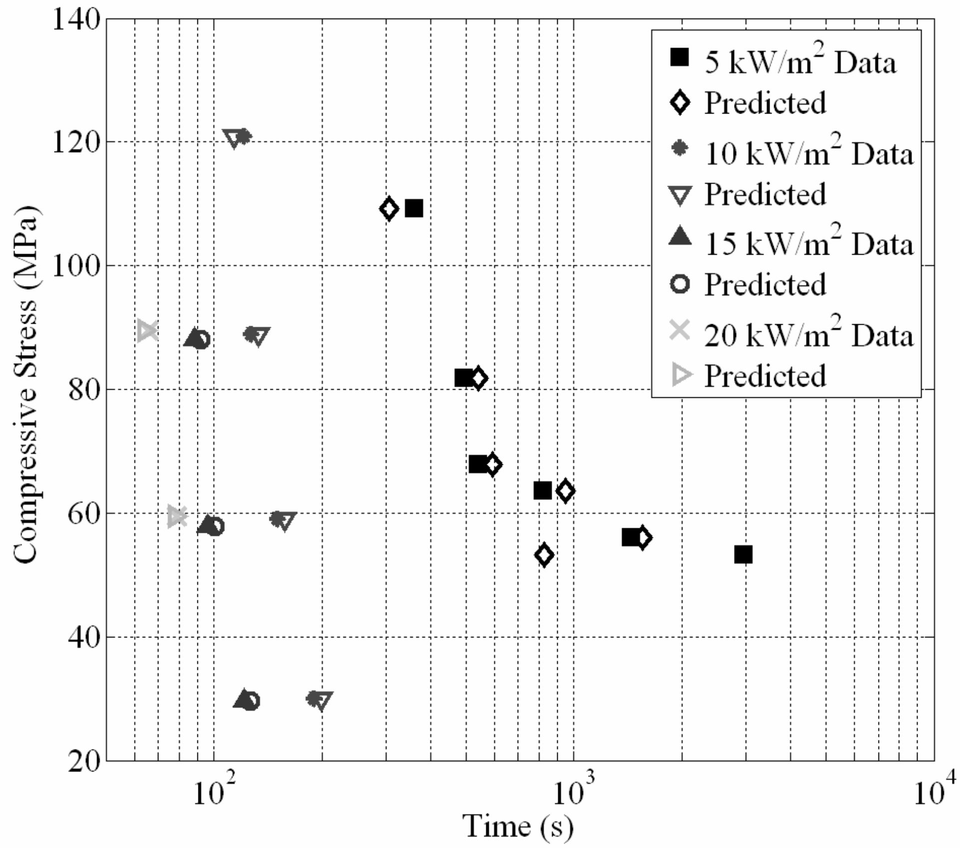

Figure 45: Compression creep rupture lifetimes of laminates ($[0/+45/90/-45/0]_S$) of Vetrotex 324/Derakane 510A – 40 subject to a one sided constant heat flux.

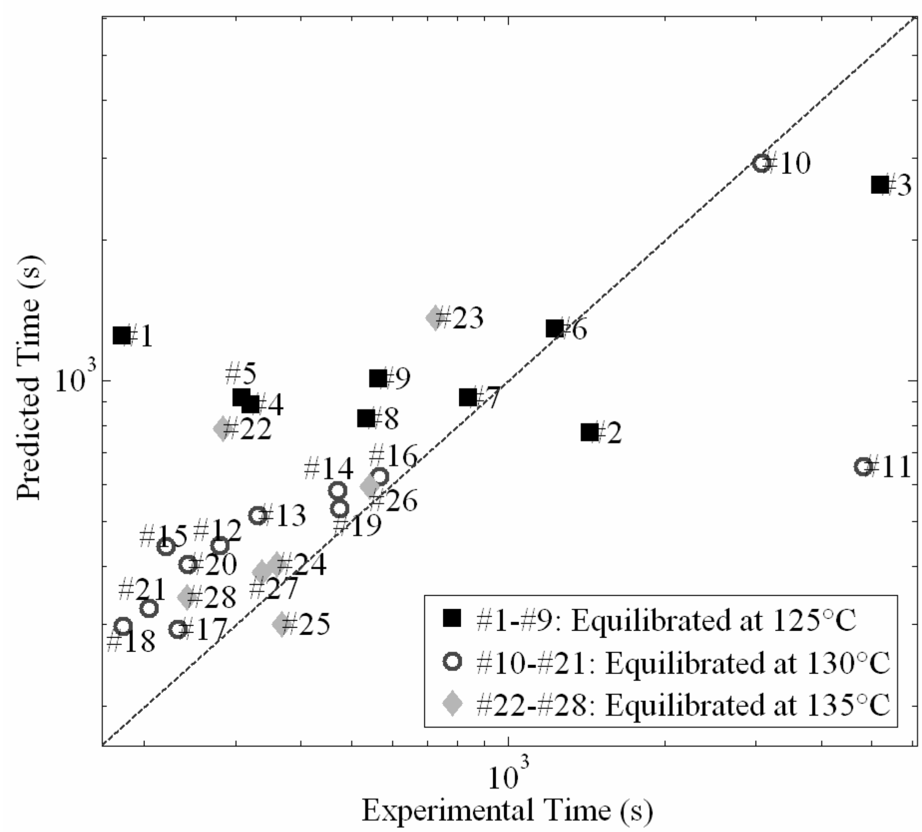

Figure 46: Compression creep rupture lifetimes of laminates ($[0/+45/90/-45/0]_S$) of Vetrotex 324/Derakane 510A – 40 subject to a one sided heat flux in which the front face temperature is held constant.

4.9 Tables

Table 2: Relevant material properties used in the analysis († values taken from Lattimer and Oullette [16])

Material Properties	Vetrotex 324/Derakane 510A - 40	
Stiffnesses and Poisson's Ratio		
$\mathbf{E_{11}}$		**33.8 GPa**
$\mathbf{E_{22}}$		**27.3 GPa**
ν_{12}		**0.15**
Coefficients of Thermal expansion		
α_1		**1.74×10^{-6}/°C**
α_2		**2.14×10^{-6}/°C**
Plasticity Parameters		
n	strain hardening	**5.3**
ϕ	initial fiber misalignment	**10°**
Thermal Analysis Parameters		
ρ	density	**1683 kg/m^3†**
k	thermal conductivity	**0.31 W/(m·°C)†**
h	coefficient of heat transfer	**30 W/(m^2·°C)**
$\mathbf{T_\infty}$	free stream temperature	**28 °C**
$\mathbf{C_p}$	specific heat capacity	**1090 J/(kg·°C)†**
α	thermal diffusivity	**1.4×10^{-7}m^2/s**

Table 3: Predictions for the constant heat flux tests. "N/A" refers to a test which was *not* used because of thermocouple failure. All calculations are performed using Matlab.

Matlab #	Compressive Stress (MPa)	Heat Flux (kW/m^2)	Failure Time (s)	Predicted Failure (s)
1	53.2	5	2962	828
2	56.0	5	1445	1549
3	63.6	5	823	945
4	67.9	5	541	593
5	81.8	5	494	542
6	109.2	5	361	306
7	15.2	10	260	N/A
8	30.0	10	190	199
9	43.6	10	168	N/A
10	59.1	10	150	157
11	88.9	10	127	133
12	120.9	10	121	113
13	29.7	15	121	126
14	57.8	15	96	100
15	88.1	15	88	91
16	4.0	20	703	N/A
17	7.0	20	289	N/A
18	59.6	20	79	78
19	89.6	20	66	64

Table 4: Predictions for the constant front temperature tests. All calculations performed using Matlab.

Matlab #	Compressive Stress (MPa)	Front Face Temperature (C)	Failure Time (s)	Predicted Failure (s)
1	52.6	125	181	1248
2	53.1	125	1438	772
3	52.1	125	5203	2632
4	55.5	125	320	890
5	54.7	125	308	919
6	55.1	125	1234	1293
7	55.8	125	838	920
8	55.4	125	534	830
9	54.9	125	564	1009
10	44.3	130	3078	2924
11	44.0	130	4822	656
12	47.3	130	279	444
13	46.9	130	330	513
14	46.6	130	471	581
15	47.5	130	220	442
16	49.8	130	567	622
17	49.9	130	232	293
18	50.1	130	182	297
19	50.2	130	474	532
20	49.3	130	243	405
21	49.8	130	204	325
22	27.9	135	283	787
23	27.7	135	727	1362
24	41.6	135	360	404
25	41.3	135	368	301
26	41.4	135	541	594
27	41.5	135	337	387
28	41.4	135	242	343

Chapter 5: Summary and Conclusions

5.1 Summary

The main goal of this research effort is to characterize and model non-linear viscoelastic behavior of an E-glass/vinyl ester composite subject to combined mechanical loading and fire exposure and integrate the effect into a structural model for the prediction of limit state variables. This structural model must be based on first principles and fundamental physics and include material property evolution (progressive thermal softening with elevating temperatures), an assessment of the thermal state of the polymer matrix and viscoelastic and viscoplastic phenomena. With fire exposure there are two temperature regions that are of interest: temperatures in the vicinity of the glass transition and temperatures at and above the decomposition temperature. Previously work has been conducted which accounts for material property evolution and the physics of the thermal state of a decomposing polymer matrix composite [18, 34]. Work has also been performed that focuses on lower temperature failure [83], but included no viscoelasticity. The contribution of this work is in developing tools and methods that allow the structural model to describe lower temperature failures that are controlled by non-linear viscoelastic/viscoplastic effects in which matrix decomposition plays no role.

In order to accomplish the goal of integrating a characterization of the non-linear viscoelastic response into the structural model, many creep and creep recovery tests were conducted over a wide temperature range and linear and non-linear creep stress levels. Over one hundred creep tests were conducted on Vetrotex 324/Derakane 510A – 40 (E-glass woven roving, vinyl ester matrix composite) at temperatures in the vicinity of the glass transition T_g (≈ 105 ºC) and in the rubbery region to T_g + 65 ºC. Since Vetrotex 324 is a woven roving with two fiber directions, the fiber direction properties were considered to be time independent and the viscoelastic characterization focused on the shear properties. An accelerated characterization method combining time – temperature superposition and Schapery's non-linear viscoelastic integral was used to reduce the data to obtain the time dependent shear compliance S_{66}. A sizeable viscoplastic component was observed in the rubbery region and the Zapas – Crissman model was adopted to characterize it. The viscoelastic and viscoplastic data reduction successfully characterized the time dependent behavior and matched the data to within ± 5 – 10% with more error encountered in the rubbery region and at stress levels in the vicinity of yield for a particular temperature.

Once the time dependent shear compliance S_{66} was known, the other necessary material properties were found through tensile and compression strength tests at temperature as previously described. Most important were the parameters for the compression strength failure criterion, the fiber imperfection ratio and the strain hardening parameter. The initial fiber misalignment for the Vetrotex 324 fibers is determined by direct microscopy (see Figure 31). Stress – strain data is collected from tension strength tests at temperature on shear coupons ($[\pm 45^o]_{2S}$) as specified by the standard test ASTM D3518/D3518M – 94 (2001). This data is fit using a Ramberg – Osgood analysis to determine the yielding shear strain and strain hardening parameter as a function of temperature.

Compression creep rupture tests were performed on unidirectional laminates (warp and weft oriented) under isothermal and one sided heating conditions. The resulting lifetimes were predicted by substituting the shear relaxation modulus G_{12} into the developed compression strenth model. The successful predictions for the isothermal compression creep rupture data indicate that the correct or dominate viscoelastic relaxation mechanism had been identified and adequately modeled. Also, reasonable predictions for both isothermal and one sided heating tests indicate that the failure mechanism described by the compression strength model of initial fiber misalignment and localized kink band formation leading to global composite failure is adequately accounted for. Though temperature is the dominant accelerating factor, the impact of stress changes in individual plies under the action of a viscoelastic and viscoplastic strain was not considered in the second manuscript (Chapter 3). Also, problems with the time – temperature profile determination exerted undue influence on the predictions causing groupings of over predictions with a cooler profile and under predictions with a warmer profile. Finally, the analysis to this point only considered viscoelastic effects and no progressive thermal softening of the Budiansky and Fleck parameters was included.

The next step in the modeling effort was to apply the non-linear viscoelastic characterization and the compression strength failure criterion to a general composite laminate. The laminate lay-up was selected by the United States Navy as $[0/+45/90/-45/0]_S$ (a pseudo-quasi-isotropic lay-up) for proposed use in topside structural components on naval ships. Compression creep rupture tests were performed on laminated coupons subject to a combined compression load and one sided heat flux. Two sets of tests were conducted to control the incident heating: constant incident heat flux and constant front face temperature. In order to account for the orthotropic symmetry of the laminate, classical lamination theory or finite element analysis may be used to determine the stress in each individual ply (CLT) or at a point (FEA). Though it is generally regarded that an FE analysis would assess the state of stress more accurately, it is challenging to implement a general viscoelastic constitutive relationship within a commercially available finite element software package such as ANSYS or ABAQUS. Though such an approach will be required if one is considering a structural component in which the composite laminate is one constituent, for life predictions of the laminated composite by itself, CLT should provide a reasonable estimate of the state of stress in each layer. Therefore CLT was used to perform the viscoelastic stress analysis under a sustained compressive load and temperature profile with the FE analysis to continue afterward.

The conventional explicit CLT algorithm presented first by Dillard et al. [78] was found to be too unstable to converge with the laminate lay-up and aggressive temperature profile of the one sided heating tests. Therefore, the implicit CLT algorithm presented by Gramoll et al. [47] was extended to include laminate curvatures, the TTSSP data reduction as presented in the first manuscript (Chapter 2) and a viscoplastic strain component to perform the stress analysis. The solution method is detailed in Figure 44 and successfully predicted the one sided heating tests further validating the modeling approach. The third manuscript (Chapter 4) corrected some of the shortcomings of the analysis in the second manuscript (Chapter 3) including developing a detailed viscoelastic stress analysis, including progressive thermal softening for some of the material properties, and developing a 1D forward time, centered space (FTCS) solution to the heat equation for a more accurate determination and extension (if necessary) of the time – temperature profile. Limitations of the analysis, however, mostly focused on the sophistication of the non-linear solver employed to converge on the state of stress in each ply and its ability to accept multiple inputs that were quickly varying with temperature and time.

5.2 Conclusions

The inclusion of creep and creep rupture phenomena into the structural modeling effort is regarded as a success. Since the model validation process focuses on lower temperature failures, the methods developed are solely mechanical models which estimate time dependent properties (viscoelasticity), temperature dependent properties (thermal softening), and laminate failure (the compression strength model). The key conclusion of this research is that viscoelastic effects play a dominant role in the delayed failure of polymer matrix composites at low heat fluxes and temperatures in the vicinity of the glass transition temperature T_g. Though the effort involved to characterize the non-linear viscoelastic response is significant and the theoretical framework involved, the characterization is necessary to successfully predict material property evolution and laminate failure at lower temperatures. Indeed, this work is among the first to provide a detailed characterization of viscoelastic effects using TTSSP and implement it within a mechanistic, phenomenological model for analysis of structures exposed to fire.

The main purpose of the first manuscript (Chapter 2) was to clearly identify the non-linear viscoelastic behavior and its onset with temperature. Above the glass transition T_g the viscoelastic response was non-linear regardless of applied shear stress level and had a significant viscoplastic strain component. Elevated temperature and *not* stress was identified as the dominant accelerating factor for the viscoelastic relaxation process. Problems with the analysis centered on the Zapas – Crissman viscoplastic functional and the difficulty of applying it with rapidly changing temperatures over large time periods (i.e. it would become unstable and diverge). Other viscoplastic models such as the approach of Nagdi [61, 62] used by Ha and Springer [53] may be more stable and deserve investigation. Also, the stress dependence of the non-linear parameters were well modeled; however, the temperature trends observed were erratic and unclear unlike those presented by Peretz and Weitsman [60]. The only parameters that demonstrated a clear temperature trend was the temperature shift fact a_T which was found to follow an Arrhenius and then Williams – Landell – Ferry relationship in temperature and the stress shift factor a_σ which followed a Erying type process. In retrospect a method of evaluating the temperature trends different from Xiao [50] should be investigated. Another issue with the non-linear viscoelastic characterization for the glass/vinyl ester composite is that its application to other composite systems with different matrix materials and different or additional relaxation mechanisms is uncertain or limited in light of the experimental time and effort required to obtain the data. Characterization of viscoelastic properties will certainly have to be simplified for implementation by naval architects who may have little time to conduct the testing and limited *a priori* knowledge of the basic physics.

As stated the inclusion of the non-linear viscoelastic constitutive relationship into the compression strength model successfully predicted the isothermal and one sided heating compression creep rupture data. The predictions for the isothermal data clearly indicate that the dominant viscoelastic relaxation mechanism was correctly identified as the shear mode and that data from tension creep testing can be used to predict compression creep phenomena. However, if the facilities and fixtures are available, it would be better to conduct compression creep testing at temperature and utilize this data for prediction. Also, the success of the compression strenght failure criterion indicates that initial fiber misalignment and matrix plasticity both play a significant role in the local compression failure of woven roving composites subject to compressive loads even though the Budianksy and Fleck model on which the compression strength model is based was original developed for unidirectional laminates. However, the compression strength model is very sensitive to input parameters such as the shear modulus and the initial fiber misalignment both of which must be accurately determined to yield good predictions. However, if the shear modulus and relaxation mechanisms are accurately modeled, the basic modeling framework should yield good predictions regardless of the material system investigated.

One of the major issues that affected the one sided heating predictions for both unidirectional (warp) and pseudo-quasi-isotropic laminates ($[0/+45/90/-45/0]_S$) was determination of the time – temperature profile. Stability and reproducibility of the temperature profiles were a significant issue. Often one sided heating tests could not be used because the front thermocouple went "open" or fell off or somehow malfunctioned giving erroneous temperature readings. Use of contact thermocouples or self adhering thermocouples may stand up to the radiant heat flux of the IR lamp better than K – type thermocouples adhered with epoxy dots. Efforts to do replicate tests were frustrated in that though the load could be reproduced, the time – temperature profiles were distinctly unique for each coupon. Another unforeseen problem with the one sided heating tests conducted on unidirectional laminates seemed to indicate that delaminations most likely due to kink band propagation were causing an insulating effect which significantly cooled the test coupon from front to back face. In retrospect the IR lamp which was used for the one sided heating tests should have been replaced with a silicon rubber resistance heater to better control the front face temperatures and the test coupons should be insulated on the back face and sides by a ceramic blanket such as the one used by Mouritz et al. [101]. This procedure would stabilize the temperature profiles making them less susceptible to ambient thermal effects, PID control for the IR lamp, and more reproducible for sets of replicate tests. As a result the more stable temperature profile would be easier to model using a simple 1D solution to the heat equation. Even so, the time – temperature profiles were stable enough to provide good temperature profile estimations and the time – temperature profile extensions calculated using the 1D FTCS discretization of the heat equation were very plausible aiding accurate prediction of times to failure.

Another issue which affected the scope of the pseudo-quasi-isotropic laminate predictions was the robust nature of the non-linear solver used in the viscoelastic stress analysis. In the third manuscript (Chapter 4) which focused on using the developing model to predict times to failure for a general laminated composite, the desire was to combine shear viscoelasticity with progressive thermal softening of the remaining properties to more accurately account for the temperature evolution of the material properties of the laminate. However, the modified Newton – Raphson method used is not guaranteed to converge unless the initial guess and Newton step remains in the region of quadratic convergence. When so many material properties and viscoelastic inputs to the CLT equations are varying with both temperature and the current state of stress, convergence is very difficult to achieve unless a more sophisticated solver is used. The Newton – Raphson method can be modified to be globally convergent with the use of linesearch/backtracking algorithms; however, it is best to adopt one of the powerful minimization or quasi – Newton methods such as the Broyden – Fletcher – Goldfarb – Shano (BFGS) method. Time limitations prohibited the coding of the BFGS method; therefore, many of the material properties known to be a function of temperature were fixed at their room temperature values in order to aid in convergence to a solution. It was possible however to include thermal softening of the fiber imperfection ratio within the compression strength model. The combination of the shear relaxation modulus and the temperature dependence of the fiber imperfection ratio did an excellent job with predicting times to failure for the pseudo-quasi-isotropic laminates indicating that the time and temperature dependencies of the composite laminate are dominated by matrix viscoelasticity and plasticity even though other temperature dependencies and the viscoplastic strain were omitted in the analysis.

Another important conclusion of this work is the benefits of implicit methods over explicit methods especially in deriving viscoelastic recursion formulas and in solving the equations of CLT. As mentioned the explicit CLT algorithm developed by Dillard et al. [78] and the viscoelastic recursion of Henriksen [93] were first attempted to perform the viscoelastic stress analysis but were unsuccessful due to stability problems associated with Henriksen's method, the laminate lay-up, and the aggressive time – temperature profile of the one sided heating tests. Fortunately, an implicit CLT algorithm was identified in the work of Gramoll et al. [47] which was successfully extended to incorporate laminate curvatures and the TTSSP viscoelastic constitutive relationship and adopted for this work. First order implicit methods worked best in the analysis for both stability and accuracy over second order methods involving the improved Euler formula. Barring the success other researchers have reported with the explicit CLT algorithm of

Dillard (including Tuttle et al. [42], Pasricha et al. [43], and more recently Guedes et al. [56]), the implicit method is a better choice given its proven stability characteristics. Though the implicit method does require a robust non-linear solver especially when multiple inputs are varying with temperature and stress, the investment is worth the coding effort since non-linear solvers such as the Newton – Raphson or BFGS method have better convergence characteristics and deal more effectively with the fact that most of the non-linear model parameters depend on the current state of stress.

The future effort will center on including the thermoviscoelastic constitutive relation within a commercially available finite element analysis code package. A first step will be to use FE to reproduce and improve the lifetime predictions for the pseudo-quasi-isotropic laminate. It is expected that the FE analysis will estimate the state of stress at a point more accurately by incorporating edge and constraint effects and inter-laminar stresses (discontinuities at the layer boundaries). Also, the FE analysis will allow for the inclusion of the viscoplastic component of the strain and temperature dependencies of various material properties which had to be omitted in the CLT analysis due to convergence issues. Once this is successfully completed, a laminated structure with basal wood core can be meshed and analyzed subject to combined mechanical load and non-uniform temperature field (more accurately simulating a fire exposure within a ship compartment).

References

1. Benson JL. The AEM/S System, a Paradigm-Breaking Mast, Goes to Sea. Naval Engineers Journal 1998;107(1995):99-103.

2. Egglestone GT, Turley DM. Flammability of GRP for use in Ship Superstructures. Fire and Materials 1994;18:255-60.

3. Fisher KJ. Is Fire a Barrier to Shipboard Composites? Advanced Composites 1993(May/June):20-26.

4. Sorathia U, Lyon R, Gann R, Gritzo L. Materials and fire threat. Sampe J. 1996;32(3):8-15.

5. Sorathia U, Gracik T, Ness J, Blum M, Le A, Scholl B, Long GL. Fire Safety of Marine Composites. 45th International SAMPE Symposium, 2000. p.1191-203.

6. Sorathia U, Ness J, Blum M. Fire Safety of Composites in the US Navy. Composites, Part A: Applied Science and Manufacturing 1999;30:707-13.

7. Sorathia U, Dapp T. Structural Performance of Glass/Vinyl Ester Composites at Elevated Temperatures. 42nd International SAMPE Symposium, 1997. p.1020-31.

8. Grand AF. Heat Release Calorimetry Evaluations of Fire Retardand Polymer Systems. 42nd International SAMPE Symposium, vol. 42, 1997. p.1062-70.

9. Hirschler MM. Heat Release in Fires. New York: Elsevier Applied Science, 1992.

10. Scudamore MJ, Briggs PJ, Prager FH. Cone Calorimetry - A Review of Tests Carried Out on Plastics for the Association of Plastic Manufacturers in Europe. Fire & Materials 1991;15:65-84.

11. Sorathia U, Beck C. Fire-Screening Results of Polymers and Composites. Fire- and Smoke-Resistant Interior Materials for Commercial Aircraft Interiors. Washington, D. C.: National Materials Advisory Board, Commission on Engineering and Technical Systems, National Research Council, 1995. p.93-114.

12. Ohlemiller T, Cleary T. Fire and Polymer II, Materials and Tests for Hazard Prevention. Washington, DC: American Chemical Society, 1995.

13. Ohlemiller T, Cleary T, Shields J. Effect of Ignition Conditions on Upward Flame Spread on a Composite Material in a Corner Configuration. 41st International SAMPE Symposium, 1996.

14. Lesko JJ, Case SW. Modeling Structural Integrity of Navy Composite Structures Subjected to and Following Fire Threat. 2002.

15. NIST. Fire Dynamics Simulator and Smokeview. Gaithersburg, MD, 2006.

16. Lattimer BY, Ouellette J. Properties of composite materials for thermal analysis involving fires. Composites Part A: Applied Science and Manufacturing 2006;37(7):1068-81.

17. Gibson AG, Chandler HW, Wu YS, Wilcox JAD, Hume J. Fire Performance of Composite Panels for Marine and Offshore Applications. Structural Materials in Marine Enrivonments, Inst. of Materials. U.K., 1994. p.35-46.

18. Gibson AG, Wright PNH, Wu YS, Mouritz AP, Mathys Z, Gardiner CP. Fire Integrity of Polymer Composites Using the Two Layer Model. Proc. of the 60th SAMPE. Long Beach, CA, 2004.

19. Mouritz AP, Gardiner CP. Compression Properties of Fire-Damaged Polymer Sandwich Composites. Composites, Part A: Applied Science and Manufacturing 2002;33:609-20.

20. Mouritz AP, Mathys Z. Post-fire mechanical properties of marine polymer composites. Compos. Struct. 1999;47(1-4):643-53.

21. Mouritz AP, Mathys Z. Mechanical Properties of Fire-damaged Glass-reinforced Phenolic Composites. Fire & Materials 2000;24:67-75.

22. Mouritz AP, Mathys Z. Post-fire mechanical properties of glass-reinforced polyester composites. Compos. Sci. Technol. 2001;61(4):475-90.

23. Pering GA, Farrell PV, Springer GS. Degradation of Tensile and Shear Properties of Composites Exposed to Fire or High Temperatures. Journal of Composite Materials 1980;14:54-68.

24. Griffis CA, Masumura RA, Chang CI. Thermal Response of Graphite Expoxy Composite Subjected to Rapid Heating. Journal of Composite Materials 1981;15:427-41.

25. Chen JK, Sun CT. Failure Analysis of Graphite/Epoxy Laminate Subjected to Combined Thermal and Mechanical Loading. Journal of Composite Materials 1985;19:408-23.

26. Griffis CA, Nemes JA, Stonesifer FR, Chang CI. Degradation In Strength Of Laminated Composites Subjected To Intense Heating And Mechanical Loading. Journal Of Composite Materials 1986;20(3):216-35.

27. Henderson JB, Wiecek TE. A Mathematical Model to Predict the Thermal Response of Decomposing, Expanding Polymer Composites. Journal of Composite Materials 1987;21.

28. Milke JA, Vizzini AJ. Thermal Response Of Fire-Exposed Composites. Journal Of Composites Technology & Research 1991;13(3):145-51.

29. McManus HLN, Springer GS. High-Temperature Thermomechanical Behavior Of Carbon-Phenolic And Carbon-Carbon Composites .1. Analysis. Journal Of Composite Materials 1992;26(2):206-29.

30. McManus HLN, Springer GS. High-Temperature Thermomechanical Behavior Of Carbon-Phenolic And Carbon-Carbon Composites .2. Results. Journal Of Composite Materials 1992;26(2):230-55.

31. Gibson AG, Wright PNH, Wu YS, Mouritz AP, Mathys Z, Gardiner CP. Modelling residual mechanical properties of polymer composites after fire. Plast. Rubber Compos. 2003;32(2):81-90.

32. Seggewiss PGB. Methods to evaluate the fire resistance of carbon fiber reinforced plastics: International SAMPE Symposium and Exhibition (Proceedings) SAMPE 2004 Conference Proceedings - Materials and Processing Technology - 60 Years of SAMPE Progress. v 49 2004. p 1463-1473.

33. Seggewiss PGB. Properties of Fire-damaged Polymer Matrix Composites. Proceedings of Composites in Fire-3, 9-10th September. University of Newcastle upon Tyne: CompositeLink, Inc., 2003.

34. Gibson AG, Wu YS, Evans JT, Mouritz AP. Laminate Theory Analysis of Composites under Load in Fire. J. Compos Mater. 2006;40(7):639-58.

35. Leaderman H. Elastic and Creep Properties of Filamentous Materials and Other High Polymers. Washington, D.C.: The Textile Foundation, 1943.

36. Schapery RA. A Theory of Non-Linear Thermoviscoelasticity Based on Irreversible Thermodynamics. Proc. 5th U.S. Nat. Cong. Appl. Mech.: ASME, 1966. p.511-30.

37. Lou YC, Schapery RA. Viscoelastic Characterization of a Nonlinear Fiber-Reinforced Plastic. Journal of Composite Materials 1971;5:208-34.

38. Glasstone S, Laidler KJ, Eyring H. The Theory of Rate Process. New York: McGraw-Hill, 1941.

39. Daugste CL. Joint Application of Time-Temperature and Time-Stress Analogies to Constructing Unified Curves. Polymer Mechanics 1974;3:359-62.

40. Griffith WI, Morris DH, Brinson HF. The Accelerated Characterization of Viscoelastic Composite Materials. Blacksburg, VA: Virginia Polytechnic Institute and State University, 1980.

41. Hiel C, Cardon AH, Brinson HF. Nonlinear Viscoelastic Response of Resin Matrix Composite Laminates. NASA Contractor Report. NASA Cr. , 1984. p.149.

42. Tuttle ME, Brinson HF. Prediction Of The Long-Term Creep Compliance Of General Composite Laminates. Exp. Mech. 1986;26(1):89-102.

43. Pasricha A, Tuttle ME, Emery AF. Time-dependent response of IM7/5260 composites subjected to cyclic thermo-mechanical loading. Compos. Sci. Technol. 1996;56(1):55-62.

44. Findley WN, Lai JSY, Onaran K. Creep and Relaxation of Nonlinear Viscoelastic Materials, with an Introduction to Linear Viscoelasticity. Amsterdam; New York: North-Holland Pub. Co., 1976.

45. Findley WN, Lai JSY. A Modified Superposition Principle Applied to Creep of Nonlinear Viscoelastic Material Under Abrupt Changes in State of Combined Stress. Transactions of the Society of Rheology 1967;11(3):361-80.

46. Onaran K, Findley WN. Combined Stress-Creep Experiments on a Nonlinear Viscoelastic Material to Determine the Kernel Functions for a Multiple Integral Representation of Creep. Transactions of the Society of Rheology 1965;9(2):299-327.

47. Gramoll KC, Dillard DA, Brinson HF. A Stable Numerical Solution Method for In-plane Loading of Nonlinear Viscoelastic Laminated Orthotropic Materials. Composites Structures 1989;13:251-74.

48. Dillard DA, Hiel C. Singularity Problems of the Power Law for Modeling Creep Compliance. Soc for Experimental Mechanics 1985:142-48.

49. Czyz JA, Szyszkowski W. An Effective Method for Nonlinear Viscoelastic Structural-Analysis. Comput. Struct. 1990;37(5):637-46.

50. Xiao X. Studies Of The Viscoelastic Behavior Of A Thermoplastic Resin Composite. Compos. Sci. Technol. 1989;34(2):163-82.

51. Brouwer R. Nonlinear Viscoelastic Characterization of Transversely Isotropic Fibrous Composites under Biaxial Loading. vol. PhD. Brussels, Belgium: Free University of Brussels, 1986.

52. Ha SK, Springer GS. Nonlinear Mechanical-Properties Of A Thermoset Matrix Composite At Elevated-Temperatures. J. Compos Mater. 1989;23(11):1130-58.

53. Ha SK, Springer GS. Time-Dependent Behavior Of Laminated Composites At Elevated-Temperatures. J. Compos Mater. 1989;23(11):1159-97.

54. Tuttle ME, Pasricha A, Emery AF. The Nonlinear Viscoelastic-Viscoplastic Behavior Of Im7/5260 Composites Subjected To Cyclic Loading. Journal Of Composite Materials 1995;29(15):2025-46.

55. Pasricha A, Van Duser P, Tuttle ME, Emery AF. The Nonlinear Viscoelastic/Viscoplastic Behavior of IM6/5260 Graphite/Bismaleimide. Proc. VII Int. Congress on Experimental Mechanics. Bethel, CT: SEM, 1992. p.35-43.

56. Guedes RM, Marques AT, Cardon AH. Analytical and Experimental Evaluation of Nonlinear Viscoelastic-Viscoplastic Composite Laminates under Creep, Creep-Recovery, Relaxation and Ramp Loading. Mechanics of Time-Dependent Materials 1998;2:113-28.

57. Guedes RM, Morais JJL, Marques AT, Cardon AH. Prediction of long-term behaviour of composite materials. Comput. Struct. 2000;76(1-3):183-94.

58. Zienkiewicz OC, Watson M, King IP. A NUMERICAL METHOD OF VISCO-ELASTIC STRESS ANALYSIS. International Journal of Mechanical Science 1968;10:807-27.

59. Peretz D. Non-Linear Viscoelastic Characterization Of Fm-73 Adhesive. J. Rheol. 1982;26(3):245-61.

60. Peretz D, Weitsman Y. The Non-Linear Thermoviscoelastic Characterizations Of Fm-73 Adhesives. J. Rheol. 1983;27(2):97-114.

61. Naghdi PM. Stress-Strain Relations in Plasticity and Thermoplasticity. In: Lee EH, Symonds PS, editors. Plasticity. Pergamon Press, 1960. p.121-67.

62. Naghdi PM, Murch SA. On the Mechanical Behavior of Viscoelastic/Plastic Solids. Journal of Applied Mechanics 1963;30:321-28.

63. Crissman JM, Zapas LJ. On The Mechanical Preconditioning Of Ultrahigh-Molecular-Weight Polyethylene At Small Uniaxial Deformations. J. Polym. Sci. Pt. B-Polym. Phys. 1985;23(12):2599-610.

64. Crissman JM. Creep And Recovery Behavior Of A Linear High-Density Polyethylene And An Ethylene-Hexene Copolymer In The Region Of Small Uniaxial Deformations. Polym. Eng. Sci. 1986;26(15):1050-59.

65. Xiao XR, Hiel CC, Cardon AH. Characterization And Modeling Of Nonlinear Viscoelastic Response Of Peek Resin And Peek Composites. Compos. Eng. 1994;4(7):681-702.

66. Kawai M, Masuko Y, Sagawa T. Off-axis tensile creep rupture of unidirectional CFRP laminates at elevated temperature. Composites Part A: Applied Science and Manufacturing;In Press, Corrected Proof.

67. Guedes RM. An energy criterion to predict delayed failure of multi-directional polymer matrix composites based on a non-linear viscoelastic model. Composites Part A: Applied Science and Manufacturing 2004;35(5):559-71.

68. Miyano Y, Nakada M, Sekine N. Accelerated testing for long-term durability of GFRP laminates for marine use. Composites Part B: Engineering 2004;35(6-8):497-502.

69. Miyano Y, Nakada M, McMurray MK, Muki R. Prediction of Flexural Fatigue Strength of CRFP Composites under Arbitrary Frequency, Stress Ratio and Temperature. J. Compos Mater. 1997;31(6):619-38.

70. Miyano Y, Nakada M, Mohri M, McMurray MK, Kitade N. Loading rate and temperature dependence of flexural behaviour of unidirectional pitch-based CFRP laminates. Composites 1995;26(10):713-17.

71. Orr RL, Sherby OD, Dorn JE. Transactions of the American Society of Mechanical Engineers 1954;46:113.

72. Larson FR, Miller J. "A Time-Temperature Relationship for Rupture and Creep Stresses". Transactions of the American Society of Mechanical Engineers 1952;74:765.

73. Dillard DA, Morris DH, Brinson HF. "Predicting Viscoelastic Response and Delayed Failures in General Laminated Composites". In: Daniel IM, editor. Composite Materials: Testing and Design (Sixth Conference), vol. ASTM STP 787. American Society for Testing and Materials, 1982. p.357-70.

74. Lyons JS. "Time and Temperature Effects on the Mechanical Properties of Glass-Filled Amide-Based Thermoplastics". Polymer Testing 1998;17:237-45.

75. Zhurkov SN. International Journal of Fracture Mechanics 1965;1:311.

76. Zhurkov SN, Korsukov VE. "Atomic Mechanisms of Fracture of Solid Polymers". Journal of Polymer Science, Part A-2: Poymer Physics Edition 1974;12(2):385-98.

77. Budiansky B, Fleck NA. Compressive Failure Of Fiber Composites. J. Mech. Phys. Solids 1993;41(1):183-211.

78. Dillard DA, Brinson HF. NUMERICAL PROCEDURE FOR PREDICTING CREEP AND DELAYED FAILURES IN LAMINATED COMPOSITES. In: O'Brien TK, editor. Long Term Behavior of Composites, ASTM STP 813, vol. ASTM STP 813. ASTM, 1983. p.23-37.

79. Dillard DA. Creep and Creep Rupture of Laminated Graphite/Epoxy Composites. PhD Dissertation in Engineering Science and Mechanics, vol. PhD. Blacksburg, Virginia: Virginia Polytechnic Institute & State University, 1981.

80. Dillard DA. Viscoelastic Behavior of Laminated Composite Materials. In: Reifsnider KL, editor. Fatigue of Composite Materials. Elsevier Science Publishers, B. V., 1990.

81. Boyd SE, Lesko JJ, Case SW. The Thermo-Viscoelastic, Viscoplastic Characterization of Vetrotex 324/Derakane 510A – 40 through Tg. Journal of Engineering Materials and Technology 2006;128(4):586-94.

82. Boyd SE, Bausano JV, Lesko JJ, Case SW. Compression Creep Rupture Behavior of a Glass/Vinyl Ester Composite Subject to Isothermal and One-sided Heat Flux Condition. submitted to Composites, Part A: Applied Science and Technology 2006.

83. Bausano JV, Lesko JJ, Case SW. Composite life under sustained compression and one sided simulated fire exposure: Characterization and prediction. Composites Part A: Applied Science and Manufacturing 2006;37(7):1092-100.

84. Halverson H, Bausano J, Case S, Lesko J. Simulation of response of composite structures under fire exposure. Sci. Eng. Compos. Mater. 2005;12(1-2):93-101.

85. Schapery RA. On the Characterization of Nonlinear Viscoelastic Materials. Polym. Eng. Sci. 1969;9(4):295-310.

86. Ferry JD. Viscoelastic Properties of Polymers. New York: John Wiley and Sons, 1980.

87. Tuttle ME, Mescher AM, Potocki ML. Mechanics of Polymeric Composites Exposed to a Constant Heat Flux. ASME 1997, Composites and Functionally Graded Materials, vol. 80, 1997. p.157-63.

88. Henderson JB, Wiecek TE. A Mathematical Model to Predict the Thermal Response of Decomposing, Expanding Polymer Composites. J. Compos Mater. 1987;21:373-93.

89. Cain JJ, Post NL, Lesko JJ, Case SW, Lin YN, Riffle JS, Hess PE. Post-Curing Effects on Marine VARTM FRP Composite Material Properties for Test and Implementation. Journal of Engineering Materials and Technology 2006;128(1):34-40.

90. Boyd SE, Bausano JV, Lesko JJ, Case SW. Mechanistic Approach to Structural Fire Modeling of Composites. In: Mouritz AP, Couchman L, editors. Modeling of Naval Composite Structures in Fire. Cooperative Research Centre for Advanced Composite Structures, 2006. p.199 - 253.

91. Leaderman H. Viscoelasticity Phenomena in Amorphous High Polymeric Systems. In: Eirich FR, editor. Rheology: Theory and Applications, vol. 2. New York: Academic Press Inc., 1958. p.1 - 61.

92. Schapery RA, Park SW. Methods of interconversion between linear viscoelastic material functions. Part II--an approximate analytical method. Int. J. Solids Struct. 1999;36(11):1677-99.

93. Henriksen M. Nonlinear Viscoelastic Stress Analysis - A Finite Element Approach. Computers and Structures 1984;18(1):133-39.

94. Roy S, Reddy JN. A Finite Element Analysis of Adhesively Bonded Composite Joints with Moisture Diffusion and Delayed Failure. Comput. Struct. 1988;29(6):1011-31.

95. Lai J, Bakker A. 3-D Schapery representation for non-linear viscoelasticity and finite element implementation. Computational Mechanics 1996;18(3):182-91.

96. Haj-Ali RM, Muliana AH. Numerical finite element formulation of the Schapery non-linear viscoelastic material model. International Journal for Numerical Methods in Engineering 2004;59(1):25-45.

97. Boyce WE, DiPrima RC. Elementary Differential Equations and Boundary Value Problems: John Wiley & Sons, Inc., 2001.

98. Pasricha A. Prediction and measurement of the long term mechanical behavior of polymeric composites. PhD Dissertation, vol. PhD: University of Washington, 1994.

99. Jones RM. Mechanics of Composite Materials: Taylor & Francis, 1999.

100. Bathe KJ. Finite Element Procedures: Prentice-Hall Inc., 1996.

101. Mouritz AP, Feih S, Mathys Z, Gibson AG. Mechanical Property Degradation of Naval Composite Materials. In: Couchman L, Mouritz AP, editors. Modeling of Naval Composite Structures in Fire. Department of the Navy: Science and Technology, 2006.